University of Alberta

Second Order Corrections to Semileptonic b-quark Decay

by

Matthew Eric Dowling ©

A thesis submitted to the Faculty of Graduate Studies and Research
in partial fulfillment of the requirements for the degree of

Master of Science

in

Department of Physics

Edmonton, Alberta
Fall 2008

Library and Archives Canada

Published Heritage Branch

395 Wellington Street
Ottawa ON K1A 0N4
Canada

Bibliothèque et Archives Canada

Direction du Patrimoine de l'édition

395, rue Wellington
Ottawa ON K1A 0N4
Canada

Your file Votre référence
ISBN: 978-0-494-47205-7
Our file Notre référence
ISBN: 978-0-494-47205-7

NOTICE:
The author has granted a non-exclusive license allowing Library and Archives Canada to reproduce, publish, archive, preserve, conserve, communicate to the public by telecommunication or on the Internet, loan, distribute and sell theses worldwide, for commercial or non-commercial purposes, in microform, paper, electronic and/or any other formats.

The author retains copyright ownership and moral rights in this thesis. Neither the thesis nor substantial extracts from it may be printed or otherwise reproduced without the author's permission.

AVIS:
L'auteur a accordé une licence non exclusive permettant à la Bibliothèque et Archives Canada de reproduire, publier, archiver, sauvegarder, conserver, transmettre au public par télécommunication ou par l'Internet, prêter, distribuer et vendre des thèses partout dans le monde, à des fins commerciales ou autres, sur support microforme, papier, électronique et/ou autres formats.

L'auteur conserve la propriété du droit d'auteur et des droits moraux qui protège cette thèse. Ni la thèse ni des extraits substantiels de celle-ci ne doivent être imprimés ou autrement reproduits sans son autorisation.

In compliance with the Canadian Privacy Act some supporting forms may have been removed from this thesis.

While these forms may be included in the document page count, their removal does not represent any loss of content from the thesis.

Conformément à la loi canadienne sur la protection de la vie privée, quelques formulaires secondaires ont été enlevés de cette thèse.

Bien que ces formulaires aient inclus dans la pagination, il n'y aura aucun contenu manquant.

Canada

University of Alberta

Library Release Form

Name of Author: Matthew Eric Dowling

Title of Thesis: Second Order Corrections to Semileptonic b-quark Decay

Degree: Master of Science

Year this Degree Granted: 2008

Permission is hereby granted to the University of Alberta Library to reproduce single copies of this thesis and to lend or sell such copies for private, scholarly or scientific research purposes only.

The author reserves all other publication and other rights in association with the copyright in the thesis, and except as herein before provided, neither the thesis nor any substantial portion thereof may be printed or otherwise reproduced in any material form whatsoever without the author's prior written permission.

_____

Signature

Matthew Eric Dowling
1104 – 111A Street
Edmonton, Alberta
Canada, T6J 6R9

University of Alberta

Faculty of Graduate Studies and Research

The undersigned certify that they have read, and recommend to the Faculty of Graduate Studies and Research for acceptance, a thesis entitled **Second Order Corrections to Semileptonic b-quark Decay** submitted by **Matthew Eric Dowling** in partial fulfillment of the requirements for the degree of **Master of Science**.

Andrzej Czarnecki (Supervisor)

Roger Moore (Chair)

Ian Blokland (External)

Alexander Penin

Date: _____

Abstract

Recent disagreements in estimating the decay rate of $b \to c\ell\nu_\ell$ have given the need to check the result first calculated in 1998. Here, we present an expansion of the second order corrections to the decay rate $b \to cW^*$ in the limit that the W^* mass equals the c-quark mass. This new expansion provides a check of the one from 1998 and has highlighted the reason for the disagreement. With these new results, the estimates of the decay rate of $b \to c\ell\nu_\ell$ now agree.

Contents

1 Introduction **1**
- 1.1 The CKM Parameter V_{cb} 1
- 1.2 Experimental Methods 2
- 1.3 Theoretical Calculation for the Determination of $|V_{cb}|$ 4

2 Methods of Calculation **7**
- 2.1 Tools For Computing Feynman Diagrams 7
- 2.2 Asymptotic Expansion 10
- 2.3 Recurrence Relations 11
- 2.4 Phase Space Integrals 14
- 2.5 Eikonal Integrals 16
  - 2.5.1 Expansions and Preparation 16
  - 2.5.2 The Eikonal Integrals 18
- 2.6 Relations Between Diagrams 20
  - 2.6.1 Gauge Independence 21
  - 2.6.2 Vertex Switching 28

3 The Decay $b \to c\bar{c}cW^*$ **32**
- 3.1 Methods of Calculation 32
- 3.2 Results 35

4 Second Order Corrections to Semileptonic b Decay **37**
- 4.1 Expansion From Zero Recoil 38
- 4.2 Expansion From Zero Mass 40
  - 4.2.1 Checks 40
  - 4.2.2 NNLO Results 41
- 4.3 The Polynomial Fit 43
  - 4.3.1 $\mathcal{O}(\alpha_s)$ Corrections 46
  - 4.3.2 The $\mathcal{O}(\alpha_s^2)$ Corrections 48

5 Conclusions **51**

Bibliography **53**

A Useful Programs **55**
A.1 Qgraf [30] 55
A.1.1 Installation and Use 55
A.1.2 Files 55
A.1.3 Indices 58
A.1.4 Example and How to Interpret the Output 59
A.2 The Mathematica Package HypExp [31] 61
A.2.1 HypExp Functions In Mathematica 62
A.2.2 Examples 63
A.3 XSummer [32] 65
A.3.1 How to Use XSummer 65
A.3.2 Goncharov Multiple Polylogarithms [33] 68

B Catalog of Diagrams **70**
B.1 Zero Recoil Expansion 70
B.2 Zero Mass Expansion 73
B.3 Topologies And Mass Expansions 75

C Full NNLO Expansions **86**
C.1 Expansion From Zero Recoil 86
C.2 Expansion From Zero Mass 92

List of Tables

2.1 The colour grouping of gauge invariance. Note that there is overlapping between the groups because of renormalization diagrams that contribute to all four groups. 21

2.2 The colour grouping of gauge invariance. Note that there is overlapping between the groups because of renormalization diagrams that contribute to all four groups. 22

4.1 Comparison of polynomial fit after correcting the renormalization. 49

4.2 Comparison of polynomial fit with extended expansions. . . . 49

4.3 Comparison of polynomial fit using no normalization. 49

List of Figures

1.1 The unitary triangle derived from Eq. (1.3). There is a lot of interest in over-constraining the parameters of this triangle in order to search for new physics [2]. 2

1.2 The kinematically allowed region for $Q \to qW^*$ decay. The different known expansions are shown with solid arrows and the expansion obtained in this thesis is shown with a dashed arrow. The analytical result is also known along the whole Zero Recoil line. 5

2.1 Two loop Feynman diagram. 9

2.2 The three possible contributions that are calculated from the imaginary part of Fig. (2.1). The zig-zags represent where the diagram has been cut. 9

2.3 A two loop topology where the solid thin line has mass m the solid thick line has mass M and the dashed line is massless. . 10

2.4 The possible regions found with the method of asymptotic expansion applied to the diagram in Fig. (2.3). 12

2.5 Massive two particle phase space. 14

2.6 In the region where $|p_1|, |p_9| < |p|$ this diagram has propagators that lead to eikonal integrals. The solid, dashed and dotted lines represent particles with mass M, m, and 0 respectively. For this calculation, we have cut the diagram through propagators 9, 3 and 6. 16

2.7 Diagram with an external gluon from a b-quark line. 23

2.8 Step 1: cancellations at the c-quark end. 24

2.9 Step 2: cancellations at the b-quark end. 24

2.10 The gauge dependent part from the contraction of Fig. (2.7) with k_ρ. 24

2.11 Rule for finding the gauge dependent part of a diagram involving a quark-gluon vertex. 24

2.12 A three gluon vertex with one of the gluons being emitted. The momentum of the gluon 1 is into the vertex and the momentum of the other two is out of the vertex. 25

2.13 The gauge dependent part from a triple gluon vertex. 26

2.14 Diagram with an external gluon from a c-quark line. 26

2.15 Cancel either b-quark lines. 26

2.16 Cancel either c-quark lines. 26
2.17 Diagram with an external gluon from a gluon line. 26
2.18 After applying the quark gluon vertex rule and three gluon rule to propagator q. 27
2.19 The result from applying the rules to propagator $q - k$. 27
2.20 After applying the three gluon rule there are two diagrams that have a gauge dependence. 27
2.21 Applying the quark gluon rule to each resulting diagram confirms our above method. 28
2.22 Diagram with a c-quark propagator. 29
2.23 Diagram with a b-quark propagator. 29
2.24 The three possible diagrams with two outgoing gluons that originate on the fermion line 30

3.1 Feynman diagrams, corresponding to amplitudes M_1 and M_2 respectively, contributing to $b \to c\bar{c}cW^*$ 32
3.2 Comparison of results from previous papers. The dashed line shows the expansion about $\rho = 1$ while the thin line shows the expansion about $\rho = 0$. The thick line shows how the result from this paper closes the gap between the two. 36

4.1 A comparison between the old and updated expansions shows a clear difference. The tail on the old expansion (dotted line) is a result of attempting to estimate the remaining contribution with a $\frac{\beta}{1-\beta}$ term. 39
4.2 The contributions to the $\mathcal{O}(\alpha_s)$ corrections. The WF and MC diagrams correspond to wave function and mass renormalization contributions respectively. 41
4.3 The matching of the $\mathcal{O}(\alpha_s)$ corrections to the decay $\Gamma(b \to cW^*)$. The dotted line is the expansion from the zero recoil line and the solid line is the expansion from zero mass. 42
4.4 The matching between the different colour contributions. The dashed line corresponds to the expansion from zero recoil and the solid line corresponds to the expansion from zero mass. . . 44
4.5 The complete $\mathcal{O}(\alpha_s^2)$ contribution. 45
4.6 Polynomial fit to the tree order calculation. 46
4.7 Polynomial fit to $\mathcal{O}(\alpha_s)$ corrections normalized to the phase space. The exact result is shown using points known along the dashed curve. 47
4.8 Polynomial fit to $\mathcal{O}(\alpha_s)$ corrections normalized to the tree level. The exact result is shown using points known along the curve. 47
4.9 Polynomial fit to $\mathcal{O}(\alpha_s)$ corrections with no normalization. The exact result is shown using points known along the curve. . . . 47

A.1 The corresponding vertices generated in the qgraf output. . . . 61

A.2 The resulting Feynman diagram when the propagators are put together. 61

B.1 Feynman diagrams of amplitudes that needed to be calculated for the zero recoil expansion. The amplitude of each diagram on the left is multiplied by the amplitude of each diagram on the right. 72
B.2 $\mathcal{O}(\alpha_s^2)$ diagrams for the zero mass expansion. 73
B.3 Topologies to be considered for the three loop contributions. . 74
B.4 $\mathcal{O}(\alpha_s^2)$ renormalization diagrams for the zero mass expansion. . 74

Chapter 1

Introduction

The field theory of Quantum Electrodynamics (QED) is among the most accurately tested physical theories to date. For example, the fine structure constant in QED, α, has been deduced from experimental and theoretical studies and is by far the most precisely known coupling constant. The value provided from g-2 measurements [1],

$$\alpha^{-1} = 137.035\,998\,83(51), \tag{1.1}$$

Accurate measurements, confronted with theoretical predictions of QED, are sensitive probes of new physics and a lot of effort is being put into increasing their precision and accuracy.

The enormous success of QED has stimulated the development of a theory of strong interactions, Quantum Chromodynamics (QCD). It has also led to the construction of the Standard Model: a quantum field theory describing the three larges subatomic forces, including weak interactions. One very active area of research, encompassing all Standard Model interactions focuses on determining the values of the Cabibbo-Kobayashi-Maskawa (CKM) quark-mixing matrix and over-constraining its unitarity.

1.1 The CKM Parameter V_{cb}

The unitary CKM matrix is parametrized by nine different parameters relating the mass eigenstates to the weak-interaction eigenstates of quarks,

$$V_{CKM} = \begin{pmatrix} V_{ud} & V_{us} & V_{ub} \\ V_{cd} & V_{cs} & V_{cb} \\ V_{td} & V_{ts} & V_{tb} \end{pmatrix}. \tag{1.2}$$

To understand better the meaning of this matrix, consider the example of a b-quark decay. When referred to by name, the quark of interest is a particle with well-defined mass. The origin of masses is not yet fully understood, but it is not necessarily related to the weak interactions responsible for quark decays. It follows that the quark does not necessarily decay into a state with a

well-defined mass, but rather into a superposition of similar quarks: u-type or d-type. The particle states involved in this superposition are restricted only by kinematics and charge conservation. For the b-quark decay, the resulting state consists of a u-quark and a c-quark with probability amplitudes given by V_{ub} and V_{cb} respectively.

The assumption that there are a total of three generations of quarks gives the condition that this three-by-three matrix must be unitary. This also leads to six off-diagonal unitary triangle relations, such as

$$V_{ud}V_{ub}^* + V_{cd}V_{cb}^* + V_{td}V_{tb}^* = 0. \tag{1.3}$$

The elements of the matrix can be expressed in terms of three angles (α, β, γ) and a phase factor δ. In light of this, we can make a triangle out of Eq. (1.3) in the complex plane with angles and side lengths defined in terms of the elements of the CKM matrix, as shown in Fig. (1.1).

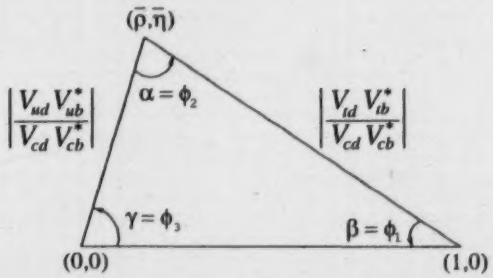

Figure 1.1: The unitary triangle derived from Eq. (1.3). There is a lot of interest in over-constraining the parameters of this triangle in order to search for new physics [2].

The strict unitary relationships in this triangle mean that measurements of the angles and side lengths can be sensitive probes to new physics. For example, if another generation of quarks existed, the measured mixing parameters might not fulfill the unitary triangle conditions Eq. (1.3). In particular the length of the side opposite to the angle β is proportional to $|V_{ub}|/|V_{cb}|$ making the determination of $|V_{ub}|$ and $|V_{cb}|$ of great interest.

In this work we will be concentrating on one of two methods used to determine $|V_{cb}|$: inclusive semileptonic decay. To date, this is the most accurate method of determining $|V_{cb}|$ and the limits of the theoretical approach come only from higher order perturbative and non-perturbative contributions.

1.2 Experimental Methods

Experimentally, $|V_{cb}|$ has become easier and easier to measure because of the increased experimental ability to detect and track b decays, increased luminosity at particle colliders, and the fact that the predominant decay mode

is $b \to c$. This makes for a clean signal so that there is a large amount of data and the determination of $|V_{cb}|$ from experimental data is mainly systematics limited. As a result, the main uncertainty comes not from experimental measurements but from the theoretical calculations as discussed in the next section.

There are two methods for determining $|V_{cb}|$ experimentally: through exclusive decays and through inclusive decays. Exclusively, the decay rate of $\overline{B}^0 \to D^{*+}\ell^-\overline{\nu}_\ell$ has been used to extract a value for $|V_{cb}|$ by considering its dependence on the recoil of the D^{*+}. The most recent measurement of $|V_{cb}|$ from exclusive decays was made by BaBar [3]. Including their data in the world average provides a value of [4],

$$|V_{cb}| = (39.3 \pm 0.9_{exp} \pm 1.7_{theo}) \times 10^{-3}.$$

It can easily be seen here that the main uncertainty comes from the theory side of the determination.

The inclusive determination is more precise than the exclusive methods and uses semileptonic decay rates. This method is also helped by the fact that two schemes can be used for the calculation: an expansion in the 1S scheme and an expansion in the kinetic mass scheme.

In order to extract values for $|V_{cb}|$ measurements of the electron energy and hadron mass spectra are needed. To measure these spectra, events from $\Upsilon(4S)$ decays are used to reconstruct fully one of the B meson decays. From these events, partial branching fractions for B^0 and B^+, moments of the electron energy spectrum and the 4-momenta of the hadronic component are determined. All of these values are then used to perform a global fit in either the 1S scheme or kinetic scheme to obtain a value for $|V_{cb}|$. These results can be further refined by including data from $b \to s\gamma$ decays to constrain the b-quark mass.

One other important consideration is what scheme to use when measuring a quark mass. This happens because quarks are confined and thus we are essentially unable to measure the properties of a free quark. In the case of top quark production we are able to measure some properties because the top quard does not live long enough to hadronize. To measure the mass of a quark, we then must rely on the mass dependence of certain properties of particles containing the quark we are interested in. In the case of the b-quark, the 1S and kinetic mass schemes have been used to measure the b-quark mass. The 1S scheme relies on the 1S $b\bar{b}$ bound state properties, while the kinetic scheme uses properties of the decay $b \to c$ when the c-quark is produced almost at rest. When all of the data is put together one finds [4]

$$|V_{cb}| = (41.69 \pm 0.33_{fit} \pm 0.20_{\tau_B}) \times 10^{-3},$$

from the 1S expansion and

$$|V_{cb}| = (41.96 \pm 0.23_{exp} \pm 0.35_{HQE} \pm 0.59_{\Gamma_{SL}}) \times 10^{-3},$$

from the kinetic mass expansion. The *fit* error comes from both theoretical and experimental errors in the fit and the τ_B error is from the uncertainty in B lifetime. In the kinetic mass expansion, the last two errors are theoretical and provide a large amount of the uncertainty in $|V_{cb}|$. As can be seen, both determinations of $|V_{cb}|$ are consistent with each other and the exclusive result.

1.3 Theoretical Calculation for the Determination of $|V_{cb}|$

The parameter $|V_{cb}|$ is a free parameter in the Standard Model (SM). As such, a combination of experimental data and theoretical calculations are needed to extract its value. The large amount of data from B factories has lead to the main uncertainty in $|V_{cb}|$ coming from our ignorance of higher order perturbative contributions to inclusive decays. In accordance with this, a lot of work has been done in attempting to calculate the complete $\mathcal{O}(\alpha_s^2)$ corrections to $\Gamma(b \to c\ell\nu_\ell)$. These corrections include both perturbative and non-perturbative corrections.

The decay $\Gamma(b \to c\ell\nu_\ell)$ can be computed perturbatively as an expansion that depends on $\left(\frac{m_c}{m_b}\right)$. To be able to compare this to experimental data though, we need $\Gamma(B \to X_c\ell\nu_\ell)$. Fortunately, the largest contribution to $\Gamma(B \to X_c\ell\nu_\ell)$ comes precisely from the decay $\Gamma(b \to c\ell\nu_\ell)$. This is called the spectator quark model, because the second quark does not participate in the decay. In reality, however, this is not true and the spectator quark contributes non-perturbative corrections. These non-perturbative corrections give terms that are proportional to Λ_{QCD}^n/m_b^n starting at $n = 2$ [5]. They have been found to be large at least in the leading order and much work has been done in calculating sufficient orders. As an example of this work, see [6]. With the non-perturbative contributions under control, it is important also to have the perturbative corrections.

The perturbative corrections are calculated using Heavy Quark Effective Field Theory (HQET). In this theory expansions are computed in terms of Λ_{QCD}/m_b and α_s. Unfortunately the second order corrections in α_s to this decay are very difficult to calculate for arbitrary lepton invariant mass $\sqrt{q^2}$. A small subset of these corrections has been calculated and resummed to all orders [7]: the Brodsky-Lepage-Mackenzie (BLM) corrections [8]. This small group of corrections contributes to a large part of the $\mathcal{O}(\alpha_s^2)$ complete result with non-BLM corrections thought to be no larger than 1%. Without the full second order corrections though, this is only an estimate. Recently K. Melnikov [9] and A. Pak and A. Czarnecki [10] were able to compute expansions that give the full $O(\alpha_s^2)$ results, thus providing a more exact calculation.

These new results, however, contradict an earlier determination [11]. This thesis is devoted to resolving this discrepancy. In [11–13] three points for the decay $d\Gamma(b \to c\ell\nu_\ell)/dq^2$ were calculated corresponding to the three circled

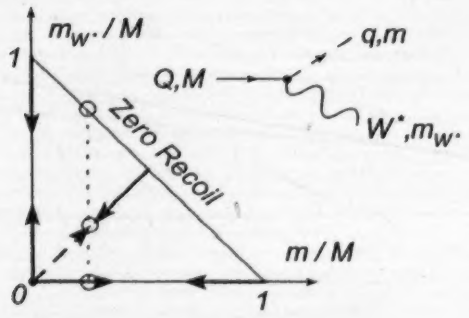

Figure 1.2: The kinematically allowed region for $Q \to qW^*$ decay. The different known expansions are shown with solid arrows and the expansion obtained in this thesis is shown with a dashed arrow. The analytical result is also known along the whole Zero Recoil line.

points in Fig. (1.2). This triangle is a plot of the allowed kinematic region for the decay $\Gamma(Q \to qW^*)$, where Q is a heavy quark and q is light compared to Q. Much work has been done to understand fully the mass dependence of $\Gamma(Q \to qW^*)$ in different limits. Each arrow in Fig. (1.2) represents a second order expansion that has been done. The most recent of these is the diagonal expansion shown by the dashed arrow and presented in this thesis. Perhaps the most interesting aspect of this diagram, is the dotted line representing the curve given by the differential decay rate $d\Gamma(b \to c\ell\nu_\ell)/dq^2$. Integrating along this line gives the full semi-leptonic decay which is then used to extract $|V_{cb}|$. Since the differential decay rate is not known to second order, the three points calculated in [11–13] were used to fit a polynomial that could then be integrated with respect to q^2 and thus give a value for the full second order correction to $\Gamma(b \to c\ell\nu_\ell)$.

The authors were able to compute these points by fixing the invariant lepton mass $\sqrt{q^2}$ and relating the differential rate to the decay $\Gamma(b \to cW^*)$. As seen in Fig. (1.2) several expansions have been computed for this decay [11, 14–17]. One way to check these earlier results is to perform an expansion along the diagonal with $m_{W^*} = m_c$ starting at the point $m_c = 0$: this is done in this thesis.

In [11] the diagonal expansion result was used to obtain an estimate for the non-BLM corrections to the decay rate $\Gamma(b \to c\ell\nu_\ell)$. The authors used the three known points for q^2 to derive a polynomial expression for the differential decay rate and integrated to obtain the non-BLM corrections. In that paper, it was found that the non-BLM corrections have a contribution of 0.9(3) to the decay rate. Recently, however, a numerical calculation was done that obtained a significantly different result that could not be explained [9]. The author arrived at a result of 1.73 for the same contribution. At the same time as well, fully analytical results [10] were computed that confirmed this difference.

The result presented here is aimed at showing that the expansion in [11] was right. We have found, however, that there were errors in the renormalization of two of the relevant points for this polynomial expansion resulting in the abnormally low estimate originally obtained. As well, we have found a method of fitting this polynomial that gives much more accurate results and brings the estimate within error of the recent exact calculation.

Chapter 2

Methods of Calculation

With the increasing need for higher order corrections in perturbative quantum field theory (QFT) comes the need for tools that will allow us to carry out these complicated calculations. Some of these tools, for example the optical theorem and dimensional regularization, have been around for some time and are widely used. Others, for example the Laporta Algorithm [18], have only recently been discussed in the literature. In this chapter we will introduce these tools and others that will be useful in the calculation of $\Gamma(b \to cW^*)$.

2.1 Tools For Computing Feynman Diagrams

In order to aid in calculating higher order corrections a number of useful tools are needed. The first of these tools is dimensional regularization. This is a mathematical method allowing us to compute integrals that would otherwise be divergent in four dimensions. Essentially the idea is to extend the dimension of the integral by a small amount, ϵ, and compute it in these D dimensions rather than the more familiar four. At the end of the calculation, any observable should be independent of ϵ when we take the limit $\epsilon \to 0$. In this thesis we will always generalize to D dimensions using $D = 4 - 2\epsilon$. This method has the added bonus of highlighting divergences. When the expansion in ϵ is done, the divergent parts appear as terms with inverse powers of ϵ. These terms end up cancelling with renormalization factors so that the result is finite, as one would expect.

To be able to use this method and take full advantage of it, there are a few properties that need to be introduced. First, we need to know the form of the D dimensional angular integral [19],

$$\int d\Omega_{D-1} = \frac{2\pi^{D/2}}{\Gamma(\frac{D}{2})}. \tag{2.1}$$

This will come in useful when we attempt to do phase space integrals later on

in this chapter. Next, we have the basic loop integral [20],

$$\int \frac{d^D k}{(2\pi)^D} \frac{1}{(k^2+m^2)^n} = \frac{1}{(4\pi)^{D/2}} \frac{\Gamma(n-\frac{D}{2})}{\Gamma(n)} \left(\frac{1}{m^2}\right)^{n-\frac{D}{2}} \tag{2.2}$$

This integral arises very often in loop calculations and is worth remembering.

Another property of dimensional regularization is the so called scaleless integral. These integrals are convenient because in dimensional regularization they give zero. Scaleless integrals are of the type

$$J_n = \int \frac{d^D k}{k^{2n}}. \tag{2.3}$$

A very simple and intuitive proof of this property can be seen by making the substitution $k = \mu\ell$ for some scalar μ [19].

$$\begin{aligned} J_n &= \int \frac{d^D(\mu\ell)}{(\mu\ell)^{2n}} \\ &= \mu^{D-2n} \int \frac{d^D\ell}{\ell^{2n}} \\ &= \mu^{D-2n} J_n. \end{aligned}$$

Now by requiring this to hold for all μ we have that $J_n = \pi\Omega_D \delta(n-\frac{D}{2})$. Note that when $n = \frac{D}{2}$, the integral becomes a delta function. For a more detailed analysis of this property, see [21]. For the purpose of this thesis, we will not need to worry about this special limit and will consider the integral to give zero identically. These few identities are by no means everything that comes from dimensional regularization. They will however be the most useful later on in this chapter.

Another very important tool in the calculation of higher order corrections in perturbative QFT is the optical theorem. The optical theorem states that the total cross section of a process is proportional to the imaginary part of the scattering amplitude for that process. In terms of amplitudes $\mathcal{M}$ it says,

$$\mathrm{Im}\mathcal{M}(\mathcal{A} \to \mathcal{A}) = \mathcal{C} \sum_B \int d\Pi_B |\mathcal{M}(\mathcal{A} \to \mathcal{B})|^2, \tag{2.4}$$

where $\mathcal{C}$ is a constant determined by the process being considered and the integration is over the phase space of the final state, Π_B. For a single particle decaying, $\mathcal{C} = \frac{1}{2}$. This means that, in order to calculate the second order corrections to a process like $\Gamma(b \to cW^*)$ we could instead calculate the amplitude of the second order b-quark self energy diagrams and keep only the imaginary part. To find out which contributions are included we cut the diagram in all possible ways. For example, calculating the imaginary part of the diagram in Fig. (2.1), would give the contributions from the three amplitudes corresponding to the three possible cuts in Fig. (2.2). Thus, we reduce the

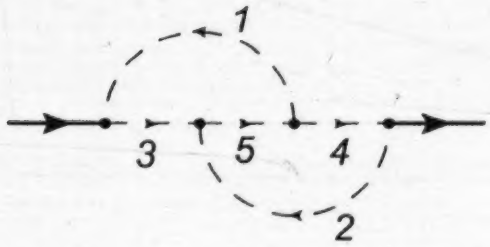

Figure 2.1: Two loop Feynman diagram.

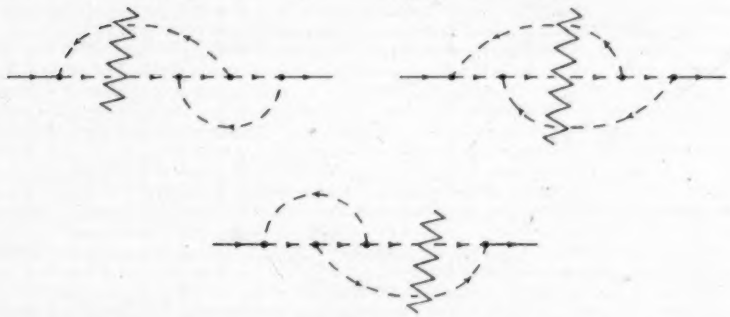

Figure 2.2: The three possible contributions that are calculated from the imaginary part of Fig. (2.1). The zig-zags represent where the diagram has been cut.

calculation of three separate contributions into one two-loop integral. Even with the symmetry considerations of the two diagrams in Fig. (2.2) with only two lines cut, this property still cuts the number of diagrams in half.

It is also important for us to know which cuts will end up having imaginary parts. This property comes from considering the optical theorem a little more closely. To make it clear let us consider an equivalent representation of the optical theorem,

$$\mathrm{Im}\mathcal{M}(\mathcal{A}\to\mathcal{A}) = C\sum_{\mathcal{B}}\int d\Pi_{\mathcal{B}}\mathcal{M}(\mathcal{A}\to\mathcal{B})\mathcal{M}^{*}(\mathcal{B}\to\mathcal{A}). \tag{2.5}$$

In this form, we can see that the only cuts that will end up having an imaginary part are those that give physically realizable processes. In the next section we will show how to reduce any multi-scale diagram to a set of single-scale diagrams. This means that the only diagrams contributing an imaginary part are those with cuts that go through massless propagators only.

The final tool we want to introduce is Feynman parameters [19]. This change of parameters is instrumental in carrying out loop integrals and will also be a useful tool when we consider eikonal integrals later in this chapter. The switch to Feynman parameters is given by

$$\frac{1}{AB} = \int_0^1 dx \frac{1}{[xA+(1-x)B]^2}. \tag{2.6}$$

A general version of the switch is also available when one needs to consider more than two factors in the denominator.

2.2 Asymptotic Expansion

The ability to calculate contributions to a process from the associated Feynman diagrams is hampered by certain problems that commonly arise. In Heavy Quark Effective Field Theory (HQET) and in particular for the decay $\Gamma(b \to cW^*)$ one runs into the problem of how to handle the different scales of the diagrams involved. One strong method that deals with this is the method of asymptotic expansion. The basic idea is to separate the integral into parts with each part contributing to a different scale. It is then possible to use one or a combination of single scale methods to compute the resulting integrals.

Let us consider the example of the diagram in Fig. (2.3). For this diagram

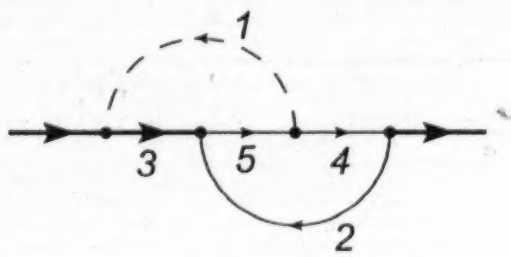

Figure 2.3: A two loop topology where the solid thin line has mass m the solid thick line has mass M and the dashed line is massless.

we define

$$[1] = (k_1 - k_2)^2,\ [2] = k_3^2 + m^2,\ [3] = (k_1 - k_3)^2 + M^2,\ [4] = k_2^2 + m^2,\ [5] = k_1^2 + m^2.$$

We then have the following integral,

$$\int \frac{d^D k_1 d^D k_3}{(k_1^2 + m^2)(k_2^2 + m^2)(k_3^2 + m^2)(k_1 - k_2)^2[(k_1 - k_3)^2 + M^2]}, \tag{2.7}$$

where, $k_2 = p_0 + k_3$. This integral has two scales, m and M, and three different momenta that can either be hard ($\sim M$) or soft ($\ll M$). The relation between k_2 and k_3 means that k_2 cannot be soft. We use this set of momenta because it will make the expansions a bit more intuitive later. Thus we have four different regions of the integral that we can consider separately. Lets start by considering the case where $|k_1|, |k_2|, |k_3|$ are all hard scale momenta. In this situation we can expand the three propagators with mass m and get

$$\sum_{n,m,l=0}^{\infty} \int \frac{d^D k_1 d^D k_3 (-m^2)^{n+m+l}}{(k_1^2)^{n+1}(k_2^2)^{m+1}(k_3^2)^{l+1}(k_1-k_2)^2[(k_1-k_3)^2+M^2]} - \tag{2.8}$$

$$\sum_{n,m,l=0}^{\infty} \int_{|k_1|,|k_3|<M} \frac{d^D k_1 d^D k_3 (-m^2)^{n+m+l}}{(k_1^2)^{n+1}(k_2^2)^{m+1}(k_3^2)^{l+1}(k_1-k_2)^2[(k_1-k_3)^2+M^2]}.$$

For now, let us consider only the second term. Since it is in the region $|k_1|, |k_3| < M$ we can also expand the last propagator to give

$$\sum_{n,m,l,j=0}^{\infty} (-1) \frac{(-m^2)^{n+m+l}}{(-M^2)^{j+1}} \int_{|k_1|,|k_3|<M} \frac{d^D k_1 d^D k_3 (k_1-k_3)^{2j}}{(k_1^2)^{m+1}(k_2^2)^{n+1}(k_3^2)^{l+1}(k_1-k_2)^2}. \tag{2.9}$$

Alone this does not seem to help at all. To evaluate this integral over the whole domain (i.e. not just in the region $|k_1|, |k_3| < M$) we need to add some parts. It can be shown [19] that these parts are scaleless integrals and thus equal zero. For simplicity, we will leave out this contribution from now on the understanding that it will not contribute to the final result.

Let us now go back and consider the eight possible regions. Taking all possible regions and carrying out the necessary expansions gives the contributions listed in Fig. (2.4). Notice that we can rule out certain regions based on the kinematics of the resulting diagram or by the optical theorem discussed earlier. The tadpoles in regions two and three indicate that the integral associated with its momentum can be separated from the rest of the integral.

With this breakup into regions, we can see how powerful asymptotic expansions are. We started out with a two loop, two scale integral and it has been reduced to three single scale integrals, two of which are one loop problems. From here it is fairly straightforward to apply one and two loop methods for single scale integrals.

2.3 Recurrence Relations

With a grasp on how to handle the multiple scales of a diagram, we are well poised to start considering how one goes about carrying out the loop integrals involved in the resulting single scale diagrams. A very well known technique involves reducing the diagram to a set of simpler so called master integrals. In recent years there have been a few attempts at finding a systematic way to carry out this reduction [18, 22, 23]. Before these, most of the work had to be carried out by hand and there was no general way to find the master integrals for a given diagram. The methods used by all of these schemes rely on recurrence relations that are found using integration by parts. In this section we will describe how recurrence relations are derived and can be used to simplify the evaluation of a diagram.

Region 1: 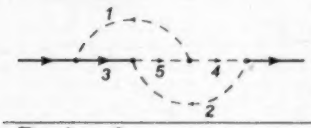	$\lvert k_1\rvert \gg m$ $\lvert k_2\rvert \gg m$ $\lvert k_3\rvert \gg m$	$[2] \to k_3^2$ $[4] \to k_2^2$ $[5] \to k_1^2$
Region 2: 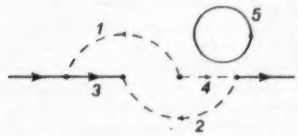	$\lvert k_1\rvert \sim m$ $\lvert k_2\rvert \gg m$ $\lvert k_3\rvert \gg m$	$[1] \to k_2^2$ $[2] \to k_3^2$ $[3] \to k_3^2 + M^2$ $[4] \to k_2^2$
Region 3: 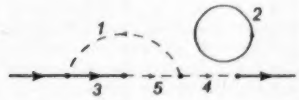	$\lvert k_1\rvert \gg m$ $\lvert k_2\rvert \gg m$ $\lvert k_3\rvert \sim m$	$[3] \to k_1^2 + M^2$ $[4] \to k_2^2$ $[5] \to k_1^2$
$\lvert k_1\rvert \sim m$ $\lvert k_2\rvert \gg m$ $\lvert k_3\rvert \sim m$	$[1] \to k_2^2$ $[3] \to M^2$ $[4] \to k_2^2$	No imaginary contributions.

Figure 2.4: The possible regions found with the method of asymptotic expansion applied to the diagram in Fig. (2.3).

Recurrence relations rely on the integration by parts identity,

$$\int \frac{\partial}{\partial(k_i)_\mu} \ell_\mu \frac{\prod_i^n [d^D k_i]}{D(k_1, k_2, \ldots, k_n, p)} = 0, \tag{2.10}$$

where $D(k_1, k_2, \ldots, p)$ is an arbitrary collection of propagators. By applying this identity for a number of momenta ℓ_μ it is possible to find some combination of these that will end up simplifying the integral to a set of well known integrals or master integrals. The question arises of whether it is possible to find an irreducible set of master integrals and if so, how to automate this procedure. The work in [18,22,23] is just a sample of the different approaches being made.

The method of how to use recurrence relations is best illustrated with an example, so let us turn back to our two loop diagram, with fermion propagators of mass M, and consider what can be done to simplify it further. We have

$$NP = \frac{1}{[1]^{a_1}[2]^{a_2}[3]^{a_3}[4]^{a_4}[5]^{a_5}}, \tag{2.11}$$

where we define

$$[1] = k_1^2,\ [2] = k_2^2,\ [3] = k_1^2 + 2k_1 \cdot p,\ [4] = k_2^2 + k_2 \cdot p,\ [5] = (k_1^2 + k_2^2) + 2(k_1 + k_2) \cdot p,$$

to make things a bit cleaner. Referring to Eq. (2.10) we see that there are six different identities we can produce by using three different momenta for ℓ_μ and two for the $(k_i)_\mu$. Let us start by applying the operator $\frac{\partial}{\partial k_2} p_\mu$ to NP to get

$$\begin{aligned} R1 &= \int [d^D k_i] \left[2(a_2 - a_4) - \frac{a_5}{[5]}([3] + 2[4] - [1] - 2[2] - 2) \right. \\ &- \left. 2a_2 \frac{[4]}{[2]} + \frac{a_4}{[4]}(2[2] + 1) \right] NP. \end{aligned} \tag{2.12}$$

where we have defined $p^2 = -1$ and rewritten scalar products in terms of the propagators. Alone, this does not help much, but if we also apply $\frac{\partial}{\partial k_2} k_{2\mu}$ we end up with another equation that will be useful,

$$R2 = \int [d^D k_i] \left[(D - 2a_2 - a_4 - a_5) - a_4 \frac{[2]}{[4]} + a_5 \frac{[3]}{[5]} \right] NP. \tag{2.13}$$

We can now combine the two of these with $R1 + 2R2$, and rearrange to give

$$\begin{aligned} \frac{1}{[4]} &= -\frac{1}{a_4} \left[(2D - 2a_2 - 4a_4 - 2a_5) - 2a_2 \frac{[4]}{[2]} \right. \\ &+ \left. \frac{a_5}{[5]} ([3] - 2[4] + [1] + 2) \right], \end{aligned} \tag{2.14}$$

where we understand that both sides are applied to the integral of NP. Now, we want to write this in the form $1 = [something]$ so that we have a relation that can be applied again and again. To do this, we need to multiply through by the propagator ($[4]$). With everything under integration though, it is not as straight forward as it seems. To get around this problem and find a recurrence relation for NP we reduce the power of the propagator ($[4]$) by one so that in Eq. (2.11) the exponent becomes $a_4 - 1$. Carrying this through the equations we have set up so far, we end up with the same relation as above except with the transformation $a_4 \to a_4 - 1$, giving

$$\begin{aligned} \int [d^D k_i] NP &= \int [d^D k_i] \frac{NP[4]}{a_4 - 1} [(2D - 4 - 2a_2 - 4a_4 - 2a_5) \\ &- 2a_2 \frac{[4]}{[2]} + \frac{a_5}{[5]}([3] - 2[4] + [1] + 2) \Big]. \end{aligned}$$

This is our recurrence relation. Notice that on the left, we have the same NP set of propagators as defined above because of the extra $\left(\frac{1}{[4]}\right)$ on the left hand side of Eq. (2.14). We can expand all of this out to create a new set of two loop integrals, however, in all of them, the power of propagator ($[4]$) will be reduced by at least one. Applying this relation recursively then, we can reduce the power of ($[4]$) to one or zero in every resulting integral leaving us with a set of one loop integrals to be calculated.

Going through and applying the other six operators will help us find other recurrence relations that are then used to reduce a diagram like NP to a set of simpler master integrals. This method is very straightforward and once these recurrence relations are found it is not difficult to implement them in a computer program that will automatically reduce the diagram to a set of known or much simpler to evaluate integrals. How exactly to evaluate these resulting integrals is well covered in the literature. For a good review of methods and tricks used to evaluate many common master integrals, see [19].

2.4 Phase Space Integrals

With the loop integrals in Feynman diagrams under control, it is now important to consider phase space integrals. These integrals come into consideration when calculating decay rates and scattering amplitudes with a final product of two or more particles. As with loop integrals, there are a few tricks we can use to aid in evaluating phase space integrals.

The phase space has a nice feature that allows one to break it up into products of smaller phase spaces so that in the end, all that is needed is the two particle phase space definition. This is done via the following relation [2]. For

$$dR_N(Q;p_1,p_2,\ldots,p_N) = (2\pi)^4\delta^4(Q-\sum_{i=1}^{N}p_i)\prod_{i=1}^{N}\frac{d^3p_i}{(2\pi)^3 2E_i}, \tag{2.15}$$

we have

$$\begin{aligned} dR_N(Q;p_1,p_2,\ldots,p_N) &= dR_{N-j+1}(Q;q,p_{j+1},\ldots,p_N)(2\pi)^3 \\ &\times\ dR_j(q;p_1,\ldots,p_j)dq^2. \end{aligned} \tag{2.16}$$

This phase space reduction formula is well known and can be a very useful tool when evaluating otherwise complicated processes [24]. In order to use this relation, we still need to know the form of the two particle phase space. Specifically we would like to know the volume of the two particle phase space.

Let us consider the process $Q \to p_1p_2$ with masses M, m_1, and m_2 respectively. The volume of the phase space is then given by

Figure 2.5: Massive two particle phase space.

$$R_2(Q;p_1,p_2) = \frac{1}{(2\pi)^{D-2}}\int\frac{d^{D-1}\mathbf{p_1}}{2E_1}\frac{d^{D-1}\mathbf{p_2}}{2E_2}\delta^D(Q-p_1-p_2). \tag{2.17}$$

The bold symbols indicate that we are working with "3-momenta" but generalized to D dimensions. We start by separating the delta function into separate energy and momentum factors. Here we are working in the rest frame of Q,

$$R_2(Q;p_1,p_2) = \int \frac{d^{D-1}\mathbf{p_1} d^{D-1}\mathbf{p_2}}{4(2\pi)^{D-2}E_1E_2}\delta(M-E_1-E_2)\delta^{D-1}(-\mathbf{p_1}-\mathbf{p_2}). \quad (2.18)$$

The second delta function can then be used to integrate over one of the momenta leaving us with a single $D-1$ dimensional integral. It is also convenient at this point to make the substitutions $E_i = \sqrt{\mathbf{p_1^2}+m_i^2}$ to give

$$\begin{aligned} R_2(Q;p_1,p_2) &= \frac{1}{4(2\pi)^{D-2}} \int \frac{d^{D-1}\mathbf{p_1}}{\sqrt{\mathbf{p_1^2}+m_1^2}\sqrt{\mathbf{p_1^2}+m_2^2}} \\ &\times \delta(M-\sqrt{\mathbf{p_1^2}+m_1^2}-\sqrt{\mathbf{p_1^2}+m_2^2}). \end{aligned} \quad (2.19)$$

In order to continue from here, we need to do two things. The first of these is the typical change of coordinates into hyper-spherical coordinates so the integral becomes an integral over the angular parts and an integral over the modulus of the momentum. The second thing we need to do is simplify the delta function so that we can properly carry out the integral. To do this second step we use the relation

$$\delta(f(x)) = \sum_i \frac{\delta(x-x_i)}{|f'(x_i)|} \quad \forall i \text{ such that } f(x_i)=0. \quad (2.20)$$

From our delta function we can see that there is one zero for $|\mathbf{p_1}|$, namely,

$$p_1' = \frac{\sqrt{[M^2-m_1^2-m_2^2]^2-4m_1^2m_2^2}}{2M}. \quad (2.21)$$

With this we can finally do the $\mathbf{p_1}$ integral with the result

$$R_2(Q;p_1,p_2) = \frac{p_1'^{D-3}}{4(2\pi)^{D-2}} \left(\frac{1}{\sqrt{p_1'^2+m_1^2}+\sqrt{p_1'^2+m_2^2}} \right) \oint d\Omega_{D-1}. \quad (2.22)$$

Finally, we plug in the angular integral from Eq. (2.1) and substitute for p_1' to give the final form of the volume of the two particle phase space,

$$R_2(Q;p_1,p_2) = \frac{2^{4-D}\pi^{3/2}M^{2-D}}{(4\pi)^{D/2}\Gamma(\frac{D-1}{2})} \left(\sqrt{[M^2-m_1^2-m_2^2]^2-4m_1^2m_2^2} \right)^{D-3}. \quad (2.23)$$

So, we have the volume of the two particle phase space. This result can then be used in conjunction with the phase space reduction formula to compute the volume of any N particle phase space.

In practice, when actually doing calculations, this becomes very handy. There are a number of tricks that allows one to get rid of the scalar products that typically show up in phase space integrals so that all that is needed in the end is the volume of the phase space.

2.5 Eikonal Integrals

Every so often when using the method of asymptotic expansion to calculate the contributions from Feynman diagrams, we run into a propagator that is of the form

$$\frac{1}{k^2 + 2k \cdot p}. \tag{2.24}$$

In the region where $|k| < |p|$ this is expanded in a Taylor series and all we are left with in the denominator is the scalar product. Such propagators are referred to as eikonal propagators. Typically when carrying out phase space integrals, the small imaginary part of each propagator can be ignored. With eikonal propagators though, these terms are important and must be accounted for. As an example we consider the following Feynman diagram,

Figure 2.6: In the region where $|p_1|, |p_9| < |p|$ this diagram has propagators that lead to eikonal integrals. The solid, dashed and dotted lines represent particles with mass M, m, and 0 respectively. For this calculation, we have cut the diagram through propagators $9, 3$ and 6.

For this diagram, it can be shown that after expanding all propagators, one ends up with only two possibilities,

$$I_{\pm} = \int \frac{d^D p_1}{p_1^2 (2p \cdot p_1 \pm 2p \cdot p_9 + i0)^n}. \tag{2.25}$$

We will start by considering the combination of propagators ([11]) and ([1 − 9]) to show the difference between this and the combination of ([5]) and ([1 − 9]).

2.5.1 Expansions and Preparation

To begin we introduce $Q = p_6 + p_3$ and $W_\perp$ such that $p_3 = Q/2 - W_\perp$ and $|W_\perp| < |p|$. Using the properties $p_9^2 = 0$, $p_3^2 = m^2$ and $p^2 = M^2$, we can expand the propagators labeled ([5], [4], [11]). We do the expansion in the region where both p_1 and p_9 are small compared to p and Q. For the propagator ([4]) we get

$$\begin{aligned} \frac{1}{p_4^2 - m^2 + i0} &= \frac{1}{Q \cdot p_1 + (p_1^2 - 2W_\perp \cdot p_1) + i0} \\ &= \frac{1}{Q \cdot p_1 + i0} + \frac{p_1^2 - 2W_\perp \cdot p_1}{(Q \cdot p_1 + i0)^2} + \ldots . \end{aligned} \tag{2.26}$$

Propagators ([5]) and ([11]) are expanded similarly, and both give

$$\frac{1}{p_{11,5}^2-(m,M)^2+i0} \to \frac{C}{(2p\cdot p_1-2p\cdot p_9+i0)}+\ldots, \tag{2.27}$$

with some constant C depending on which propagator is being expanded.

Effectively we are left with six cases. To make writing everything easier we will drop the $i0$ dependence as it does not play a role in this part. we will introduce it back in later, when it is needed.

$$J_1 = \frac{1}{[p_1^2]^m}\frac{1}{(2Q\cdot p_1-2Q\cdot p_9)^n} \tag{2.28}$$

$$J_2 = \frac{1}{[p_1^2(p_1-p_9)^2]^m}\frac{1}{(2Q\cdot p_1-2Q\cdot p_9)^n} \tag{2.29}$$

$$J_3 = \frac{1}{[(p_1-p_9)^2]^m}\frac{1}{(2Q\cdot p_1)^n} \tag{2.30}$$

$$J_4 = \frac{1}{[p_1^2(p_1-p_9)^2]^m}\frac{1}{(2Q\cdot p_1)^n} \tag{2.31}$$

$$J_5 = \frac{1}{[p_1^2]^m}\frac{1}{(2Q\cdot p_1)^n} \tag{2.32}$$

$$J_6 = \frac{1}{[(p_1-p_9)^2]^m}\frac{1}{(2Q\cdot p_1-2Q\cdot p_9)^n}. \tag{2.33}$$

Note that J_5 and J_6 lead to scaleless integrals in dimensional regularization and give zero contribution. We notice that J_1 is in the form of I_- given earlier so we will leave it alone for now. Looking at J_3 we immediately see that making the transformation $p_1 \to p_1+p_9$ gives an integral of the form I_+. J_2 and J_4, however require a little bit more work. Starting with J_4 we apply Feynman parameters, Eq. (2.6), to the first term to get

$$J_4 = \int_0^1 \frac{dx}{[p_1^2(1-x)+(p_1^2-2p_1\cdot p_9+p_9^2)x]^{2m}}\frac{1}{(2Q\cdot p_1)^n}. \tag{2.34}$$

Expanding inside the brackets and completing the square gives

$$\begin{aligned} J_4 &= \int_0^1 \frac{dx}{[(p_1-p_9x)^2+p_9^2x(1-x)]^{2m}}\frac{1}{(2Q\cdot p_1)^n} \\ &= \int_0^1 \frac{dx}{[(p_1-p_9x)^2]^{2m}}\frac{1}{(2Q\cdot p_1)^n}, \end{aligned} \tag{2.35}$$

where we have used the fact that $p_9^2=0$ to get rid of that term. Now we are in a position to shift $p_1 \to p_1+p_9x$, and right after this make another transformation $p_1 \to p_1x$. This introduces an extra factor of x^D from the Jacobian in the p_1 phase space integral. We end up with

$$\begin{aligned} J_4 &= \int_0^1 \frac{dx}{[(p_1)^2]^{2m}}\frac{1}{(2Q\cdot p_1+2Q\cdot p_9x)^n} \\ &= \int_0^1 dx\frac{x^D}{[(p_1)^2]^2x^{4m}}\frac{1}{(2Q\cdot p_1+2Q\cdot p_9)^n x^n}. \end{aligned} \tag{2.36}$$

Setting $D = 4 - 2\epsilon$ and taking extra terms out of the integral, we get

$$J_4 = \frac{1}{[(p_1)^2]^{2m}(2Q\cdot p_1 + 2Q\cdot p_9)^n}\int_0^1 dx\, x^{4-4m-n-2\epsilon}, \tag{2.37}$$

which can easily be integrated and the propagators are left in the form of I_+ after one more step to reduce the power of p_1.

The same steps can be applied to J_2 except this time using $p_1 \to p_1(1-x)$ instead of $p_1 \to p_1 x$. This gives a beta function for the solution of the x-integral and leaves the propagators in the form of I_-,

$$J_2 = \frac{1}{[(p_1)^2]^{2m}(2Q\cdot p_1 - 2Q\cdot p_9)^n}\int_0^1 dx\, x^{(4m+1)-1}(1-x)^{(5+n-2\epsilon)-1}. \tag{2.38}$$

The final thing we need to do before carrying out the p_1 phase space integral is to reduce the powers of p_1 that appear to one. To do this we use the integration by parts identity that we used earlier in deriving the recurrence relations

$$0 = \int \frac{\partial}{\partial p_1^\mu}\frac{Q^\mu}{p_1^2(2Q\cdot p_1 \pm 2Q\cdot p_9)^a(2Q\cdot p_1)}. \tag{2.39}$$

Applying the partial derivative yields

$$\begin{aligned} 0 \;=\; & -\int \frac{1}{p_1^4(2Q\cdot p_1 \pm 2Q\cdot p_9)^a} - \int \frac{2aQ^2}{p_1^2(2Q\cdot p_1 \pm 2Q\cdot p_9)^{a+1}(2Q\cdot p_1)} \\ & -\int \frac{2Q^2}{p_1^2(2Q\cdot p_1 \pm 2Q\cdot p_9)^a(2Q\cdot p_1)^2}, \end{aligned} \tag{2.40}$$

or

$$\begin{aligned} \int \frac{1}{[p_1^2]^2(2Q\cdot p_1 \pm 2Q\cdot p_9)^a} \;=\; & -\int \frac{2aQ^2}{p_1^2(2Q\cdot p_1 \pm 2Q\cdot p_9)^{a+1}(2Q\cdot p_1)} \\ & -\int \frac{2Q^2}{p_1^2(2Q\cdot p_1 \pm 2Q\cdot p_9)^a(2Q\cdot p_1)^2}. \end{aligned} \tag{2.41}$$

Applying this repeatedly will end up giving integrals with only single powers of p_1^2 as in I_- and I_+. To deal with the new $2Q\cdot p_1$ factors that arise, we can simply use partial fractions with $(2Q\cdot p_1 \pm 2Q\cdot p_9)$ to separate the terms. Again, all resulting integrals with $2Q\cdot p_1$ are scaleless integrals because of the p_1^2, and thus do not contribute. In the end, we are left with just two eikonal integrals that must be done,

$$I_\pm = \int \frac{d^D p_1}{p_1^2(2Q\cdot p_1 \pm 2Q\cdot p_9)^n}. \tag{2.42}$$

2.5.2 The Eikonal Integrals

We have finally simplified the propagators of the diagram in Fig. (2.6) to two eikonal forms. Now we want to carry out the phase space integral so that we

can get our final result. We start by using a substitution akin to Feynman parameters [25],

$$\frac{1}{A^\alpha C^\beta} = \frac{1}{\beta(\alpha,\beta)} \int_0^\infty d\lambda \frac{\lambda^{\beta-1}}{[A + C\lambda]^{\alpha+\beta}}. \tag{2.43}$$

Applying this to $I_\pm$ gives

$$I_\pm = \frac{1}{\beta(1,n)} \int d^D p_1 \int_0^\infty d\lambda \frac{\lambda^{n-1}}{[p_1^2 + 2\lambda Q \cdot p_1 \pm 2\lambda Q \cdot p_9]^{n+1}}. \tag{2.44}$$

Now adding and subtracting $Q^2\lambda^2$ in the denominator allows us to collect all p_1 terms in a square. Then we shift p_1 to $p_1 - Q\lambda$ and make a Wick rotation to simplify the expression a bit,

$$\begin{aligned} I_\pm &= n \int d^D p_1 \int_0^\infty d\lambda \frac{\lambda^{n-1}}{[(p_1 + Q\lambda)^2 - Q^2\lambda^2 \pm 2\lambda Q \cdot p_9]^{n+1}} \\ &= i(-1)^{n+1} n \int d^D p_1 \int_0^\infty d\lambda \frac{\lambda^{n-1}}{[p_1^2 + Q^2\lambda^2 \mp 2\lambda Q \cdot p_9]^{n+1}}. \end{aligned} \tag{2.45}$$

Switching the order of integration now leads to a well known integral in dimensional regularization, so it can easily be done, leaving us with only the parameter to integrate. Simplifying the result and making the change of variables $\lambda \to \lambda \frac{2Q\cdot p_9}{Q^2}$, leaves us with a common integral. We end up with

$$\begin{aligned} I_\pm &= i\pi^{\frac{D}{2}} (-1)^{n+1} \frac{\Gamma(n+1-\frac{D}{2})}{\Gamma(n)} \left(\frac{2Q\cdot p_9}{Q^2}\right)^{\frac{D}{2}-1} (2Q\cdot p_9)^{\frac{D}{2}-n-1} \\ &\times \int_0^\infty \lambda^{\frac{D}{2}-2} (\lambda \mp 1)^{\frac{D}{2}-n-1} d\lambda. \end{aligned} \tag{2.46}$$

At this point we must consider the two integrals individually. This is because of the possibility of a singularity at $\lambda = 1$ in the case of I_+. We first consider the simpler case I_- and notice that it just gives a beta function. So we have

$$\begin{aligned} I_- &= i\pi^{\frac{D}{2}} (-1)^{n+1} \frac{\Gamma(n+1-\frac{D}{2})}{\Gamma(n)} \left(\frac{2Q\cdot p_9}{Q^2}\right)^{\frac{D}{2}-1} (2Q\cdot p_9)^{\frac{D}{2}-n-1} \\ &\times \beta\left(\frac{D}{2} - 1, 2 + n - D\right). \end{aligned} \tag{2.47}$$

In the case of I_+ we need to separate the integral into two parts: $\lambda \in (0,1)$ and $\lambda \in (1,\infty)$ and bring back the factor of $i0$ that we have been leaving out. Including this factor gives

$$I_+^{(0,1)} = \int_0^1 \lambda^{\frac{D}{2}-2} (\lambda - 1 \pm i0)^{\frac{D}{2}-n-1} d\lambda \tag{2.48}$$

$$= \int_0^1 \lambda^{\frac{D}{2}-2} [(1-\lambda) e^{\pm i\pi}]^{\frac{D}{2}-n-1} d\lambda \tag{2.49}$$

$$= e^{\pm i\pi(\frac{D}{2}-n-1)} \beta\left(\frac{D}{2} - 1, \frac{D}{2} - n\right). \tag{2.50}$$

Note that this has an imaginary part. We can choose to keep this term or take the real part of it because of the fact that the imaginary part will be cancelled by other cuts that contribute.

Now we have to treat the other part,

$$I_+^{(1,\infty)} = \int_1^\infty \lambda^{\frac{D}{2}-2}(\lambda-1)^{\frac{D}{2}-n-1}d\lambda. \tag{2.51}$$

To do this integral we make a change of variables to $u = \frac{1}{\lambda}$ to transform the integral to a familiar form,

$$\begin{aligned} I_+^{(1,\infty)} &= \int_0^1 u^{2-\frac{D}{2}}\left(\frac{1}{u}-1\right)^{\frac{D}{2}-n-1}\frac{du}{u^2} && (2.52)\\ &= \int_0^1 u^{n+1-D}(1-u)^{\frac{D}{2}-n-1} && (2.53)\\ &= \beta\left(2+n-D, \frac{D}{2}-n\right). && (2.54) \end{aligned}$$

The final result for I_+ is then the sum of the two parts and we end up with

$$\begin{aligned} I_+ &= i\pi^{\frac{D}{2}}(-1)^{n+1}\frac{\Gamma(n+1-\frac{D}{2})}{\Gamma(n)}\left(\frac{2Q\cdot p_9}{Q^2}\right)^{\frac{D}{2}-1}(2Q\cdot p_9)^{\frac{D}{2}-n-1}\times \\ &\left[e^{\pm i\pi\left(\frac{D}{2}-n-1\right)}\beta\left(\frac{D}{2}-1, \frac{D}{2}-n\right)+\beta\left(2+n-D, \frac{D}{2}-n\right)\right] \end{aligned} \tag{2.55}$$

In this result, the sign of $e^{\pm i\pi}$ is determined by the sign of the $i0$ term so it is important to keep track of this.

2.6 Relations Between Diagrams

Today computers play a pivotal role in our ability to compute higher order corrections to processes in perturbative QFT. They give us the benefit of the speed at which such calculations can be carried out. There is, however, a prominent bottleneck that can greatly lengthen the time it takes to complete a full calculation. Many of the calculations that need to be done require programs to be written that will carry out the expansions, reductions, and integrals needed. Along with creating these programs come the inevitable bugs. These bugs, sometimes as small as a missed two or a sign error, can take an incredible amount of time to find and fix.

Fortunately there are some useful tricks one can use quickly to check the consistency of results for small groups of diagrams and quickly isolate any bugs that are present. In HQET, certain relations between diagrams can be used to check (at least) the leading order terms and often highlight any problems encountered. One of these properties, gauge independence, is at the center of QFT and is often used to simplify calculations. The other is based on the expansions used in HQET and relates the leading order of different diagrams.

2.6.1 Gauge Independence

Gauge independence is a vital part of field theory. This is a useful property in that it can greatly simplify calculations by proper choice of gauge. Indeed, when calculations are done, they are typically done in a pre-defined gauge instead of a general one. It may however also be useful to use a general gauge to check the gauge invariance of a group of diagrams. Gauge invariance requires that all gauge dependent terms of diagrams contributing to a physical process sum up to zero. For higher order calculations like $\mathcal{O}(\alpha_s^2)$ corrections to $b \to cW^*$, this requires cancellations in 73 separate amplitudes. With no other requirements, it would be next to impossible to find out which terms are not contributing properly by looking at the gauge dependent parts. It would make things much easier if it were possible to group the diagrams into separately gauge invariant parts. This way, one would only need to consider a few gauge dependent terms when looking for errors making this an effective check for debugging purposes. There are two ways that we can achieve this grouping: separate by colour factors and separate by number of loops. Here, we will consider only the gauge dependence of gluon propagators.

Property Groups

One helpful property of perturbative QCD is that the colour tensor structure appearing in diagram amplitudes can be separated leaving us with a colour factor multiplied by a colourless amplitude. It is then possible to separate the diagrams into groups that each have the same colour factor in such a way that the colour factors are all independent. The colourless amplitudes are then known to obey certain properties [26], one of which is gauge invariance. One such separation is into the commonly used Abelian, Non-Abelian, Heavy Quark Loop and Light Quark Loop colour groups; C_F^2, $C_F\left(C_F - \frac{C_A}{2}\right)$, $T_R N_H$ and $T_R N_L$ respectively. N_H and N_L refer to the number of heavy and light quarks, respectively, in the HQET being used. This separation nicely leads to four different gauge invariant subgroups. In the example of $b \to cW^*$ decay, we now have the groups in Tab. (2.1). There is, however another association

Colour Factor	C_F^2	$C_F\left(C_F - \frac{C_A}{2}\right)$	$T_R N_H$	$T_R N_L$
# of Diagrams	45	43	6	8

Table 2.1: The colour grouping of gauge invariance. Note that there is overlapping between the groups because of renormalization diagrams that contribute to all four groups.

we can use to separate the groups even more.

Another independent set of colour tensors involves the terms C_F^2 and $C_F C_A$ separately. These two groups must also be separately gauge invariant. From our original groupings, we see that there is a set of diagrams that will contribute to both C_F^2 and $C_F C_A$. This means that, if one already knows that the

abelian group is gauge invariant, you know that those diagrams contributing $C_F\left(C_F - \frac{C_A}{2}\right)$ have the proper gauge dependence because they contribute to the gauge independent abelian group. Now, the only diagrams that need to be checked are those contributing an independent $C_F C_A$ factor. This reasoning also works the other way around when the non-abelian part is gauge invariant and the abelian part has some problematic terms.

The grouping in Tab. (2.1) is useful if the problem ends up being in either of the quark loop groups, but it does not help too much with the other two groups. The colour groups, however, are not all we can do to simplify gauge dependence.

Another way to separate gauge invariant groups is to consider the number of external gluons, or equivalently, the number of loops. Each group of diagrams with the same number of external gluons should be gauge invariant. When we combine this requirement with the colour factor requirement from above, we get the groups show in Tab. (2.2)

Colour Factor	C_F^2			$C_F\left(C_F - \frac{C_A}{2}\right)$			$T_R N_H$			$T_R N_L$		
External Gluons	0	1	2	0	1	2	0	1	2	0	1	2
Diagrams	10	23	12	11	17	15	3	3	0	5	3	0

Table 2.2: The colour grouping of gauge invariance. Note that there is overlapping between the groups because of renormalization diagrams that contribute to all four groups.

We can see that we have greatly simplified the task by reducing the greatest number of diagrams that need to be considered to 23. On top of that, the two quark loop subsets have a sufficiently small number of diagrams to be able to stop here and compare. For the other two subsets though, we still have too many diagrams. This grouping will be very useful in the next section where we will visually compare diagrams to find even smaller gauge invariant groups.

Comparing Diagrammatically

In 1996 some work was done on what gauge transformations look like diagrammatically in order to create an easy and systematic way of finding gauge invariant subsets of diagrams and to develop specific gauges that would simplify the calculations in each of these subsets [27]. Here we would like to develop something similar, but instead of looking for gauges to simplify the calculations we want to find the relations between diagrams that will cause the gauge dependent parts to cancel. For a general gauge the gluon propagator is given by

$$\frac{i}{k^2}\left(-g^{\mu\nu} + \xi\frac{k^\mu k^\nu}{k^2}\right). \tag{2.56}$$

Here, we have already factored out the colour dependence in accordance with the previous section and instead of the typical gauge dependence of $(1-\xi)$ we

simply use ξ. This makes the notation a bit simpler and will not affect the end result.

To check gauge independence we use the Ward identity. It says that for a process $M(k)$ involving an external photon (gluon) with polarization $\epsilon_\mu(k)$ we have

$$M^\mu(k)k_\mu = 0, \tag{2.57}$$

where $M(k) = M^\mu(k)\epsilon_\mu(k)$. Let us consider the diagram in Fig. (2.7). Applying

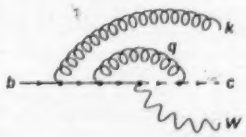

Figure 2.7: Diagram with an external gluon from a b-quark line.

Feynman rules and factoring out the colour dependence gives

$$\begin{aligned} M_1^\rho(k)k_\rho &= \frac{iQ^3}{q^2}\left[\overline{u}(c)\gamma^\mu \frac{1}{\hat{q}+\hat{c}-m}\Gamma^W \right. \\ &\times \left. \frac{1}{\hat{b}+\hat{q}-\hat{k}-M}\gamma^\nu \frac{1}{\hat{b}-\hat{k}-M}\gamma^\rho u(b)\right]\left[-g_{\mu\nu}+\xi\frac{q_\mu q_\nu}{q^2}\right]k_\rho. \end{aligned} \tag{2.58}$$

Since we are only interested in the gauge dependent term, we can forget about the term from $-g_{\mu\nu}$ and concentrate on the rest. Here, we have grouped the outgoing W and the associated vertex dependence into the term Γ^W for simplicity.

Now, instead of simply writing $\hat{q} = \gamma^\nu q_\nu$ for the momenta contracted with associated gamma matrices, we will add a fat zero that will make some convenient cancellations,

$$\begin{aligned} &= \frac{i\xi Q^2}{(q^2)^2}\left[\overline{u}(c)\frac{(\hat{q}+\hat{c}-m)-(\hat{c}-m)}{\hat{q}+\hat{c}-m}\Gamma^W \right. \\ &\times \left. \frac{(\hat{b}+\hat{q}-\hat{k}-M)-(\hat{b}-\hat{k}-M)}{(\hat{b}+\hat{q}-\hat{k}-M)(\hat{b}-\hat{k}-M)}\hat{k}u(b)\right]. \end{aligned} \tag{2.59}$$

We notice right away that these added zeros simplify the expression quite a bit. In the case of the c-quark propagator we have two terms: one that cancels the propagator and another that, combined with the associated wave function, simply gives zero according to the Dirac equation. The term associated with the b-quark is not as nice but still simplifies the result by cancelling one or the other b-quark propagators. Looking at the resulting propagators, we can picture this process in the following steps.

In the first step, notice that the diagram on the right gives zero. This corresponds to the zero from the Dirac equation.

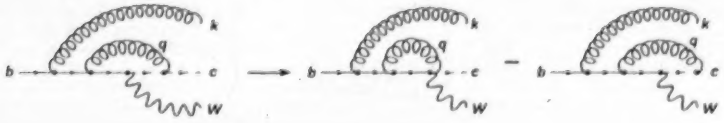

Figure 2.8: Step 1: cancellations at the c-quark end.

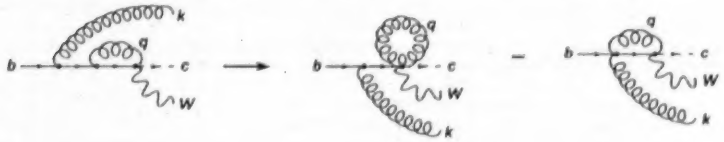

Figure 2.9: Step 2: cancellations at the b-quark end.

In essence the extra momenta terms, q_μ and k_ρ in this case, give a sum of diagrams where one of the propagators attached to their associated vertex is cancelled. We end up with the equation

$$M_1^\rho(k)k_\rho = \frac{i\xi Q^2}{(q^2)^2}\left[\overline{u}(c)\Gamma^W\left(\frac{1}{\hat{b}-\hat{k}-M} - \frac{1}{\hat{b}+\hat{q}-\hat{k}-M}\right)\hat{k}u(b)\right]. \quad (2.60)$$

The final simplification we can make is in the first term. Since this term does not involve the loop momentum q at all, we are left with a scaleless integral which gives zero in dimensional regularization. In the end, we are left with only one contribution, given by

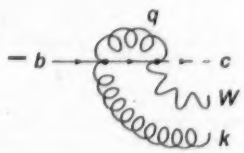

Figure 2.10: The gauge dependent part from the contraction of Fig. (2.7) with k_ρ.

From this example, we can create a rule for dealing with quark gluon vertices:

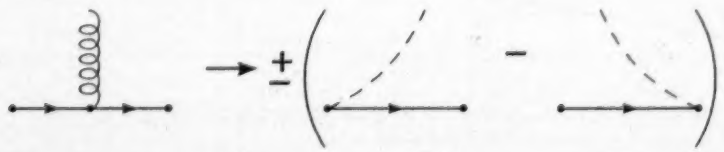

Figure 2.11: Rule for finding the gauge dependent part of a diagram involving a quark-gluon vertex.

The $\pm$ is determined by looking at the quark propagators involved. If they are the same flavour as the incoming quark it is a $-$ and if they are the same flavour as the outgoing quark it is a $+$.

Similar to this we also need a rule for dealing with triple gluon vertices. We start with a three gluon vertex where two of the gluons are propagators, Fig. (2.12). We apply the Feynman rules to the gluon propagator and the

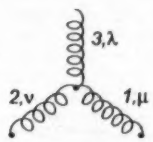

Figure 2.12: A three gluon vertex with one of the gluons being emitted. The momentum of the gluon 1 is into the vertex and the momentum of the other two is out of the vertex.

vertex to get

$$\begin{aligned} G_3 &= -\frac{Q}{k_1^2 k_2^2}\left(-g^{\mu\rho}+\xi\frac{k_1^\mu k_1^\rho}{k_1^2}\right)\left(-g^{\nu\sigma}+\xi\frac{k_2^\nu k_2^\sigma}{k_2^2}\right) \\ &\times \left[g_{\mu\nu}(k_1+k_2)_\lambda + g_{\nu\lambda}(k_3-k_2)_\mu - g_{\lambda\mu}(k_1+k_3)_\nu\right] k_3^\lambda. \end{aligned} \tag{2.61}$$

Expanding this and keeping only the gauge dependent part ends up simplifying to

$$G_3 = -Q\xi\left[\frac{1}{k_1^2}\frac{k_1^\rho k_1^\sigma}{k_1^2} - \frac{1}{k_2^2}\frac{k_2^\rho k_2^\sigma}{k_2^2} - \frac{k_1^\rho k_2^\sigma (k_1\cdot k_2)}{k_1^2 k_2^2}\left(\frac{1}{k_1^2}-\frac{1}{k_2^2}\right)\right]. \tag{2.62}$$

Notice, the first term in this equation is exactly the gauge dependent term from the previous diagram except with opposite sign. The second term will end up matching with another diagram with the external gluon coming from a c-quark line. The last term, however is a bit more complicated but is easy to deal with given the quark-quark-gluon rule from before. It ends up giving a scaleless integral in dimensional regularization and thus does not contribute to the result. Let's rewrite this result a bit more suggestively by using the momentum relationships between the three momenta,

$$G_3 = -Q\xi\left[\frac{1}{k_1^2}\frac{k_1^\rho k_3^\sigma}{k_1^2} + \frac{1}{k_2^2}\frac{k_2^\sigma k_3^\rho}{k_2^2} + \frac{k_1^\rho k_2^\sigma (k_1\cdot k_2)}{k_1^2 k_2^2}\left(\frac{1}{k_1^2}-\frac{1}{k_2^2}\right)\right]. \tag{2.63}$$

We can now see that, in the first term, the k_1^ρ will act to cancel either the propagator on the left or the one on the right and the k_3 is associated with the outgoing gluon. A similar thing happens in the second term. The final term corresponds to something similar to the scaleless integral found before. Diagrammatically, we have the situation

Let us now apply these rules to two more diagrams in order to find something that will completely cancel the gauge dependent part in Fig. (2.10). First we consider the diagram in Fig. (2.14). Applying the quark-gluon rule to this diagram we see that we have a diagram similar to that of Fig. (2.10) except with a c-quark propagator and opposite sign.

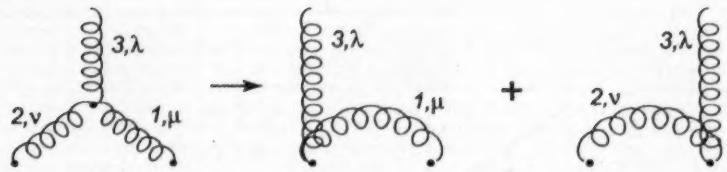

Figure 2.13: The gauge dependent part from a triple gluon vertex.

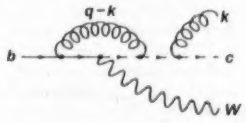

Figure 2.14: Diagram with an external gluon from a c-quark line.

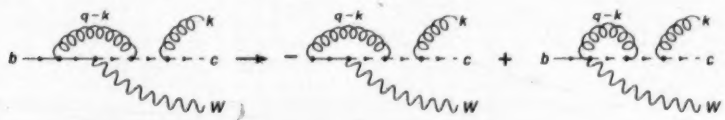

Figure 2.15: Cancel either b-quark lines.

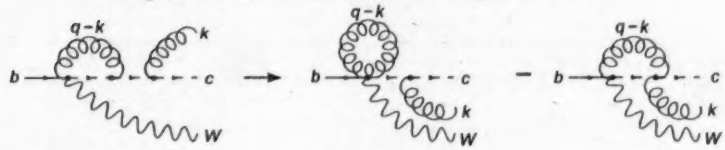

Figure 2.16: Cancel either c-quark lines.

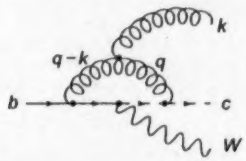

Figure 2.17: Diagram with an external gluon from a gluon line.

The last diagram we need to consider is one with a three gluon vertex Fig. (2.17). There is an important distinction that must be made here before we proceed. In general, it doesn't matter in what order you apply the above rules to a diagram like this. We must, however, make note of a few important details. When treating a three gluon vertex, we are effectively taking into account two gluon propagators at the same time. The sum of the two diagrams effectively comes from the separate treatment of one propagator and then the other. In Fig. (2.13) the first diagram comes from the effect that propagator 1 has on the diagram and the second one is the result of propagator 2.

On the other hand, when treating a quark gluon vertex, the sum of diagrams comes from the treatment of a single gluon propagator and its effect

on the two quark lines attached to it. These two sums are different in nature and this must be remembered when applying the rules. The best way to stay out of trouble when using these rules is to apply them to one propagator at a time. The following will illustrate this subtlety.

We start by applying the quark gluon rule to the propagator with momentum q. After being applied, it can be seen that there is only one non-zero contribution from the cancellation of the c-quark propagator. We then apply the three gluon rule but only the q propagator part of the rule. This is because, the rest of the rule only affects a diagram where the q propagator has not been modified.

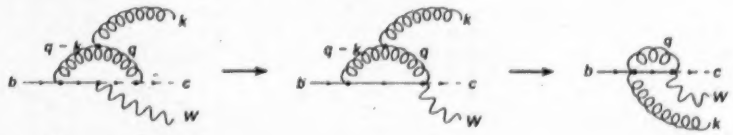

Figure 2.18: After applying the quark gluon vertex rule and three gluon rule to propagator q.

Next we add to this the result from treating the $q - k$ propagator.

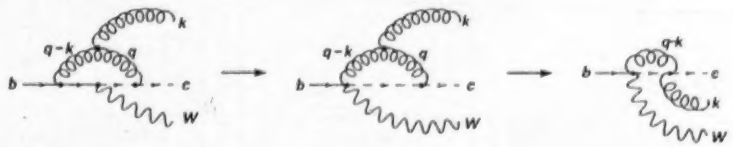

Figure 2.19: The result from applying the rules to propagator $q - k$.

Finally, all we need to do is add these two diagrams to obtain the gauge dependent part of Fig. (2.17). Comparing this result with the other two above, we see that the sum of the gauge dependent parts of the three diagrams do indeed cancel. This can be confirmed by working through the tedious calculations to arrive at a result that only involves scaleless integrals and is thus zero.

Another way we can confirm our above method is by applying the rules to Fig. (2.17) in the opposite order. We start by applying the three gluon rule to the main diagram Fig. (2.20).

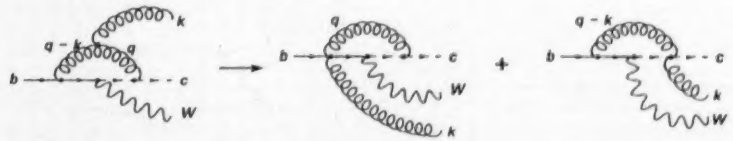

Figure 2.20: After applying the three gluon rule there are two diagrams that have a gauge dependence.

Now we can apply the quark gluon rule to each diagram. Notice that each diagram will only need one application of the rule on the vertex that is purely a quark gluon vertex. The other vertex (attached to the outgoing gluon) has just been dealt with. Applying the rule and getting rid of the scaleless parts, we arrive at our result that confirms the previous method.

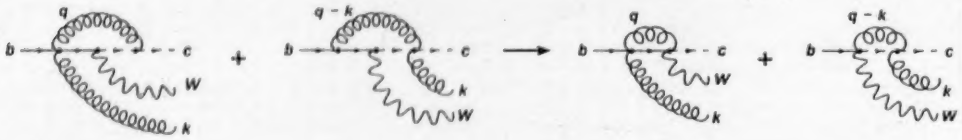

Figure 2.21: Applying the quark gluon rule to each resulting diagram confirms our above method.

In the end, we have developed a fast and easy method to look visually for gauge independent subsets of a complete calculation. This method enables us to check for errors in our method of calculation simply by computing the expansions of select diagrams in perturbative QFT instead of re-calculating the complete set of diagrams and hoping for the best. Combining the two methods of finding gauge independent groups makes for a fast and efficient method of isolating the error so that bugs can easily be found.

2.6.2 Vertex Switching

Vertex switching is based on a simple mathematical trick to find relations between the leading order terms of two similar diagrams. The method is very basic. Starting with the expression derived from the Feynman rules for the diagram, simplify the expression keeping only leading order terms. Once this has been simplified compare this to a similar expression from the second diagram. One should have similar expressions that differ only by a constant factor so that their leading terms can be easily compared.

Simple Example

Here we will outline the procedure with a simple example. We start by writing out the expression from the Feynman rules for the diagrams we are interested in.

For both diagrams we assume that the gluon is created at threshold so that the momentum k_1 is small compared to both b and c.

For the diagram in Fig. (2.22) we have

$$\langle 1| = \bar{u}(c)\gamma^{\mu}\frac{\hat{c}+\hat{k}_1+m_c}{(c+k_1)^2-m_c^2}u(b), \tag{2.64}$$

where $\hat{p} = p_{\nu}\gamma^{\nu}$. Now we expand the denominator and use the Dirac equation

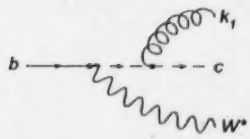

Figure 2.22: Diagram with a c-quark propagator.

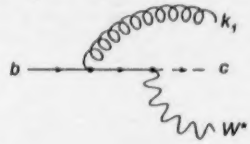

Figure 2.23: Diagram with a b-quark propagator.

$\bar{u}(c)(\hat{c} - m_c) = 0$ to simplify

$$\langle 1| = \bar{u}(c)\gamma^\mu \frac{\hat{k}_1 + 2\hat{c}}{2c \cdot k_1 + k_1^2} u(b). \tag{2.65}$$

Now we can use the assumption that k_1 is small and drop both the $\hat{k}_1$ and k_1^2 terms. In reality what we do is Taylor expand the denominator around k_1^2 with the leading term being $\frac{1}{2c \cdot k_1}$. We end up with

$$\langle 1| = \bar{u}(c) \frac{c^\mu}{c \cdot k_1} u(b). \tag{2.66}$$

The last step makes use of the fact that we are doing a threshold calculation. In this case, we can say that to leading order the c-quark is produced at rest and its momentum is parallel to the b-quark. This leads to the relations

$$b^\mu = m_b \begin{pmatrix} 1 \\ 0 \\ 0 \\ 0 \end{pmatrix} = m_b \vec{R} \qquad \text{and} \qquad c^\mu = m_c \begin{pmatrix} 1 \\ 0 \\ 0 \\ 0 \end{pmatrix} = m_c \vec{R}. \tag{2.67}$$

So we end up with the leading order of Fig (2.22) being

$$\langle 1| = \bar{u}(c) \frac{R^\mu}{R \cdot k_1} u(b). \tag{2.68}$$

Going through the same procedure for the second diagram, Fig (2.23), we see that the only thing that changes is the sign of the scalar product in the denominator. This gives

$$\langle 2| = -\bar{u}(c) \frac{R^\mu}{R \cdot k_1} u(b). \tag{2.69}$$

We have now shown that any two diagrams that differ only by moving the gluon vertex to the opposite side of the virtual W vertex only have a difference

in sign in the leading order. This relation between the two diagrams is very easy to check as it only needs a leading order calculation and can be very useful to quickly discover errors in an expansion.

From this simple example, it would be nice if we could generalize it and say that moving any outgoing gluon vertex across the virtual W vertex results in a change of sign. Unfortunately it is not quite that simple as will be shown in the next section.

Complicated Example

The case of one outgoing gluon gives a nice introduction to this procedure, but what if there is more than one? In this case, the relations are not quite so easy to see. For example, consider what happens if we add another outgoing gluon to the diagrams in Fig (2.22) and Fig (2.23).

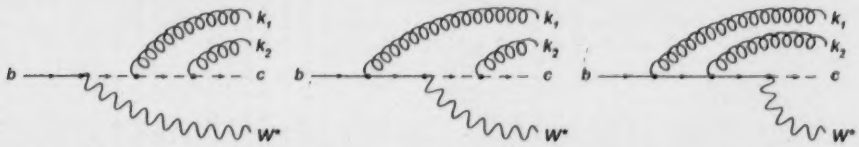

Figure 2.24: The three possible diagrams with two outgoing gluons that originate on the fermion line

Now we have two propagators and two outgoing gluon momenta to consider. Same as we did with the one gluon case, we will consider the gluon momenta to be small such that the c-quark is produced at threshold. First we will consider the middle diagram with one gluon on either side of the W. This diagram is not as complicated because the b-propagator is only associated with one gluon momentum and the c-propagator with the other. In this case, each propagator can be treated completely analogously to the one gluon case,

$$\langle g2| = \bar{u}(c)\gamma^{\mu}\frac{\hat{c}+\hat{k}_2+m_c}{(c+k_2)^2-m_c^2}\frac{\hat{b}-\hat{k}_1+m_b}{(b-k_1)^2-m_b^2}\gamma^{\nu}u(b). \tag{2.70}$$

Simplifying this leads to

$$\langle g2| = -\bar{u}(c)\frac{R^{\mu}}{R\cdot k_2}\frac{R^{\nu}}{R\cdot k_1}u(b). \tag{2.71}$$

The other two diagrams however are not quite as simple. This is because of the fact that the c and b-propagators are now associated with both gluon momenta. Still following the same procedure outlined above, we compute the first order for the diagram with the c-quark propagators,

$$\langle g1| = \bar{u}(c)\gamma^{\mu}\frac{\hat{c}+\hat{k}_2+m_c}{(c+k_2)^2-m_c^2}\gamma^{\nu}\frac{\hat{c}+\hat{k}_1+\hat{k}_2+m_c}{(c+k_1+k_2)^2-m_c^2}u(b). \tag{2.72}$$

The first term is easy enough to deal with and we can write the leading order right away as

$$\langle g1| = \bar{u}(c)\frac{R^\mu}{R\cdot k_2}\gamma^\nu\frac{\hat{c}+\hat{k}_1+\hat{k}_2+m_c}{(c+k_1+k_2)^2-m_c^2}u(b). \tag{2.73}$$

It is the second term that gives us a problem however. Using the same procedure we get

$$\langle g1| = \bar{u}(c)\frac{R^\mu}{R\cdot k_2}\frac{R^\nu}{R\cdot(k_1+k_2)}u(b). \tag{2.74}$$

Ideally we would want to simplify this to something that looks like the second term in $\langle g2|$. Unfortunately, with just this there is no hope. However, we still have to calculate the contribution from the final diagram. Looking at this and working through the calculation we see that

$$\langle g3| = \bar{u}(c)\frac{R^\mu}{R\cdot(k_1+k_2)}\frac{R^\nu}{R\cdot k_1}u(b). \tag{2.75}$$

Now, lets see what happens if we combine $\langle g1|$ and $\langle g3|$,

$$\langle g1| + \langle g3| = \bar{u}(c)\frac{R^\mu R^\nu}{R\cdot(k_1+k_2)}\left(\frac{1}{R\cdot k_2}+\frac{1}{R\cdot k_1}\right)u(b) \tag{2.76}$$

$$\langle g1| + \langle g3| = \bar{u}(c)\frac{R^\mu}{R\cdot k_2}\frac{R^\nu}{R\cdot k_1}u(b) = -\langle g2|. \tag{2.77}$$

So we see, this time, that the sum of the two diagrams with either c or b-propagators is equal to the diagram with both a c and a b-propagator with the opposite sign. Note however, that there is no guarantee that $\langle g1|$ and $\langle g3|$ will be the same and in general they won't be. Fortunately we are able to take advantage of their sum and we can still find a useful relation between the diagrams that will further allow us to debug our code.

Chapter 3

The Decay $b \to c\bar{c}cW^*$

Recent papers [12,17] were devoted to the precise determination of the c-quark mass-dependent $\mathcal{O}(\alpha_s^2)$ corrections to the decay $b \to cW^*$ in the maximum recoil limit. In those papers, results were presented as series in small parameters $\frac{m_c}{m_b}$ and $(1-\frac{m_c}{m_b})$, respectively. In these series the invariant mass of the leptons, q^2, is taken to 0 and the papers give expansions which match smoothly over almost the whole range of m_c. There is a region, however, where they don't agree smoothly, $m_c < \frac{m_b}{3}$. This was thought to be due to the omission of the $b \to c\bar{c}c\ell\nu_\ell$ process in the result of [12] because the contribution would be strongly suppressed by the fact that $3m_c \approx m_b$.

As an exercise in the use of some of the methods discussed in Chapter 2, and to show that this assumption is indeed true, we would like to present this calculation. We show that with this correction the results of [12] match those of [17] to within 1% down to $\frac{m_c}{m_b} \approx 0.05$. This matching is then only limited by the breakdown of the expansion presented here due to infrared divergences.

3.1 Methods of Calculation

We want to calculate the threshold decay rates of a b-quark into two massive c-quarks, a massive anti-c-quark, and a virtual W: $\Gamma(b \to c\bar{c}cW^*)$. The two Feynman diagrams that contribute to this process are shown in Fig. (3.1).

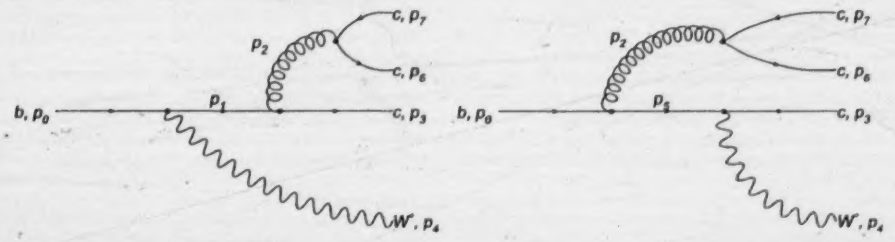

Figure 3.1: Feynman diagrams, corresponding to amplitudes M_1 and M_2 respectively, contributing to $b \to c\bar{c}cW^*$

In order to carry out this calculation, we need a small parameter that we will be able to expand around. This is given by δ in

$$m = \frac{M}{3}(1-\delta), \tag{3.1}$$

where $m = m_c$ and $M = m_b$. When $\delta < 0$, the decay is not allowed by conservation of 4-momentum and if $\delta = 1$ the decay becomes divergent indicating the presence of infrared divergences. To do this expansion we take advantage of phase space reduction, Eq. (2.16), so that we only need to deal with two particle phase spaces,

$$\begin{aligned} &\int dR_4(p_0; p_3, p_4, p_6, p_7) = \\ &\int dR_2(p_0; U, p_3) dU^2 (2\pi)^3 dR_2(U; p_2, p_4) dp_2^2 (2\pi)^3 dR_2(p_2; p_6, p_7). \end{aligned} \tag{3.2}$$

With $U = p_2 + p_4$, this break up of the phase space allows us to use one integration scheme for both diagrams and the cross term that appears. The different contributions that we need to calculate are given by the total spin averaged amplitude,

$$\langle |M_T|^2 \rangle = \langle |M_1 + M_2|^2 \rangle = \langle |M_1|^2 \rangle + 2\langle |M_1 M_2| \rangle + \langle |M_2|^2 \rangle, \tag{3.3}$$

so that we have three terms to compute. For simplicity we define $\langle |M_3|^2 \rangle \doteq 2\langle |M_1 M_2| \rangle$. These terms are then integrated to get the decay rate $\Gamma(b \to c\bar{c}cW^*)$ using

$$d\Gamma(b \to c\bar{c}cW^*) = \frac{(2\pi)^4}{2M} \langle |M_T|^2 \rangle dR_4(p_0; p_3, p_4, p_6, p_7). \tag{3.4}$$

After plugging in Eq. (3.3) this becomes the sum of three decay rates that can be calculated seperately,

$$d\Gamma(b \to c\bar{c}cW^*) = d\Gamma_1 + d\Gamma_2 + d\Gamma_3. \tag{3.5}$$

Here $d\Gamma_n$ corresponds to the term in the total decay rate corresponding to $\langle |M_n|^2 \rangle$.

With the phase space taken care of for now, we need to concentrate on the spin averaged amplitudes. As is, the denominators from the propagators make the two particle phase space integrals fairly difficult. To deal with this we use the fact that this is a threshold calculation. Since this expansion is done at threshold the decay products from each two particle decay are produced with very little motion. This means that the four-momenta have very small spatial components and the following approximations can be made: $p_6 \cdot p_7 \approx m^2$, $p_0 \cdot p_2 \approx 2Mm$, and $p_2 \cdot p_3 \approx 2m^2$. Using these we can manipulate the

denominators into forms that are suitable for expansion in a Taylor series. For $(p_1^2 - m^2)^{-1}$ we have,

$$p_1^2 - m^2 = (p_2 + p_3)^2 - m^2 = p_2^2 + 2p_2 \cdot p_3 = 2m^2 + 2p_6 \cdot p_7 + 2p_2 \cdot p_3 \quad (3.6)$$

$$= 2m^2 + 2(p_6 \cdot p_7 - m^2) + 2m^2 + 2(p_2 \cdot p_3 - 2m^2) + 4m^2 \quad (3.7)$$

$$= 8m^2 + \underbrace{2(p_6 \cdot p_7 + p_2 \cdot p_3 - 3m^2)}_{\lambda}. \quad (3.8)$$

With the above approximations we can see that the term on the right, λ, is small so that the denominator can easily be expanded to give,

$$\frac{1}{p_1^2 - m^2} = \frac{1}{8m^2} - \frac{\lambda}{(8m^2)^2} + \ldots. \quad (3.9)$$

The same can be done for $(p_5^2 - M^2)^{-1}$,

$$p_5^2 - M^2 = -4m(M - m) + \underbrace{2(p_6 \cdot p_7 - p_0 \cdot p_2 - m^2 + 2Mm)}_{\lambda'}, \quad (3.10)$$

and so

$$\frac{1}{p_5^2 - M^2} = -\frac{1}{4m(M - m)} - \frac{\lambda'}{(4m(M - m))^2} - \ldots. \quad (3.11)$$

Now the denominators contain only constants so the phase space integrals are easier to deal with. After expanding the propagators and taking traces the R_2 integrals are in the form

$$\int dR_2(Q; q_1, q_2)(Q \cdot q_1)^a (Q \cdot q_2)^b \quad (3.12)$$

for any $a, b > 0$. This general integral can effectively be treated according to the method explained in [16](Sec. III.A).

All that is left to be done now are the integrals over U^2 and p_2^2. The ranges of integration for these variables are $4m^2 < U^2 < (M - m)^2$ and $4m^2 < p_2^2 < U^2$. To simplify the integrals we make a change of variables with the definitions $p_2^2 = 4m^2(1+\omega x_1)$ and $U^2 = 4m^2(1+\omega x_1 x_2)$ and $x_1, x_2 \in [0, 1]$. When substituting in $m = \frac{M}{3}(1 - \delta)$, ω is given by

$$\omega = \frac{3\delta(4 - \delta)}{4(1 - \delta)^2}. \quad (3.13)$$

Finally, the only terms left to expand are the phase space integrals in Eq. (3.2). These can be expressed in terms of x_1, x_2 and ω,

$$(2\pi)^6 \int dR_2(p_2; p_6, p_7) \Rightarrow \frac{\pi}{2}\sqrt{w}\sqrt{x_1 x_2}\sqrt{\frac{1}{1 + \omega x_1 x_2}}, \quad (3.14)$$

$$(2\pi)^6 \int dR_2(U; p_2, p_4) \Rightarrow \frac{\pi}{2}\frac{\omega x_1(x_2 - 1)}{1 + \omega x_1 x_2}, \quad (3.15)$$

and

$$(2\pi)^6 \int dR_2(p_0; U, p_3) \Rightarrow \frac{2\pi m}{\sqrt{3}M}\sqrt{w}\sqrt{1-x_1}\sqrt{1-\frac{\delta^2}{4}-\frac{x_1\delta}{4}(4-\delta)}. \quad (3.16)$$

Since $\omega \sim \delta$ and $0 \leq x_1, x_2 \leq 1$ the term $\omega x_1 x_2$ is small and can be used as an expansion parameter in the first two volumes. The third volume has a factor of the form $\sqrt{1-\lambda}$, where λ is small so that it can be expanded as well. The choice of x_1 and x_2 as integration parameters is particularly useful here because, after expanding, we end up with half integer powers of x_1 and x_2, which give well known integrals.

3.2 Results

The results from [17] were presented as an expansion in $\rho = \frac{m}{M}$, while the results from [12] were presented as an expansion in $\delta = (1-\rho)$. Here we present our new results as an expansion in $\delta = (1-3\rho)$ and when comparing the three, all expansions are plotted as functions of ρ. This expansion only affects the light quark loop contributions as defined in [17]. Our three expansions begin at $\mathcal{O}(\delta^6)$ and are calculated up to $\mathcal{O}(\delta^{14})$. The first five terms of the expansions are presented here,

$$\Gamma_1 = \frac{\Gamma\sqrt{3}\delta^6}{4\pi}\left(\frac{3}{10}+\frac{27}{35}\delta+\frac{1737}{2240}\delta^2+\frac{4269}{4480}\delta^3+\frac{38121}{35840}\delta^4\ldots\right) \quad (3.17)$$

$$\Gamma_2 = \frac{\Gamma\sqrt{3}\delta^6}{4\pi}\left(\frac{3}{10}+\frac{9}{35}\delta+\frac{117}{448}\delta^2+\frac{2157}{4480}\delta^3+\frac{3957}{7168}\delta^4\ldots\right) \quad (3.18)$$

$$\Gamma_3 = \frac{\Gamma\sqrt{3}\delta^6}{4\pi}\left(\frac{1}{5}+\frac{11}{70}\delta-\frac{1063}{1120}\delta^2-\frac{3103}{2240}\delta^3-\frac{483}{512}\delta^4\ldots\right), \quad (3.19)$$

where we have defined

$$\Gamma = \frac{G_F|V_{cb}|^2M^3}{8\sqrt{2}\pi}C_F T_R N_L\left(\frac{\alpha_s}{\pi}\right)^2, \quad (3.20)$$

with $C_F = \frac{4}{3}$, $T_R = \frac{1}{2}$, and N_L the number of light quarks. We see that this contribution is indeed suppressed quite a bit. The leading contribution starts at $\mathcal{O}(\delta^6)$. As a result of this, the expansion had to be done to $\mathcal{O}(\delta^{14})$ in order to achieve good matching with the previous results. This expansion was added to the results presented in [12] and compared to A. Pak's expansion obtained in [17]. All three results are normalized to the tree level result, Γ_{Born}.

The plot in Fig. (3.2) shows how the results from this section contribute to the expansion about $\left(1-\frac{m}{M}\right) \ll 1$ in the region $0 \leq \rho \leq \frac{1}{3}$. At $\rho = 0.1$ the addition of this result brings the decay rate to within 0.75% as compared to the previous 2%. This agreement can be improved with a higher order expansion in δ but more computing resources would be required.

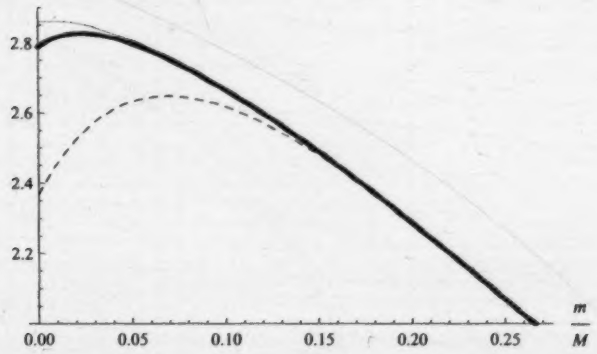

Figure 3.2: Comparison of results from previous papers. The dashed line shows the expansion about $\rho = 1$ while the thin line shows the expansion about $\rho = 0$. The thick line shows how the result from this paper closes the gap between the two.

With this example, we have shown the power of some of the methods described in the previous section, particularly the reduction of phase space. Now we can start apply them to a full $\mathcal{O}(\alpha_s^2)$ calculation, the main topic in this thesis.

Chapter 4

Second Order Corrections to Semileptonic b Decay

We have now developed the machinery needed to compute the second order corrections to the decay $\Gamma(b \to cW^*)$ at intermediate recoil. For this calculation we will use the limit $q^2 = m_c^2$ for the invariant mass squared of the leptons. As stated in the introduction, there is a discrepancy between results calculated ten years ago in [11] and those done quite recently in both [9, 10]. Naturally, we would like to resolve or at least find a reason for this discrepancy. Our goals here are three fold. First, we would like to extend the calculation done in [11] to be sure the expansion is accurate at the desired value of $\frac{m_c}{m_b}$. Second, we want to present the expansion from the opposite limit to check the consistency of the original expansion. With this, we will show that the two expansions do agree smoothly and finally proceed to recalculate the full decay $\Gamma(b \to c\ell\nu_\ell)$ as done in [11] using updated values [28].

In this section, it will be useful to make a couple of definitions here at the beginning. For the masses, we use $m = m_c$, $M = m_b$ and $\rho = \frac{m}{M}$. It will also be convenient to define an overall factor

$$\Gamma^0 = \frac{g^2 |V_{cb}|^2 M^3}{64\pi m_{W^*}^2}.$$

Finally, the second order contribution can be separated into contributions from different colour factors. For this, we introduce

$$\Gamma(b \to cW^*) = \Gamma^0 \left(X_{Born} + \left(\frac{\alpha_s}{\pi}\right) C_F X_1 + \left(\frac{\alpha_s}{\pi}\right)^2 C_F X_2 + \mathcal{O}(\alpha_s^3) \right), \quad (4.1)$$

with

$$X_2 = T_R N_H X_H + T_R N_S X_S + T_R N_L X_L + C_A X_A + C_F X_F, \quad (4.2)$$

where the H, S, and L subscripts refer to heavy (b-quark), soft (c-quark), and light quark contributions.

4.1 Expansion From Zero Recoil

One of the problems that was run into in [11] was computer power. When doing their calculation, the authors were only able to compute the first five terms in the expansion with the computing resources available. Because of this, the authors used an argument about the convergence of the series that allowed them to estimate the contribution from the remainder of the series. Ten years later, fortunately, we have the computing resources that allow us to double the number of terms calculated and thus give a much more accurate result without needing to approximate the remaining contribution.

To do this calculation, we consider 73 amplitudes shown in Fig. (B.1) and calculate cut by cut instead of using the optical theorem. This requires up to a four particle phase space and the calculation of two loop integrals. In order to carry out the calculation of the 73 diagrams, a total of 14 regions were needed with only one having an eikonal integral.

In [11] the results were presented in a scheme that differs from more recent results. We have recalculated this expansion using the same scheme as recent results to ensure that the matching can be done properly. The scheme used in [11] defined

$$S_1: \quad \alpha_s(\sqrt{Mm}),\ N_f = 4,\ \text{and}\ \frac{m}{M} = 0.3,$$

where N_f is the number of light quarks used in the BLM estimate. In [9, 10] a different scheme was used,

$$S_2: \quad \alpha_s(M),\ N_f = 3,\ \text{and}\ \frac{m}{M} = 0.25.$$

In order to be sure of our results we first computed the expansion in the S_1 scheme to reproduce the original results from [11]. While doing this, it was found that the charge renormalization was not done correctly. The authors mistakenly included a term to renormalize the b-quark loop diagrams. However, because the mass of the b-quark is larger than the renormalization scale, $\sqrt{mM}$, this term should not be included. Along with this, it would be convenient to separate the contributions from c-quark loops and b-quark loops. Correcting this mistake and separating the two contributions gives, to second order in the S_1 scheme,

$$\begin{aligned} X_H &= \sqrt{\beta}\left[\frac{509}{48} + \frac{999}{32}R_2 + \frac{87}{16}\ln 2 + \frac{337}{64}\ln^2 2 + \frac{75\pi^2}{128}\right. \\ &+ \beta\left(\frac{7937}{864} + \frac{1449}{32}R_2 + \frac{275}{144}\ln 2 + \frac{767}{64}\ln^2 2 + \frac{655\pi^2}{384}\right) \\ &+ \beta^2\left(\frac{610309}{51840} + \frac{204969}{2560}R_2 + \frac{59519}{17280}\ln 2 + \frac{973327}{46080}\ln^2 2\right. \\ &\left.\left. + \frac{317957\pi^2}{92160}\right) + \ldots\right], \end{aligned}$$

$$
\begin{aligned}
X_S &= \sqrt{\beta}\left[\frac{361}{96} - \frac{621}{256}R_2 - \frac{89}{64}\ln 2 + \frac{45}{512}\ln^2 2 - \frac{1445\pi^2}{3072}\right. \\
&- \beta\left(\frac{1189}{864} + \frac{207}{256}R_2 + \frac{49}{192}\ln 2 + \frac{1}{6}\ln 2 \ln\beta + \frac{979}{1536}\ln^2 2 - \frac{433\pi^2}{3072}\right) \\
&+ \beta^2\left(\frac{47159}{414720} - \frac{1}{12}\ln\beta - \frac{3243}{20480}R_2 + \frac{414637}{230400}\ln 2 - \frac{7}{45}\ln 2 \ln\beta\right. \\
&\left.\left. - \frac{200189}{368640}\ln^2 2 - \frac{51907\pi^2}{442368}\right) + \ldots\right],
\end{aligned}
$$

where $\beta = 1 - 4(\frac{m}{M})^2$.

After reproducing the original results, we then extended the expansions to $\mathcal{O}(\beta^8)$ so that we could be sure of the value of X_2 at the values of m/M in both schemes. The full expansion of these results is given in Appendix C. Both extending the expansion and correcting the heavy quark contribution significantly changed the value of X_2. In [11] the value was quoted as

$$X_2 = -4.72.$$

With the more accurate results, this changes to

$$X_2 = -4.45,$$

a change of about 6%. This can be clearly seen when we plot the old and updated expansion. It will be clear later on in this chapter that we now have

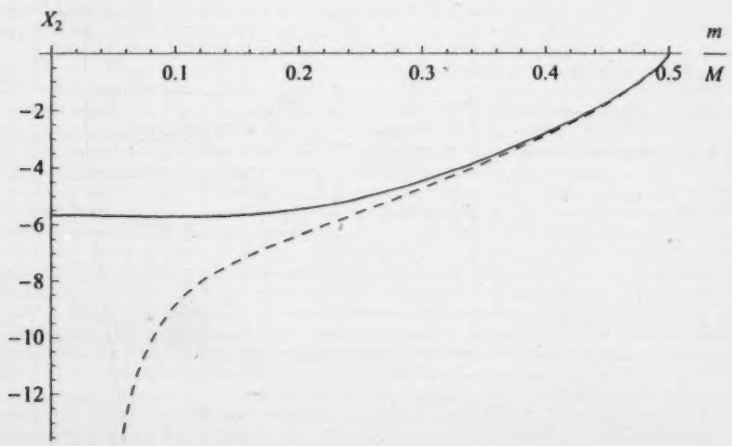

Figure 4.1: A comparison between the old and updated expansions shows a clear difference. The tail on the old expansion (dotted line) is a result of attempting to estimate the remaining contribution with a $\frac{\beta}{1-\beta}$ term.

enough terms to give an accurate value of X_2 and to show clearly the matching of this and the zero mass expansion presented in the next section.

4.2 Expansion From Zero Mass

With the expansion from zero recoil now known much more accurately, we would now like to do the same expansion from the opposite limit as a definitive check that nothing was missed and that we do indeed have enough terms to provide a precise value of X_2.

For this expansion we have used the optical theorem, reducing the number of diagrams to consider significantly. To calculate the $\mathcal{O}(\alpha_s^2)$ contributions to this decay, we need to consider the 39 three loop diagrams in Fig. (B.2) and the 19 one and two loop renormalization diagrams in Fig. (B.4). The 39 diagrams that contribute can be grouped into ten topologies. This is less than were used before in a similar calculation [17] because three of the topologies were found to be the same as ones already being considered. These ten topologies can be reduced to regions that have known expressions from [19] by the method of asymptotic expansion. The contributing regions to each topology are described in Appendix B.

4.2.1 Checks

As with any calculation, we would like to preform some kind of check to make sure we are carrying it out properly. A quick check of consistency is done by first considering the massless case $\rho = 0$. In this case, only the first regions of each topology plus region 5 of diagram D38 contribute. The result of this calculation is

$$\begin{aligned}
\Gamma^{(2)}(b \to c, W|m=0) &= C_F[T_R(N_L X_L^0 + N_H X_H^0 + N_S X_S^0) \\
&+ C_F X_F^0 + C_A X_A^0] \\
X_L^0 &= -\frac{4}{9} + \frac{23}{108}\pi^2 + \zeta(3) \\
X_H^0 &= \frac{12991}{1296} - \frac{53}{54}\pi^2 - \frac{1}{3}\zeta(3) \\
X_S^0 &= -\frac{4}{9} + \frac{23}{108}\pi^2 + \zeta(3) \\
X_F^0 &= 5 - \frac{119}{48}\pi^2 + \frac{19}{4}\pi^2 \ln 2 - \frac{53}{8}\zeta(3) - \frac{11}{720}\pi^4 \\
X_A^0 &= \frac{521}{576} + \frac{505}{864}\pi^2 - \frac{19}{8}\pi^2 \ln 2 + \frac{9}{16}\zeta(3) + \frac{11}{1440}\pi^4,
\end{aligned} \tag{4.3}$$

which is in agreement with other expansions done in the same limit.

Two other checks that were done are carrying out the expansion for the tree level and $\mathcal{O}(\alpha_s)$ corrections and making sure that they agree with the expected results. For the tree level, X_{Born}, we find,

$$X_{Born} = 1 - 3\rho^2 - 2\rho^6 - 6\rho^8. \tag{4.4}$$

We can compare this with the exact result,

$$X_{Born}^{Ex} = \sqrt{1-4\rho^2}(1-\rho^2). \tag{4.5}$$

It will be more instructive, though, to expand the exact result in a series around $\rho = 0$. Carrying this expansion out,

$$X_{Born}^{Ex} = 1 - 3\rho^2 - 2\rho^6 - 6\rho^8 + \ldots, \tag{4.6}$$

we see that our result agrees perfectly with the exact result up to $\mathcal{O}(\rho^8)$.

For the $\mathcal{O}(\alpha_s)$ results, we have three two loop diagrams and two one loop renormalization diagrams, Fig. (4.2). These diagrams can be easily integrated

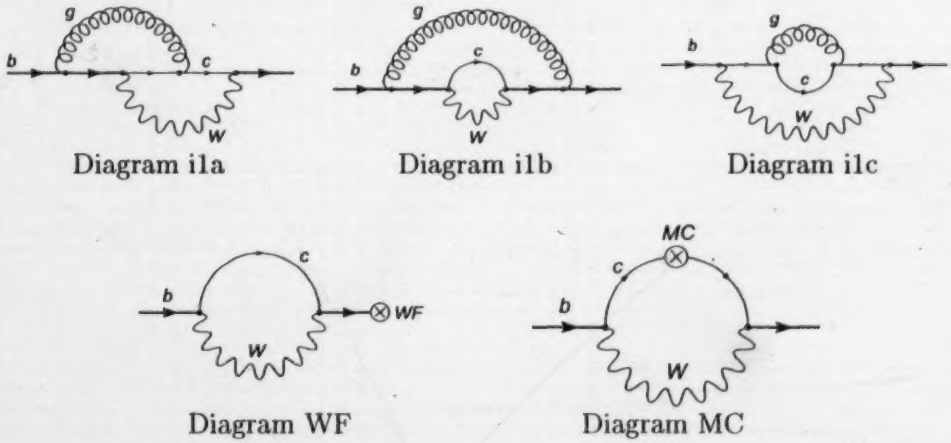

Figure 4.2: The contributions to the $\mathcal{O}(\alpha_s)$ corrections. The WF and MC diagrams correspond to wave function and mass renormalization contributions respectively.

using one two loop topology and the method of asymptotic expansion, which was done as an example in Chapter 2. After carrying out the expansion, we end up with

$$X_1 = \frac{5}{4} - \frac{\pi^2}{3} + \rho^2\left(\frac{\pi^2}{3} - \frac{5}{4} - 9\ln\rho\right) + \rho^4\left(9\ln\rho - \frac{15}{4}\right) + \ldots. \tag{4.7}$$

If we plot this along with the first order result from [11] we see that the expansions match very well in the range we are interested in, Fig. (4.3). We can be confident that our method gives the proper second order contribution with these checks and the overall gauge invariance of the second order result.

4.2.2 NNLO Results

With all of this done, we can now proceed with calculating the $\mathcal{O}(\alpha_s^2)$ corrections. This requires a total of 63 asymptotic regions to be considered for the 39 three loop diagrams and 10 topologies. To carry out these calculations we used FORM [29].

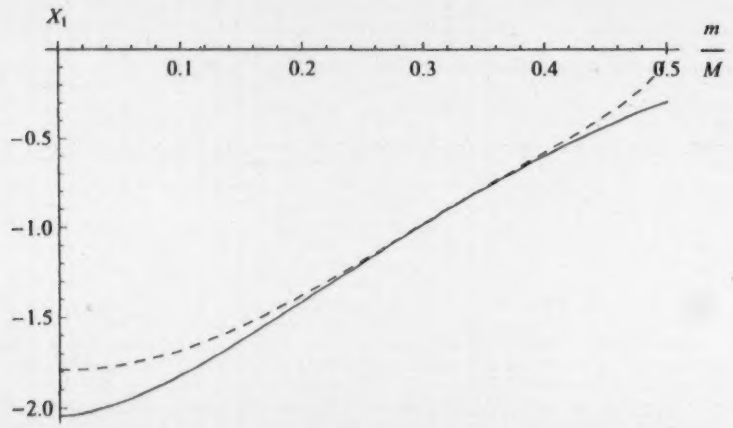

Figure 4.3: The matching of the $\mathcal{O}(\alpha_s)$ corrections to the decay $\Gamma(b \to cW^*)$. The dotted line is the expansion from the zero recoil line and the solid line is the expansion from zero mass.

Up to $\mathcal{O}(\rho^4)$ the result is

$$\begin{aligned} X_L &= \frac{23\pi^2}{108} - \frac{4}{9} + \zeta(3) - \rho^2\left(\frac{1}{18} - \frac{13}{2}\ln\rho + 3\ln^2\rho + \zeta(3) + \frac{77\pi^2}{108}\right) \\ &+ \rho^4\left(\frac{865}{72} - \frac{34}{3}\ln\rho + 6\ln^2\rho\right) \end{aligned} \tag{4.8}$$

$$\begin{aligned} X_H &= \frac{12991}{1296} - \frac{1}{3}\zeta(3) - \frac{53\pi^2}{54} + \rho^2\left(\frac{89\pi^2}{54} - \frac{137567}{6480} + \frac{13}{3}\zeta(3)\right) \\ &+ \rho^4\left(\frac{4\pi^2}{3} - \frac{10081601}{705600} - \frac{23}{840}\ln\rho\right) \end{aligned} \tag{4.9}$$

$$\begin{aligned} X_S &= \frac{23\pi^2}{108} - \frac{4}{9} + \zeta(3) - \rho\left(\frac{3\pi^2}{4}\right) \\ &+ \rho^2\left(\frac{4}{9} + \frac{13}{2}\ln\rho - 3\ln^2\rho - \zeta(3) + \frac{157\pi^2}{108}\right) \\ &- \rho^3\left(\frac{25\pi^2}{18}\right) + \rho^4\left(\frac{1193}{36} - \frac{61}{3}\ln\rho + 9\ln^2\rho - \frac{16\pi^2}{3}\right) \end{aligned} \tag{4.10}$$

$$\begin{aligned} X_F &= 5 - \frac{53}{8}\zeta(3) - \frac{119\pi^2}{48} + \frac{19\pi^2}{4}\ln 2 - \frac{11\pi^4}{720} \\ &+ \rho^2\left(\frac{743\pi^2}{48} - \frac{97}{2} - \frac{75}{8}\ln\rho - \frac{27}{2}\ln^2\rho + \frac{151}{8}\zeta(3) + \pi^2\ln\rho\right. \\ &\left. - \frac{57\pi^2}{4}\ln 2 - \frac{127\pi^4}{360}\right) - \rho^3\left(\frac{4\pi^2}{3}\right) \\ &+ \rho^4\left(\frac{7145}{288} - \frac{329}{24}\ln\rho + 18\ln^2\rho + \frac{547}{32}\zeta_3 - \frac{83\pi^2}{12} + \frac{25\pi^2}{12}\ln\rho\right. \end{aligned} \tag{4.11}$$

$$
\begin{aligned}
&+ \frac{201\pi^2}{16}\ln 2 + \frac{19\pi^4}{72}\Big) \\
X_A &= \frac{521}{576} + \frac{9}{16}\zeta(3) + \frac{505\pi^2}{864} - \frac{19\pi^2}{8}\ln 2 + \frac{11\pi^4}{1440} \\
&- \rho^2\left(\frac{1223}{576} + \frac{185}{8}\ln\rho - \frac{33}{4}\ln^2\rho + \frac{107}{16}\zeta(3) + \frac{145\pi^2}{864}\right. \\
&- \left.\frac{57\pi^2}{8}\ln 2 + \frac{161\pi^4}{720}\right) + \rho^3\left(\frac{2\pi^2}{3}\right) \\
&+ \rho^4\left(\frac{27\pi^2}{8} - \frac{13391}{288} + \frac{2027}{48}\ln\rho - \frac{33}{2}\ln^2\rho - \frac{403}{64}\zeta_3\right. \\
&- \left.\frac{23\pi^2}{8}\ln\rho - \frac{201\pi^2}{32}\ln 2 - \frac{31\pi^4}{720}\right),
\end{aligned}
\tag{4.12}
$$

and the expansions have been computed up to $\mathcal{O}(\rho^{10})$. The full results are given in Appendix C. We can now compare these results graphically with those obtained in [11]. To do this though, we must make sure that both expansions are expressed in the same scheme S_1 or S_2. This expansion has been done in the scheme S_2 and so we have calculated the expansion from zero recoil in the same scheme so that it is possible to compare them properly. Using these new expansions and the results given above we obtain the plots in Fig. (4.4).

We can see that each contribution has an area where the matching is smooth, showing that the two expansions do indeed agree. With everything put together, we end up with a plot that clearly shows the importance of expanding the zero recoil expansion to higher powers. The two expansions match smoothly in the region ~ 0.22 to ~ 0.4 so that both of our schemes S_1 and S_2 are valid with either expansion. Now that we have verified the expansions, we can redo the polynomial fit that was presented in [11] and see how the estimate changes.

4.3 The Polynomial Fit

Three points of the decay $\Gamma_{sl}(b \to c\ell\nu_\ell)$ are known from the decay $\Gamma(b \to cW^*)$ evaluated at different values of the W^* mass [11–13]. From this decay, it is possible to compute the decay into leptons using,

$$
\Gamma_{sl}(b \to c\ell\nu_\ell) = \frac{8G_F}{3\sqrt{2}M_w^2}\int_0^{(m_c-m_b)^2}\frac{dq^2}{(4\pi)^2}q^2\Gamma(b \to cW^*)|_{m_{W^*}^2=q^2}. \tag{4.13}
$$

As an example, let us calculate the tree level decay rate which is known completely analytically so it will be a good check of this formula.

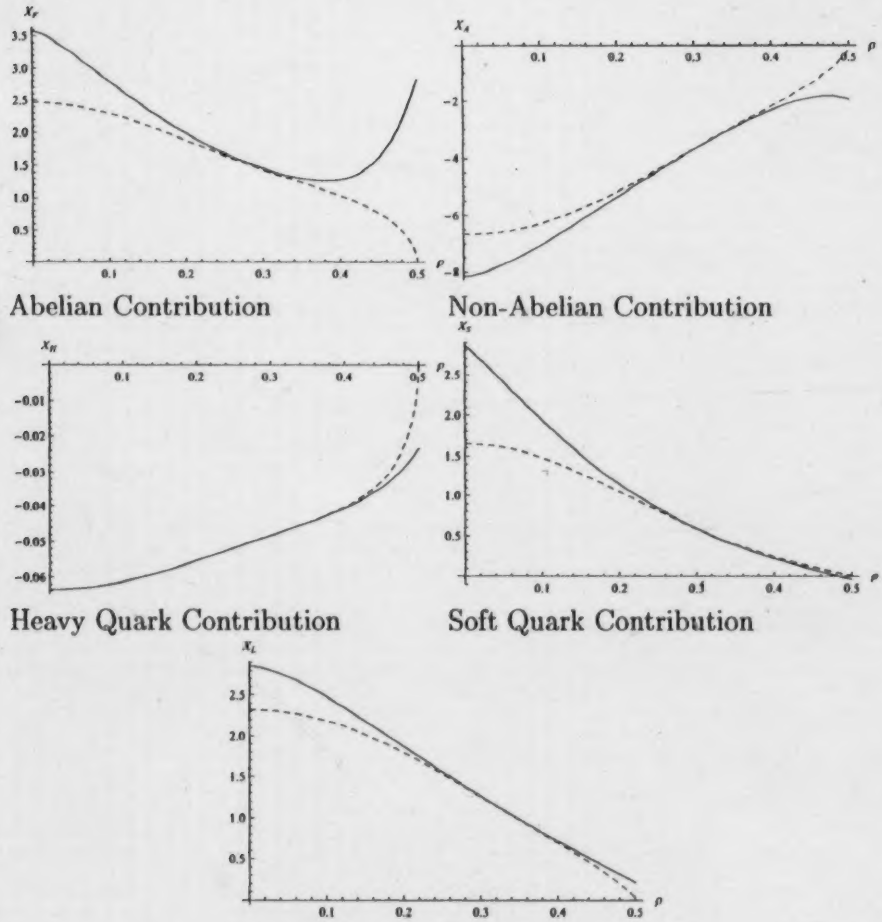

Figure 4.4: The matching between the different colour contributions. The dashed line corresponds to the expansion from zero recoil and the solid line corresponds to the expansion from zero mass.

$$\Gamma(b \to cW^*)|_{m_{W^*}^2=q^2} = \frac{g^2|V_{cb}|^2 m_b^3}{64\pi q^2} \overbrace{(1 - 2\frac{q^4}{m_b^4} + \rho^2\frac{q^2}{m_b^2} + \rho^4 + \frac{q^2}{m_b^2} - 2\rho^2)}^{\xi(q^2)} \times \underbrace{\sqrt{\left[1 - \rho^2 - \frac{q^2}{m_b^2}\right]^2 - 4\rho^2\frac{q^2}{m_b^2}}}_{PS[q^2,\rho]}. \quad (4.14)$$

Note that here, G_F is in its explicit form to highlight the q^2 dependence. This factor is compensated for in the integration by the q^2 term appearing in

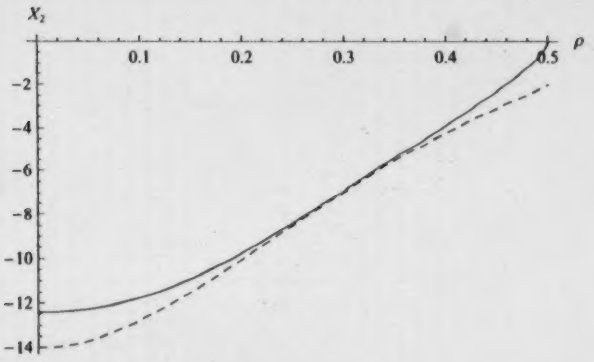

Figure 4.5: The complete $\mathcal{O}(\alpha_s^2)$ contribution.

Eq. (4.13). The square root term that appears in this equation is from the phase space and so will appear quite often. We should note that as PS goes to zero, the first derivative becomes infinite. Carrying out the integration and restoring G_F, we end up with

$$\Gamma_{sl}(b \to c\ell\nu_\ell) = \frac{G_F^2|V_{cb}|^2 m_b^5}{192\pi^3}(1 - 8\rho - 24\rho^4 \ln\rho + 8\rho^6 - \rho^8), \tag{4.15}$$

in agreement with the known result.

For second order corrections, we do not know the exact result in terms of q^2. Instead we calculate the decay $\Gamma(b \to cW^*)$ for different values of q^2 and then fit a polynomial to those values to approximate the total q^2 dependence. Let us check this method with the tree level results to show how it works. Using Eq. (4.14), we calculate the value of $\xi(q^2)$ at three points, $q^2 = 0$, $q^2 = m_c^2$, and $q^2 = (m_b - m_c)^2$. If we were to include the phase space factor PS, we would end up with a curve that had a value of zero at $q^2 = (m_b - m_c)^2$. This would work fine except for the fact that the derivative at this point is infinity, so a polynomial fit would not give an accurate result. Using a value of $\rho = 0.25$, we end up with

$$\Gamma_0 = 0.879, \quad \Gamma_{m_c^2} = 0.938, \quad \Gamma_{(m_b - m_c)^2} = 0.844. \tag{4.16}$$

We then fit these to a second order polynomial given by

$$0.879 + 1.063q^2 - 2q^4. \tag{4.17}$$

If we plot this polynomial as compared to the function $\xi(q^2)$, we find that they agree perfectly.

Now integrating this polynomial multiplied by $PS[q^2, 0.25]$, gives a number that is in perfect agreement with the tree level decay using the defined parameters,

$$\Gamma(b \to c\ell\nu_\ell) = 0.631903.$$

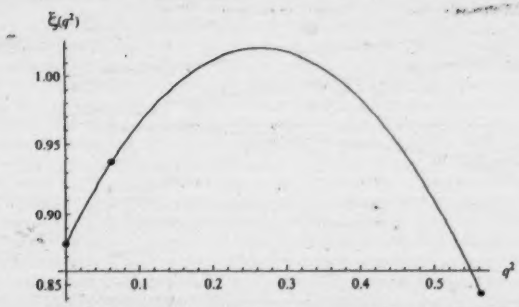

Figure 4.6: Polynomial fit to the tree order calculation.

we should note, that with the exact dependence on q^2 known, we can see that a second order polynomial will give a perfect result because $\xi(q^2)$ is a second order polynomial. This, unfortunately is not true for the first and second order corrections that we will be discussing.

4.3.1 $\mathcal{O}(\alpha_s)$ Corrections

Now that we know the method of integration used, we can apply this to the first order corrections to see how they agree and whether a polynomial fit still works. We will see that another important question must also be answered to arrive at consistent results. That is, how should we normalize the points before we fit the data? To start we will do exactly as in the previous section and only divide out the factor $PS[q^2, \rho]$. For consistency, we define

$$\Gamma(b \to cW^*) = \Gamma^0 \left[\Delta_{Born} + \frac{\alpha_s}{\pi} C_F \Delta_1 + \left(\frac{\alpha_s}{\pi}\right)^2 C_F \Delta_2 \right]. \tag{4.18}$$

This means that the first curve is fit to,

$$\xi_1^{(1)}(q^2) = \frac{\Delta_1}{PS[q^2, \rho]}, \text{ with } \rho = 0.25. \tag{4.19}$$

After doing the fit, we end up with the curves shown below.

We then integrate $\xi_1^{(1)} \cdot PS$ to give -0.799 as compared to the exact result which is -0.843. This polynomial fit has about 5% error, which is not bad. We would like to know, however if other normalizations give better results.

Next we look at normalizing to the full tree level result so that we have

$$\xi_1^{(2)}(q^2) = \frac{\Delta_1}{\Delta_{Born}}. \tag{4.20}$$

This time we actually end up doing worse. Looking at the exact result, we can clearly see that the curve is not a polynomial. The value of the integral we end up with is -0.780, which has an error of about 7%. This is still not too bad, but we can do better.

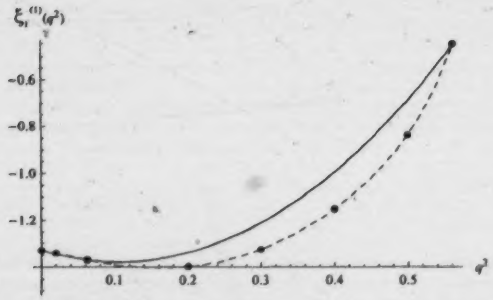

Figure 4.7: Polynomial fit to $\mathcal{O}(\alpha_s)$ corrections normalized to the phase space. The exact result is shown using points known along the dashed curve.

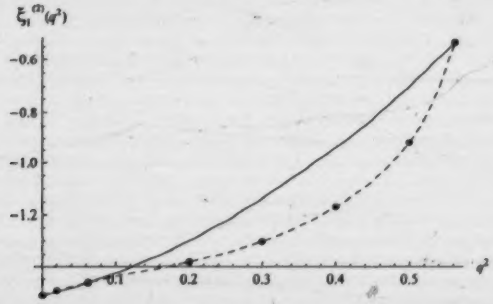

Figure 4.8: Polynomial fit to $\mathcal{O}(\alpha_s)$ corrections normalized to the tree level. The exact result is shown using points known along the curve.

The last normalization we want to consider is no normalization. We use the full $\mathcal{O}(\alpha_s)$ result, (i.e $\xi_1^{(3)}(q^2) = \Delta_1$) and do a fit to that. One would expect this fit to be worse because this result includes the phase space factor PS that causes the first derivative to be divergent. Looking at the resulting curve, however, we can plainly see that this is not the case. Here we see that the

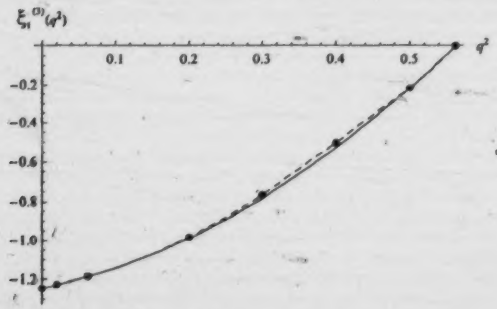

Figure 4.9: Polynomial fit to $\mathcal{O}(\alpha_s)$ corrections with no normalization. The exact result is shown using points known along the curve.

polynomial fit approximates the exact curve very well. Integrating over this

curve, we end up with -0.852, which gives an error of about 1%. This is much better than the previous two estimates so we can conclude that this is the best normalization of the three shown here to use for higher order corrections.

4.3.2 The $\mathcal{O}(\alpha_s^2)$ Corrections

We are now well poised to do a fit of the three points known to second order. Recently, the exact value of the integral has been calculated, however, the shape of the q^2 curve is unknown. We will therefore only be able to compare the resulting numbers as opposed to the shape of the curve itself.

When doing this calculation we will not only be interested in the full second order correction, but also the non-BLM corrections. For this we will need a formula for finding the BLM corrections, namely,

$$\Delta_2^{BLM} = T_R X_L \left(N_f - \frac{33}{2} \right). \tag{4.21}$$

As well, we need to know how to switch between the two normalization schemes S_1 and S_2. This is done using the $\mathcal{O}(\alpha_s)$ corrections and the relation

$$\alpha_s(\sqrt{m_b m_c}) = \alpha_s(m_b) \left(1 - \frac{\frac{11}{2} C_A - 2T_R (N_L + N_S)}{3} \frac{\alpha_s(m_b)}{\pi} \ln \sqrt{\rho} \right). \tag{4.22}$$

We will be comparing the results from our fits to the known exact results that were recently computed in [9, 10].

To start, we normalize to the Born amplitude because this is how the original fit was done in 1998. In this section, we will be giving three different results, Δ_2, Δ_2^{BLM}, and ξ_2, for comparison purposes. Each of these can be obtained from

$$\xi_2(q^2) = \frac{\Delta_2(q^2) - \Delta_2^{BLM}(q^2)}{\Delta_{Born}(q^2)}$$

in such a way that the three result are normalized the same way. Three points are then obtained from the three expansions done at $q^2 = 0$, $q^2 = m_c^2$, and $q^2 = (m_b - m_c)^2$. For this normalization, we get

$$\xi_2(0) = 1.24, \quad \xi_2(m_c^2) = 1.27, \quad \xi_2((m_b - m_c)^2) = 0.19,$$

in the S_1 scheme. Notice that all three numbers presented here are different than those presented in [11]. Unfortunately, it was found that in the previous papers that calculated $\xi_2((m_b - m_c)^2)$, $\xi_2(m_c^2)$ and $\xi_2(0)$ [11–13], the wrong charge renormalization term was used. They included a renormalization proportional to N_H that should not have been there because the scale of $m_b > \sqrt{m_b m_c}$. Correcting this and using the same method as described above to fit these numbers to a polynomial and integrating, we end up with the numbers in Tab. (4.I).

	Δ_2^{BLM}		Δ_2		ξ_2	
Scheme	S_1	S_2	S_1	S_2	S_1	S_2
Polynomial	-8.6	-14.6	-7.21	-12.7	1.44	1.95
Exact	-9.8	-17.3	-8.07	-13.9	1.73	3.40

Table 4.1: Comparison of polynomial fit after correcting the renormalization.

This method of polynomial fit corresponds to the second method in the previous section and as such, we do not expect an exact answer. Looking at the BLM and Δ_2 estimates, we would expect the method to give an answer with an error of no more than about 25% (the sum of errors from BLM and Δ_2). We notice that, with these corrected numbers, the fit gives a much better estimate than previously calculated. With an error of about 17%, this fits nicely within the expected error. The non-BLM estimate in the S_2 scheme is not quite as good however. This value has an error of about 43%. The important result to note here is the S_1 non-BLM result from the polynomial fit is 1.44 as opposed to 0.9(3) given in [9], a nice improvement.

We saw at the beginning of this chapter that the original expansion from zero recoil did not include enough terms. With the extra terms, this updated expansion and new one from $\rho = 0$ give the results shown in Tab. (4.2).

	Δ_2^{BLM}		Δ_2		ξ_2	
Scheme	S_1	S_2	S_1	S_2	S_1	S_2
Old	-8.6	-14.1	-7.03	-12.1	1.54	2.04
New	-8.6	-14.2	-7.05	-12.1	1.54	2.11
Exact	-9.8	-17.3	-8.07	-13.9	1.73	3.40

Table 4.2: Comparison of polynomial fit with extended expansions.

Here, "Old" refers to the results in [11], "New" refers to the results presented here, and "Exact" refers to the results recently obtained in [9, 10]. We see here that the estimates of Δ_2 seem to have gotten worse, even though the two opposite expansions agree very well with each other. It is clear now that fitting a polynomial in this normalization does not work, even though the non-BLM corrections give more reasonable results.

At $\mathcal{O}(\alpha_s)$ the fit with no normalization worked very well, so let us try that, with the results shown in Tab. (4.3). Looking at the numbers, it is clear that

	Δ_2^{BLM}		Δ_2		ξ_2	
Scheme	S_1	S_2	S_1	S_2	S_1	S_2
Old	-9.5	-16.4	-7.70	-13.1	1.75	3.28
New	-9.5	-16.5	-7.71	-13.2	1.76	3.37
Exact	-9.8	-17.3	-8.07	-13.9	1.73	3.40

Table 4.3: Comparison of polynomial fit using no normalization.

this estimate does much better. All results now agree to within $\sim 5\%$, showing that this is a much better method of fitting than the one previously used. As a final check of this method, we want to calculate the hadron energy moments and compare to exact results. This is done by including a factor of

$$E_n = \left(\frac{m_b^2 + m_c^2 - q^2}{2m_b} \right)^n$$

in the integral to give $H^{(n)}$. When done in the S_2 scheme with our most accurate results, we find

$$H^{(1)} = -5.631 \text{ and } H^{(2)} = -2.468,$$

to be compared with the exact results,

$$H^{(1)} = -5.331 \text{ and } H^{(2)} = -2.045.$$

These values have $\sim 6\%$ and $\sim 21\%$ error respectively.

This section gave a detailed explanation of the different methods to determine the second order corrections to $\Gamma(b \to c\ell\nu_\ell)$. Using a polynomial fit to three known points, the non-BLM part of the corrections were determined to be 0.9(3) in [11]. It was found, however, that the renormalization in this result was not done correctly. At the scale used, $\sqrt{m_b m_c}$, the b-quark loop corrections are already accounted for because its mass, m_b, is larger than the renormalization scale. This means that the b-quark loop renormalization term in [11] was not needed. This mistake with renormalization was present in all three points used for the polynomial fit. It was also found that the method of fitting the polynomial could be improved. This was done by not normalizing the second order results unlike in [11] where the results were normalized to the tree level result. When the fitting is done with these corrections a value of 1.76(4) is obtained. This value agrees with the exact value of 1.73(4) obtained in [9,10]. With these results, we have successfully resolved the large discrepancy between the old and new calculations of the second order non-BLM corrections to the decay $\Gamma(b \to c\ell\nu_\ell)$, the main motivation for this thesis.

Chapter 5

Conclusions

The precise determination of V_{cb} is an important endeavour for both experimental and theoretical particle physicists. It is directly related to some of the free parameters of the Standard Model, and when combined with other parameters can used in the search for new physics. One way we have of measuring V_{cb} is to fit experimental data to the theoretical inclusive decay rate $\Gamma(B \to X_c \ell \nu_\ell)$. To obtain a precise value for V_{cb} from this, good knowledge of higher order corrections is needed. With two recent calculations [9, 10], this decay is now known perturbatively to second order. These two calculations however were in disagreement with an estimate done ten years ago in [11] that was used in an analysis to find V_{cb}. The objective of this thesis was to check the expansion presented in [11] to be sure of the values used in determining $\Gamma(b \to c \ell \nu_\ell)$ and find the reason for the disagreement between this old estimate and the new exact values of the second order non-BLM corrections.

In order to check the expansion from zero recoil presented in [11], we carried out an expansion from the opposite limit (zero mass) and compared the two to see how well they matched. In doing this, we determined that more orders in the expansion from zero recoil were needed. This was not originally done because of available computer resources at the time. Fortunately we were able to compute the necessary terms that ultimately showed how well the two expansions match. In addition to needing more terms in the expansion, it was found that the authors of [11] included a renormalization term that should not have been there. This term was for the charge renormalization due to b-quark loops in the calculation. However, because of the renormalization scheme used in the calculation, this term is not needed and as such has been corrected here. With these two improvements, we were able to show excellent matching between the two expansions, thus achieving our first objective.

With the new expansion from zero mass presented here, we were also able to compute a much more accurate value for the second order corrections to $\Gamma(b \to cW^*)$ at intermediate recoil. This then meant that the polynomial fitting done in order to calculate the full second order corrections to $\Gamma(b \to c \ell \nu_\ell)$ could be preformed again in order to bring the value into agreement with the recently calculated exact value. For this polynomial fitting to be done

correctly though, we found that the value obtained at zero recoil needed to be corrected. This is because the same charge renormalization mistake present in [11] was also present in this expansion [13]. We corrected for this and found that the value for the non-BLM corrections changes from 0.9(3) to 1.5(2). These should be compared to the exact value of 1.73 found in [9]. A 15% error is included with the second number here based on the accuracy of the polynomial fit to the BLM corrections. It is clear that these mistakes with renormalization and the limited number of terms in the intermediate recoil expansion are what caused such a low estimate of the non-BLM corrections.

Finally, by looking at different ways of performing this polynomial fitting at first order, we were able to find a much more accurate method of determining the second order corrections to $\Gamma(b \to c\ell\nu_\ell)$. This fitting method used the values of the full second order corrections to $\Gamma(b \to cW^*)$ at the points $m^2_{W^*} = 0, m_c^2, (m_b - m_c)^2$ instead of normalizing them to the tree level result. When done this method brings the fitted estimate to 1.76(4), which is only $\sim 2\%$ higher than the exact value, showing that this is an accurate way of obtaining full second order corrections using only a few known data points. All said and done, it is expected that this change in the value of non-BLM corrections will only cause the measurement of V_{cb} to change by about 0.5% [9]. This change, however, is favourable because it brings the values obtained from inclusive and exclusive decays closer together.

Bibliography

[1] T. Kinoshita and M. Nio, Phys. Rev. D **73**, 013003 (2006) [arXiv:hep-ph/0507249].

[2] W. M. Yao *et al.* [Particle Data Group], J. Phys. G **33**, 1 (2006).

[3] B. Aubert *et al.* [BABAR Collaboration], Phys. Rev. D **74**, 092004 (2006) [arXiv:hep-ex/0602023].

[4] E. Barberio, Nucl. Phys. Proc. Suppl. **170**, 102 (2007).

[5] C. W. Bauer, (2004) arXiv:0408100 [hep-ph].

[6] I. I. Y. Bigi, M. A. Shifman, N. G. Uraltsev and A. I. Vainshtein, Phys. Rev. Lett. **71**, 496 (1993) [arXiv:hep-ph/9304225].

[7] P. Ball, M. Beneke and V. M. Braun, Phys. Rev. D **52**, 3929 (1995).

[8] S. J. Brodsky, G. P. Lepage and P. B. Mackenzie, Phys. Rev. D **28**, 228 (1983).

[9] K. Melnikov, arXiv:0803.0951 [hep-ph].

[10] A. Pak and A. Czarnecki, Phys. Rev. Lett. **100**, 241807 (2008) [arXiv:hep-ph/0803.0960].

[11] A. Czarnecki and K. Melnikov, Phys. Rev. D **59**, 014036 (1999) [arXiv:hep-ph/9804215].

[12] A. Czarnecki and K. Melnikov, Phys. Rev. Lett. **78**, 3630 (1997) [arXiv:hep-ph/9703291].

[13] A. Czarnecki, Phys. Rev. Lett. **76**, 4124 (1996) [arXiv:hep-ph/9603261].

[14] A. Czarnecki and K. Melnikov, Phys. Rev. Lett. **88**, 131801 (2002) [arXiv:hep-ph/0112264].

[15] I. R. Blokland, A. Czarnecki, M. Slusarczyk and F. Tkachov, Phys. Rev. D **71**, 054004 (2005) [arXiv:hep-ph/0503039].

[16] A. Czarnecki and K. Melnikov, Phys. Rev. D **56**, 7216 (1997) [arXiv:hep-ph/9706227].

[17] A. Pak, I. R. Blokland and A. Czarnecki, Phys. Rev. D **73**, 114009 (2006) [arXiv:hep-ph/0604233].

[18] S. Laporta, Int. J. Mod. Phys. A **15**, 5087 (2000) [arXiv:hep-ph/0102033].

[19] Ian Blokland, *PhD Thesis* (2004).

[20] M. E. Peskin and D. V. Schroeder, *An Introduction to Quantum Field Theory* (Perseus, Cambridge, MA, 1995).

[21] S. G. Gorishnii and A. P. Isaev, Theor. Math. Phys. **62**, 232 (1985) [Teor. Mat. Fiz. **62**, 345 (1985)].

[22] T. Gehrmann and E. Remiddi, Nucl. Phys. B **601**, 248 (2001) [arXiv:hep-ph/0008287].

[23] O. V. Tarasov, Nucl. Phys. B **480**, 397 (1996) [arXiv:hep-ph/9606238].

[24] A. Czarnecki and K. Melnikov, Nucl. Phys. B **544**, 520 (1999) [arXiv:hep-ph/9806244].

[25] V. A. Smirnov, *Evaluating Feynman Integrals*, Springer Tracts Mod. Phys., **211**, 1 (2004).

[26] M. L. Mangano and S. J. Parke, Phys. Rept. **200**, 301 (1991) [arXiv:hep-th/0509223].

[27] Y. J. Feng and C. S. Lam, Phys. Rev. D **53**, 2115 (1996) [arXiv:hep-ph/9503311].

[28] M. Dowling, A. Pak, A. Czarnecki, Alberta-Thy 09-08, to be published.

[29] J. A. M. Vermaseren (2000), [arXiv:math-hp/0010025].

[30] P. Nogueira, J. Comput. Phys. **105**, 279 (1993).

[31] T. Huber and D. Maitre, Comput. Phys. Commun. **175**, 122 (2006) [arXiv:hep-ph/0507094].

[32] S. Moch and P. Uwer, Comput. Phys. Commun. **174**, 759 (2006) [arXiv:math-ph/0508008].

[33] S.Moch, P. Uwer and S.Weinzierl, [arXiv:hep-ph/0110083].

[34] J.M.Borwien *et al.*, [arXiv:math.CA/9910045].

Appendix A

Useful Programs

In this section we have written a few helpful 'manuals' for some programs that are useful when computing Feynman diagrams. They are basically distilled versions of the full manuals that should enable the user to install and start using the programs. For more advanced use of the programs described here, we refer the reader to the full manuals cited in the titles.

A.1 Qgraf [30]

A.1.1 Installation and Use

Qgraf is a Fortran program that symbolically generates all Feynman diagrams that belong to a given process. The program is available as source code from

`http://cfif.ist.utl.pt/paulo/qgraf.html`.

It needs to be compiled and linked with Fortran 77 and depending on the system used the source files may need to be slightly modified. In order to use qgraf three files need to be edited or created. These are the model, style and data files, each of which will be described in the following sections. Note the qgraf package comes with sample style files form.sty, array.sty and sum.sty as well as a sample data file qgraf.dat.

To run qgraf all that needs to be done is run the executable. The program searches the current directory for the 'qgraf.dat' file which has all options defined that qgraf needs to run properly. For this reason the 'qgraf.dat' file should be in the directory that qgraf is called from.

A.1.2 Files

The Model File

The model file contains all of the information about the propagators, vertices and their properties that will be used to create the diagrams. It is separated

into three sections: constants, propagators, and vertices. The constants section is optional whereas the propagators and vertices must be defined for the diagrams to be generated.

Propagators are defined in the following way:

```
[part1, part2, +/-; functions]
```

part_1 and part_2 refer to the fields that make up the propagator and are conjugates. It is also convenient to call the fields particle and antiparticle, respectively, for labelling purposes that will appear later. The +/- defines the fields as fermionic - or bosonic +. Finally the functions are user defined functions that can be used to store various properties of the fields. The functions must be defined in the following way:

```
function = ( S1, S2 )
```

in the case that part_1 is different from part_2 and:

```
function = ( S )
```

in the case that they are the same. An example of a properly declared propagator is:

```
[electron, positron, -; C = (-1,+1), m=me]
```

where C can be seen as the charge of the field and m the mass.

Note: the images of functions should be in quotes (e.g. C=('-1','+1') or m='me') but they can be omitted when the image is a valid rational, integer, or identifier. Images with brackets, spaces, or mathematical expressions should be enclosed in quotes.

A vertex is defined by naming all particles that the vertex is connected to:

```
[part1, part2, ..., partn]
```

Qgraf will accept vertices of degree between 3 and 6. If you need a higher degree there is a parameter that must be changed in the source code. Some care should be taken when defining propagators and vertices. The above propagator defines $< \psi\overline{\psi} >$. If the electron and positron are reversed you may end up with the wrong sign. Similar considerations should be made when defining a vertex.

The last part of the model file is the definition of constants. These should be strings that you want to appear in the output file like the name of the model being described. For example:

```
[ model = 'QED in D=4-ep dimensions']
```

Data File

The data file contains all options that are passed to qgraf. The structure or name of the file should not be changed. Here is what it should look like:

```
output= 'filename' ;
style= 'style.sty' ;
model= ' model';
in= parta, partb ;
out= partc, partd ;
loops= 2;
loopmomentum= k ;
options= ;
```

Output This should be the name of the file you want qgraf to write the diagrams in. If left blank (`''`) qgraf will run without writing a file. This is recommended as a first run to make sure the output file will not be too large. If a file with the same name already exists qgraf will not over-write it and you will get an error message in the terminal output.

Style This should be the name and path of the style file that you want to use.

Model This is the name and path of the model file to use.

In(Out) These should include the names of the particles coming in or going out of the diagram respectively. It is also possible to define the external momenta in these fields by using `part_a[p1]` where `p1` is the momenta of particle a. By default the incoming momenta are labelled with `p1,p2,` and outgoing momenta are labeled with `q1,q2,`. They are labeled in the order that they are declared.

Loops The number of loops you want in each diagram.

Loop_momentum This is the prefix used to enumerate the loop momenta. In this case qgraf would create 2 loop momenta labeled k1 and k2.

Options Should include the different options that you want to use. These are described below.

The options statement lets you pick what kind of diagrams qgraf will generate. The possible options and their counterparts in brackets are listed below with a small description of what they do. There are a few terms that should be defined first though. 'Tadpole' refers to a one particle loop (starts and ends on the same vertex) that is attached to the rest of the diagram by a propagator. 'Snail' refers to a one particle loop that can be directly attached to the rest of the diagram or connected through a propagator.

onepi(onepr) One-particle irreducible diagrams only.

onshell(offshell) No self energy insertions on external lines.

nosigma(sigma) No self energy insertions anywhere.

nosnail(snail) No snail diagrams.

notadpole(tadpole) No diagrams with tadpoles.

simple(notsimple) A maximum of one propagator can connect two vertices and no one-particle loops that start and end on the same vertex.

floop Discards diagrams with fermion loops that have an odd number of interactions in accordance with Furry's theorem in QED.

topol Generates only one diagram with each possible topology. This can only be used with a single neutral field (i.e. a single bosonic field).

It should be noted that diagrams generated with one option will not be in the set of diagrams generated with the converse of that option. For example the option `snail` will only produce diagrams with snails. More general and therefore advanced options are available and for those we refer you to section 4.3 of the documentation provided with qgraf.

Style File

The style file is a small program that tells qgraf what information to include in the output file and how it should be formatted. Three sample files are included in the qgraf package. For details on how to create or edit a style file we refer you to sections 6 and 7 of the qgraf documentation provided in the package. The output generated by the form.sty file will be looked at in detail after we have explained how qgraf labels the diagrams in the next section.

A.1.3 Indices

Qgraf uses six separate indices to label the diagrams it creates. They are the vertex, propagator, leg, field, ray, and field type indices. Not all are needed to construct the diagrams but each has information that may be useful to you or the program that is going to use the information in the output file.

Vertex Each vertex is labeled with a positive integer starting at 1.

Propagator Each internal propagator is labeled with a positive integer starting at 1.

Leg Each external propagator (leg) is labeled with a positive integer starting at 1. The indices are separated between incoming and outgoing particles and the order is determined by the order in which the particles are defined in the data file. In the sample data file the particles would get leg indices `part_a`, `part_c` = 1 and `part_b`, `part_d` = 2.

Field The field index uses the propagator and leg indices to label the particles and antiparticles. For a propagator k it labels the particle $2k-1$ and antiparticle $2k$. This labelling scheme helps to determine the direction of momentum flow. For a leg j it labels the incoming legs $-2j+1$ and the outgoing legs $-2j$. This provides a convenient way of differentiating between incoming and outgoing particles and propagators.

Ray The ray index looks at a vertex and gives all associated particles an integer starting at 1. The order is determined by how the vertex is defined in the model file. For example `[e,p,ph]` corresponds to `[1,2,3]`.

Field The field type index is given to differentiate between incoming, outgoing, and internal fields. The indices are in=1, out=2 and internal=3.

A.1.4 Example and How to Interpret the Output

Running Qgraf

In this section we present a very basic and trivial example of how to use the program. The model file we use is:

```
%constants
%propagators
 [electron, positron, -]
 [photon, photon, +]
%vertex
 [electron, positron, photon]
```

This defines a very basic QED model. The style file we use is one that comes with the package: form.sty. It was created to be used with older versions of FORM and provides very basic output.

To run qgraf we have all files in the same directory and run the program from there with:

```
> ./qgraf
```

The terminal output is:

```
------------------------------------------------------
                      qgraf-3.1
------------------------------------------------------

output= 'test' ;
style= 'form.sty' ;
model= ' model';
in= electron, positron ;
out= photon, photon ;
loops= 1;
```

```
loopmomentum= k ;
options= floop, onshell ;

-------------------------------------------------------

2P --- 1+ 1- --- 1N+ 1C-

1V --- 31

-------------------------------------------------------

34 --- 8 diagrams

total = 8 diagrams
```

The first part of the output shows the contents of the data file qgraf.dat. As can be seen from this information qgraf has generated all onshell one-loop diagrams associated with electron positron annihilation and the loop has been given momentum k1.

The next bit of information has to do with what qgraf found in the model file. `2P` and `1V` refer to the fact that there are 2 propagators and 1 vertex defined respectively. On the propagator line qgraf then tells you how many are fermionic (`1-`) and how many are bosonic (`1+`). The `N` and `C` in the next bit tell you if the particle differs from the antiparticle in the propagator definition. In this case there is one bosonic propagator where the particle and antiparticle are the same `1N+` and one fermionic propagator where the particle and antiparticle are different `1C-`. On the vertex line the `3^1` refers to the fact that there is 1 vertex of degree 3 defined.

The last section of the output will either give you an error or, if the program runs successfully, the number of diagrams generated. In this example the first line tells you that there are 8 diagrams that contain 4 vertices with degree 3. This is the only kind of diagram possible so 8 is also the total number of diagrams generated.

Reading the Output File

If a file name is given in the output field of the data file qgraf will save the information for each graph generated according to the style file used. In the example above the form.sty file was used. The first diagram in the output is shown below.

```
*--#[ d1:
*
      1
      *vx(electron(-1),positron(1),photon(-2))
      *vx(electron(2),positron(-3),photon(-4))
```

```
      *vx(electron(1),positron(3),photon(4))
      *vx(electron(3),positron(2),photon(4))
*
*--#] d1:
```

The form.sty file tells qgraf to look at each vertex and then for each field attached to it print either the propagator index (for internal propagators) or the field index (for external fields). The fields with the same index correspond to the same propagator. When each vertex is considered separately you get:

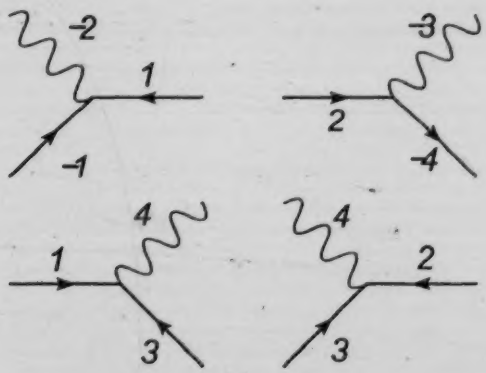

Figure A.1: The corresponding vertices generated in the qgraf output.

With everything put together the Feynman diagram then looks like:

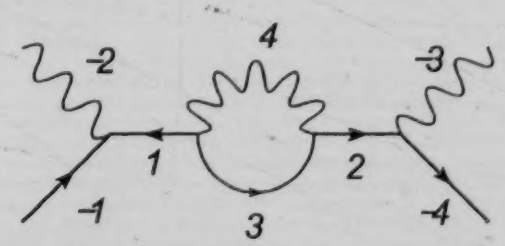

Figure A.2: The resulting Feynman diagram when the propagators are put together.

It should be noted that, because it only uses one index to label the graph, the form.sty style can produce ambiguities. The other two style files provided, however, are able to resolve these ambiguities because they produce more information about the graphs.

A.2 The Mathematica Package HypExp [31]

The package is available for download from:

`http://www-theorie.physik.unizh.ch/~maitreda/HypExp/`

A.2.1 HypExp Functions In Mathematica

- `HypergeometricPFQ[{...},{...},x]` This defines the hypergeometric function ${}_JF_{J-1}$. A special case of this is present in the form `Hypergeometric1F2[...,x]` for the ${}_2F_1$ hypergeometric function. The arguments used must be in the form $a + \alpha\epsilon$ where $a \in \mathbb{Z}$ and $\alpha \in \mathbb{R}$ or can be left as a variable.

- `HypExp[HypergeometricPFQ[ ], ϵ, n]` This is the main command of the package. It gives the ϵ expansion of ${}_PF_Q$ in terms of elementary functions up to order n. `HypExp` can be used on any function but it will only be applied to the hypergeometric functions in the expression. If you want to apply `HypExp` to an expression containing a hypergeometric function $f()_PF_Q$ it should be called as in the following example or nothing will be expanded.

```
HypExp[#1,e,n] & //@ (f() HypergeometricPFQ[...])
```

- `HypExpInt[`$\chi_1, \chi_2, \chi_3, \chi_4, \chi_5, z$ `]`
This function evaluates integrals of the form,

$$\int_0^1 du \frac{u^{\chi_1} \ln^{\chi_2}(u) \ln^{\chi_3}(1-u) \ln^{\chi_4}(1-zu)}{(uz-1)^{\chi_5}}, \tag{A.1}$$

the arguments must satisfy the conditions,
$\chi_i \in \{\mathbb{N}, 0\}$, $\chi_2 + \chi_3 + \chi_4 + 1 - \delta_{\chi_5,0} \leq 5$.
For $z = 0, 1$ the second condition can be dropped. If these conditions are not met the original command is returned and nothing is done.

- `HypExpU[n,m,p]`
This function evaluates integrals of the form,

$$\int_0^1 du \ln^n(u) \ln^m(1-u) u^p, \tag{A.2}$$

where $p \in \mathbb{Z}$ and n, m non-negative integers. In the case $p < 0$, $m+p \geq 0$ must be satisfied for the integral to be convergent.

- `HypExpAddToLib[`$a_1, \ldots, a_J, b_1, \ldots, b_{J-1}$`,n]`
This function computes the expansion for arbitrary ϵ additions to the arguments. It then adds the expansion to the library for use later on. This is especially convenient if you need to expand ${}_JF_{J-1}$ fairly frequently.

- `HypExpIsKnownToOrder[`$a_1, \ldots, a_J, b_1, \ldots, b_{J-1}$`,n]`
This function returns True if the expansion is available in the library. The above 2 functions require numbers for a_i, b_j, n as shown in the examples provided below. The HypExp package also updates the `Series` command to allow expansion of functions containing hypergeometric functions. For details on the methods used to calculate the expansions see [31].

A.2.2 Examples

- HypExp

```
In[1]:= (HypExp[#1, e, 1] & ) //@
          (Log[1-e] Hypergeometric2F1[1+e,1,2-e,x])
```

$$\text{Out[1]:= Log[1-e]}\left(-\left(\frac{\text{Log[1-x]}}{x}\right) + e\left(\frac{\text{Log[1-x]}}{x} + \frac{\text{Log[1-x]}^2}{x} + \frac{\text{PolyLog[2,x]}}{x}\right)\right)$$

```
In[2]:= (HypExp[#1, e, 1] & ) //@
          (Log[1-e] HypergeometricPFQ[{1+2e,1-e,2},
            {2-e,2+3e},x])
```

$$\text{Out[2]:= Log[1-e]}\left(-\left(\frac{\text{Log[1-x]}}{x}\right) + e\left(-\left(\frac{2\ \text{Log[1-x]}}{x}\right) - \frac{\text{Log[1-x]}^2}{2\ x} - \frac{2\ \text{PolyLog[2,x]}}{x}\right)\right)$$

- HypExpInt

```
In[3]:= HypExpInt[1,1,1,1,1,1]
```

$$\text{Out[3]:= } -6 + \frac{\pi^2}{3} + \frac{\pi^4}{45} + 2\ \text{Zeta[3]}$$

- HypExpU

```
In[4]:= HypExpU[2,4,-1]
```

$$\text{Out[4]:= } -\frac{2}{3}\pi^4\text{Zeta[3]} - 16\pi^2\ \text{Zeta[5]} + 240\ \text{Zeta[7]}$$

- HypExpIsKnownToOrder

```
In[5]:= HypExpIsKnownToOrder[2,5,1,3]
Out[5]:= True

In[6]:= HypExpIsKnownToOrder[2,6,1,3]
Out[6]:= False
```

- HypExpAddToLib

```
In[7]:= HypExpAddToLib[2,6,1,3]
```

Note that there is no output when this has finished running.

- Series

```
In[8]:= f = Log[1-e] Hypergeometric2F1[1+e,1,2-e,x]
Out[8]:= Hypergeometric2F1[1+e,1,2-e,x] Log[1-e]
In[9]:= Series[f,{e,0,2}]
```

$$\text{Out[9]:= } \frac{\text{Log[1-x]}e}{x} -$$

$$\left(\frac{\text{Log}[1-x]}{2x} + \frac{\text{Log}[1-x]^2}{x} + \frac{\text{PolyLog}[2,x]}{x}\right)e^2 + O[e]^3$$

A.3 XSummer [32]

The XSummer package is written for FORM and can be downloaded from:

`http://www-zeuthen.desy.de/moch/xsummer`

A.3.1 How to Use XSummer

XSummer adds a few main routines to be used and a whole bunch of internal routines that are used by the main processes. Another thing that XSummer adds are objects which it uses for pattern matching in order to carry out the sums properly. The following is a list of these with how they should be implemented into the FORM program. These objects are all described in the file 'declvars.h' which should be included when you use the XSummer package.

bino	`bino(a,i)`$= \binom{a}{i}$
delta	`delta(x)` $= \delta(x) = \begin{cases} 1 & x = 0 \\ 0 & x \neq 0 \end{cases}$
deltap	`deltap(x)` $= (1 - \delta(x))$
den	`den(x)` $= \frac{1}{x}$
ep	`ep` $= \epsilon$ this symbol must be used for the expansion parameter.
epow	`epow(n)` $= \epsilon^n$
fac	`fac(n)` $= n!$
inf	`inf` $= \infty$ used to represent upper limit of infinity
invfac	`invfac(n)` $= \frac{1}{n!}$
num	`num(x)` $= x$ puts x in the numerator
pow	`pow(x,a)` $= x^a$
sign	`sign(n)` $= (-1)^n$
sum	`sum(n,i1,i2)*f(n)` $= \sum_{n=i1}^{i2} f(n)$
theta	`theta(x)` $= \begin{cases} 1 & x \geq 0 \\ 0 & x < 0 \end{cases}$
z2,z3,...	`z2` $= \zeta(2)$
Gamma	`Gamma(x)` $= \Gamma(x)$
InvGamma	`InvGamma(x)` $= \frac{1}{\Gamma(x)}$

S-sum `S(R(`$m_1,\ldots$`),X(`$x_1,\ldots$`),n)`

$$= \sum_{j_1=1}^{n} \frac{x_1^{j_1}}{j_1^{m_1}} S(j_1; m_2, \ldots; x_2, \ldots), \quad S(n) = \begin{cases} 1 & n > 0 \\ 0 & n \leq 0 \end{cases}$$

Z-sum `Z(R(`$m_1,\ldots$`),X(`$x_1,\ldots$`),n)`

$$= \sum_{j_1=1}^{n} \frac{x_1^{j_1}}{j_1^{m_1}} Z(j_1 - 1; m_2, \ldots; x_2, \ldots), \quad Z(n) = \begin{cases} 1 & n \geq 0 \\ 0 & n < 0 \end{cases}$$

These functions must be used when describing indices to conform with the pattern matching routines used by XSummer. For example:

```
x/j1
```

should be written

```
x*den(j1)
```

As well the pow function is reserved for variables to an index power so

```
pow(j1,2)
```

would not work.

Next are the main processes that can be called. These processes rely on many other internal processes that will not be described here. For more information on these internal routines we refer you to the documentation provided with XSummer (XSummer.tex) which can also be downloaded in pdf format from [32].

DoSum This is the main process for the package. It is called using the line `#call DoSum(a,b)` where a is the index of the innermost summation and b is the index of the outermost sum that should be done. Note that all indices should be written as `jn` with $n = 1, 2, \ldots$. DoSum will then evaluate the innermost sum first and work its way out to the outermost sum. For example:

```
#call DoSum(3,1)
```

would evaluate sums in the order j_3, j_2, j_1.

BasisS This will express products of S-sums in terms of single S-sum sums. It is called using `#call BasisS()`. Note that the brackets need to be there. FORM interprets this as `(0)`. Changing the value inside the brackets to something other than 0 tells the BasisS process to do nothing.

ConvStoZ This is provided to convert S-sums into Z-sums in case it is more convenient to work with Z-sums. It is called using `#call ConvStoZ(S,Z)`.

Example

What follows is an example of a properly formatted FORM file that uses XSummer. In the next section we will refer back to this example to help explain the notation used.

```
#define MAXWEIGHT "20"
#define MAXSUM "1"
#include declvars.h
```

These pre processor variables are used in the internal routines that `DoSum` calls. If you are doing an ϵ expansion you should also include the variable `EXPANDEP` which tells XSummer what power of ϵ you want the expansion done to.

```
CF Li;
autodeclare s a;

L demo1 = sum(j1,1,inf)*pow(x,j1)*den(j1)*sum(j2,1,j1-1)*den(j2)
          *sum(j3,1,j2-1)*den(j3);

L demo2 = sum(j1,1,inf)*pow(x,j1)*den(j1)2*sum(j2,1,j1-1)*den(j2);

#call DoSum(3,1)

#call ConvStoZ(S,Z)

id Z(R(?a),X(?x),inf) = Li(R(reverse(?a)),X(reverse(?x)));
id acc(x?) = x;
.sort;

id Li(R(?a),X(?y)) = Li(?a,?y);
```

The above three `id` statements format the output in terms of Goncharov multiple polylogarithms which will be explained in the next section.

```
B x;
Print;
.end
```

The resulting output is:

```
demo1 =
    + Li(2,1,1,1,1,x);
demo2 =
    + Li(1,2,1,x);
```

In more readable notation demo1 and demo2 are defined as

$$\text{demo1} = \sum_{j_1=1}^{\infty} \frac{x^{j_1}}{j_1} \sum_{j_2=1}^{j1-1} \frac{1}{j_2} \sum_{j_3=1}^{j2-1} \frac{1}{j_3},$$

and

$$\text{demo2} = \sum_{j_1=1}^{\infty} \frac{x^{j_1}}{j_1^2} \sum_{j_2=1}^{j1-1} \frac{1}{j_2}.$$

A.3.2 Goncharov Multiple Polylogarithms [33]

When it is convenient XSummer displays its output in the form of Goncharov multiple polylogarithms. This is because for $n = \infty$ Z-sums are equivalent to the multiple polylogarithms with the following relation,

$$Z(\infty; m_1, \ldots, m_k; x_1, \ldots, x_k) = Li_{m_k,\ldots,m_1}(x_k, \ldots, x_1).$$

$Li_{m_k,\ldots,m_1}(x_k, \ldots, x_1)$ is defined as [34]

$$Li_{m_k,\ldots,m_1}(x_k, \ldots, x_1) = \sum_{j_1,\ldots,j_k=1}^{\infty} \prod_{i=1}^{k} x_i^{j_i} \left(\sum_{n=i}^{k} j_n \right)^{-m_i}.$$

For special cases the multiple polylogarithms can be reduced to simpler forms like Neilsen's generalized polylogarithms, harmonic polylogarithms, or even classical polylogarithms.

In the case $x_k, \ldots, x_2 = 1$ the multiple polylogarithms are related to harmonic polylogarithms in the following way,

$$Li_{m_k,\ldots,m_1}(x_k, \ldots, x_1) = H_{m_1,\ldots,m_k}(x_1),$$

where the harmonic polylogarithms are defined recursively by

$$H_0(x) = \ln(x), \qquad H_1(x) = -\ln(1-x), \qquad H_{-1}(x) = \ln(1+x)$$

$$f_0(x) = \frac{1}{x}, \qquad f_1(x) = \frac{1}{1-x}, \qquad f_{-1}(x) = \frac{1}{1+x},$$

and

$$H_{m_1+1,m_2,\ldots,m_k} = \int_0^x dt f_0(t) H_{m_1,m_2,\ldots,m_k}(t)$$

$$H_{\pm 1,m_2,\ldots,m_k} = \int_0^x dt f_{\pm 1}(t) H_{m_2,\ldots,m_k}(t).$$

Multiple polylogarithms are also related to Nielsen's generalized polylogarithms, $S_{n,p}$, in the following way,

$$S_{n,p}(x) = Li_{1,\ldots,1,n+1}(\underbrace{1, \ldots, 1}_{p-1}, x),$$

where

$$S_{n,p}(x) := \frac{(-1)^{n-1+p}}{(n-1)!p!}\int_0^1 dt \frac{\ln^{n-1}(t)\ln^p(1-tx)}{t}.$$

Finally, in the case that the multiple polylogarithm only has two arguments, it is equivalent to classical polylogarithms.

Examples

We start by looking at the answer for `demo2` provided in the example program for XSummer. As you recall

```
demo2 = Li(1,2,1,x)
```

which should be interpreted as

$$Li_{1,2}(1,x).$$

The difficult way of simplifying this would be to apply the relation to harmonic polylogarithms. Using the definitions above and the relation

$$H_{1,1}(x) = \frac{1}{2}\ln^2(1-x)$$

gives

$$Li_{1,2}(1,x) = H_{2,1}(x) = \int_0^x dt \frac{1}{t} H_{1,1}(x)$$

$$= \int_0^1 dt \frac{\ln^2(1-xt)}{2t} = S_{1,2}.$$

Using the relation to Neilsen generalized polylogarithms it is clear that this is true. The integral can then be done in a program like Mathematica or even FORM to give an answer in terms of logarithms, classic polylogarithms, and zeta functions.

The second example can only be expressed as a harmonic polylogarithm,

$$Li_{2,1,1}(1,1,x) = H_{1,1,2}(x) = \int_0^x dt \frac{1}{1-t} H_{1,2}(t)$$

$$= \int_0^x dt \frac{1}{1-t}\int_0^t ds \frac{1}{1-s} H_2(s) = \int_0^x dt \frac{1}{1-t}\int_0^t ds \frac{1}{1-s}\int_0^s du \frac{1}{u} H_1(u)$$

$$= -\int_0^x dt \frac{1}{1-t}\int_0^t ds \frac{1}{1-s}\int_0^s du \frac{1}{u}\ln(1-u).$$

After integrating over u,s and t this gives

$$Li_{2,1,1}(1,1,x) = \frac{2\pi^4 + 5\pi^2\ln^2(1-x)}{60} - 3Li_4(1-x) + \ln(1-x)[Li_3(1-x) + 2\zeta(3)],$$

for $0 < x \leq 1$.

Appendix B

Catalog of Diagrams

B.1 Zero Recoil Expansion

Two Gluon Radiation

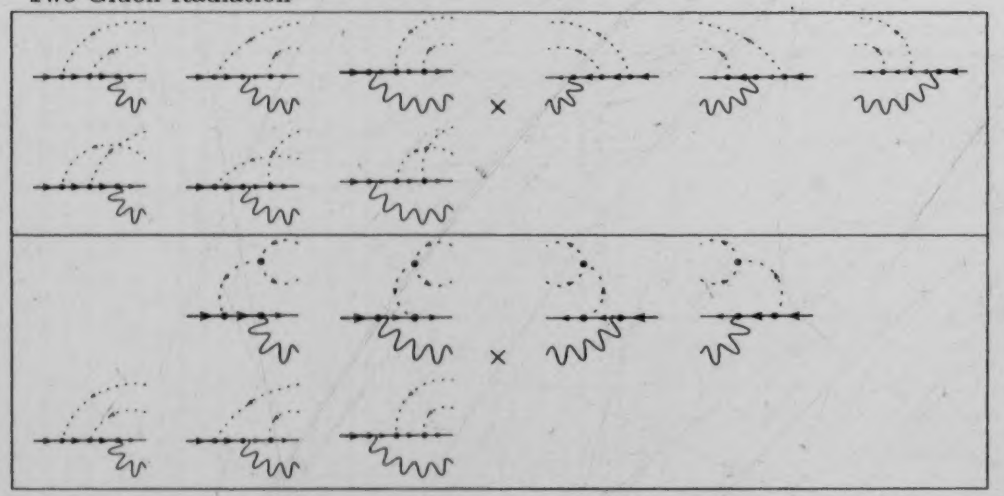

Ghost And Light Quark Radiation

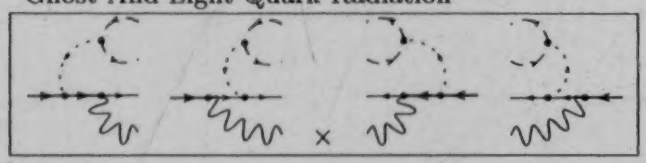

One Gluon Radiation

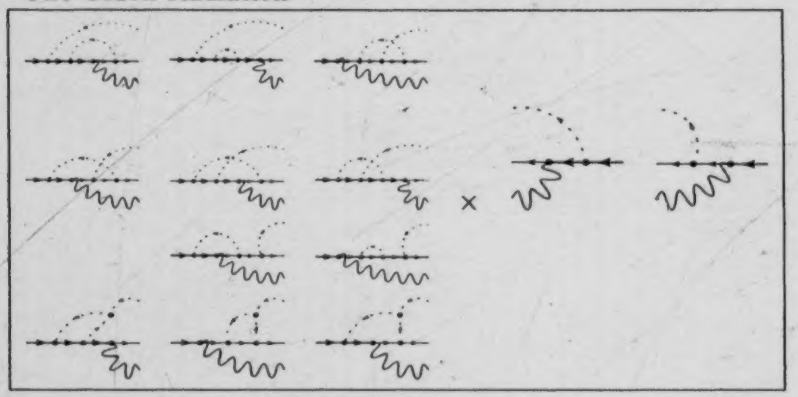

No Gluon Radiation

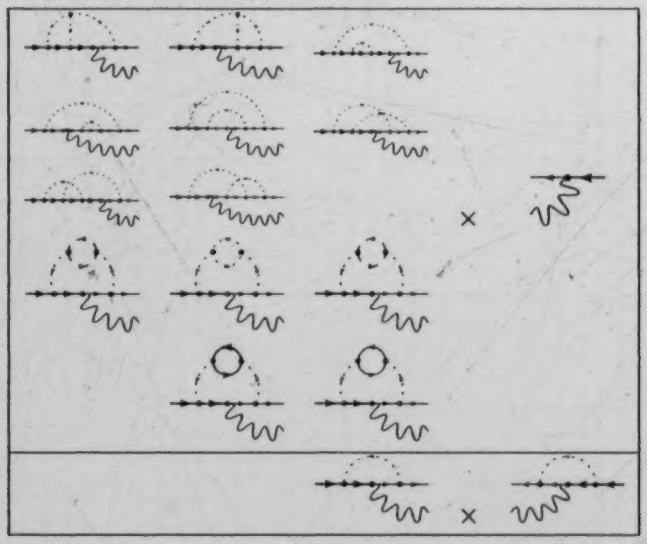

Renormalization Diagrams

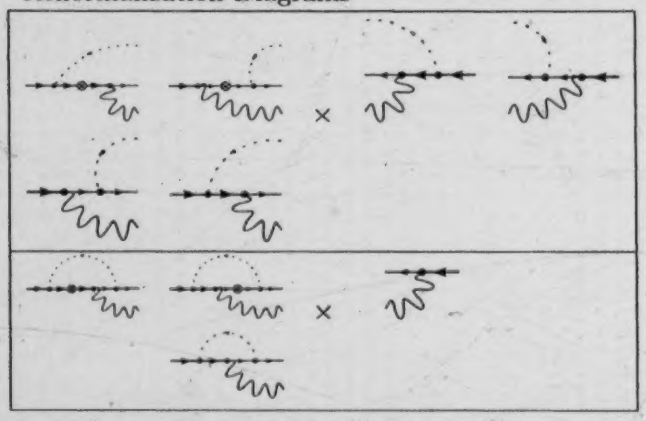

Figure B.1: Feynman diagrams of amplitudes that needed to be calculated for the zero recoil expansion. The amplitude of each diagram on the left is multiplied by the amplitude of each diagram on the right.

B.2 Zero Mass Expansion

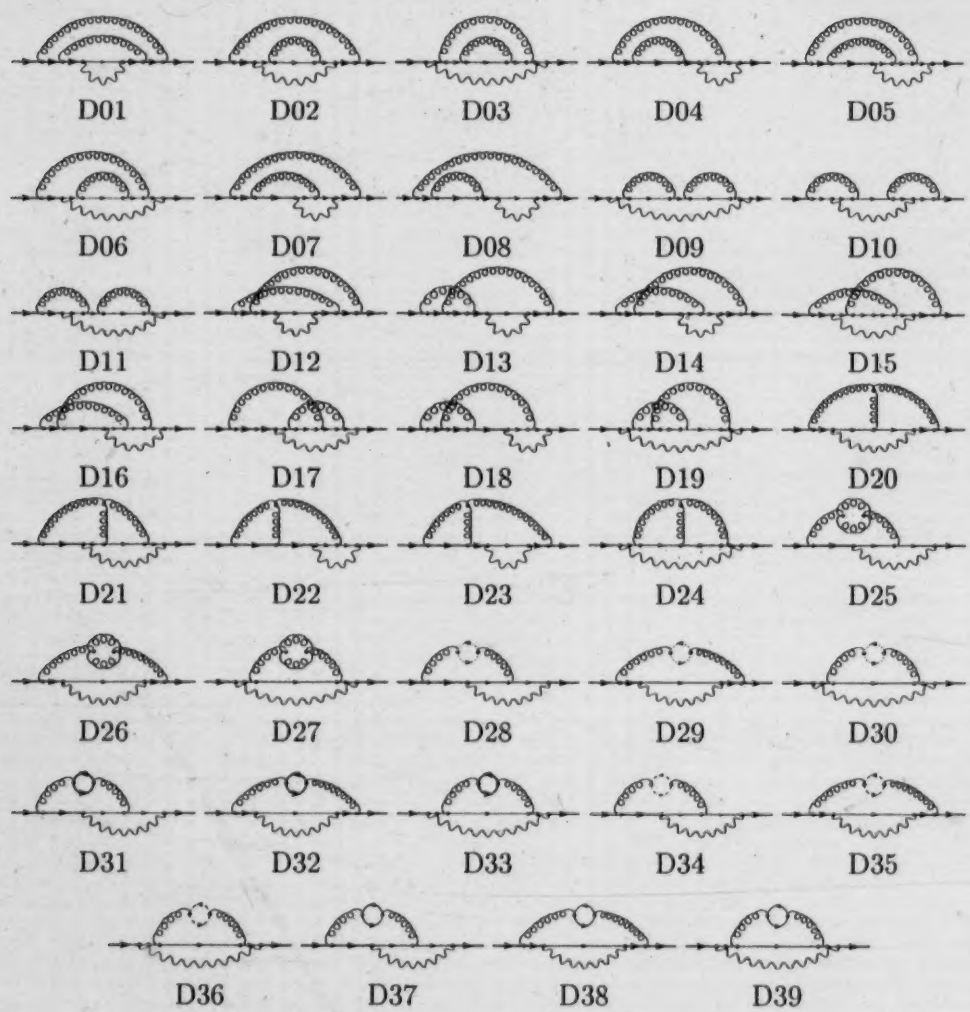

Figure B.2: $\mathcal{O}(\alpha_s^2)$ diagrams for the zero mass expansion.

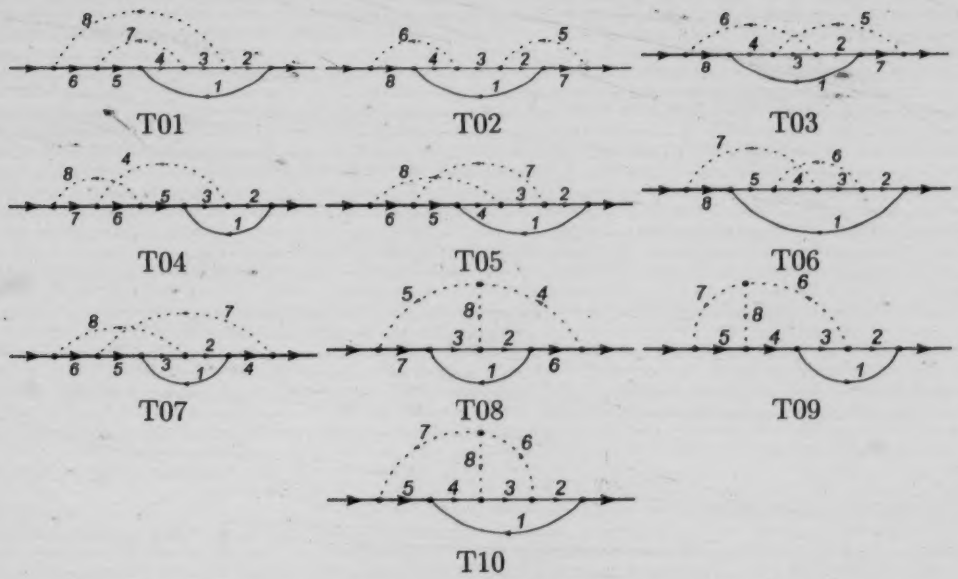

Figure B.3: Topologies to be considered for the three loop contributions.

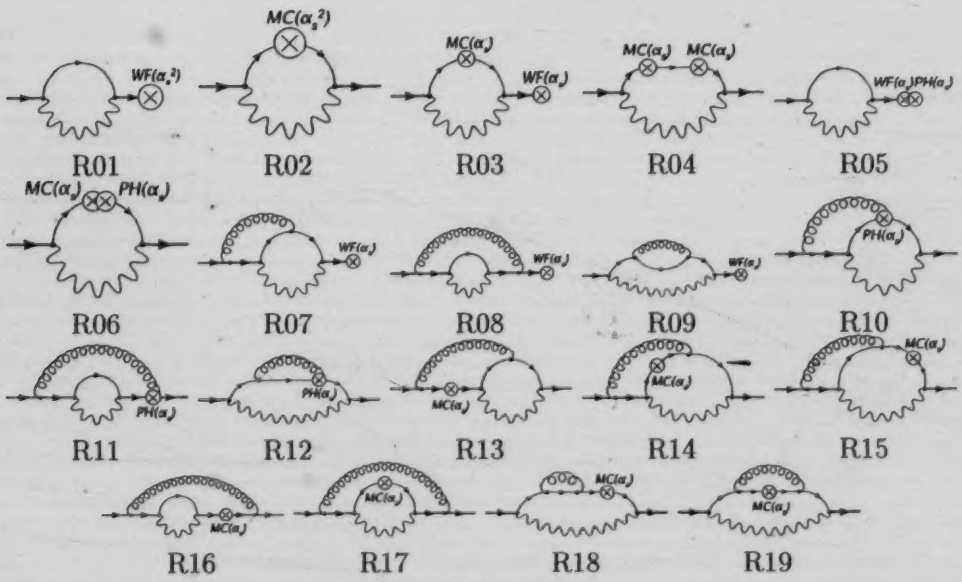

Figure B.4: $\mathcal{O}(\alpha_s^2)$ renormalization diagrams for the zero mass expansion.

B.3 Topologies And Mass Expansions

Topology T01 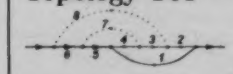	$[1] = k_1^2 + m^2$ $[2] = k_2^2 + m^2$ $[3] = k_3^2 + m^2$ $[4] = k_4^2 + m^2$ $[5] = (k_4 - k_1)^2 + M^2$ $[6] = (k_3 - k_1)^2 + M^2$ $[7] = (k_4 - k_3)^2$ $[8] = (k_3 - k_2)^2$		
Region 1 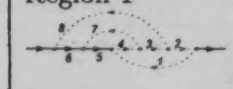	$\lvert k_1\rvert \gg m$ $\lvert k_2\rvert \gg m$ $\lvert k_3\rvert \gg m$ $\lvert k_4\rvert \gg m$	$[1] \to k_1^2$ $[2] \to k_2^2$ $[3] \to k_3^2$ $[4] \to k_4^2$	$T3c$
Region 2 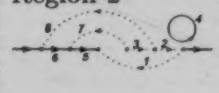	$\lvert k_1\rvert \gg m$ $\lvert k_2\rvert \gg m$ $\lvert k_3\rvert \gg m$ $\lvert k_4\rvert \sim m$	$[1] \to k_1^2$ $[2] \to k_2^2$ $[3] \to k_3^2$ $[5] \to k_1^2 + M^2$ $[7] \to k_3^2 = [3]$	$T1, gm2$
Region 3 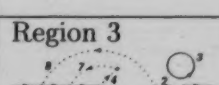	$\lvert k_1\rvert \gg m$ $\lvert k_2\rvert \gg m$ $\lvert k_3\rvert \sim m$ $\lvert k_4\rvert \gg m$	$[1] \to k_1^2$ $[2] \to k_2^2$ $[4] \to k_4^2$ $[6] \to k_1^2 + M^2$ $[7] \to k_4^2 = [4]$ $[8] \to k_2^2 = [2]$	$T2, gm2$
Region 4 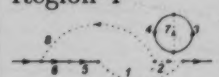	$\lvert k_1\rvert \gg m$ $\lvert k_2\rvert \gg m$ $\lvert k_3\rvert \sim m$ $\lvert k_4\rvert \sim m$	$[1] \to k_1^2$ $[2] \to k_2^2$ $[5] \to k_1^2 + M^2$ $[6] \to k_1^2 + M^2 = [5]$ $[8] \to k_2^2 = [2]$	$gm3, M3$
Region 5 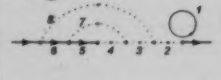	$\lvert k_1\rvert \sim m$ $\lvert k_2\rvert \gg m$ $\lvert k_3\rvert \gg m$ $\lvert k_4\rvert \gg m$	$[2] \to k_2^2$ $[3] \to k_3^2$ $[4] \to k_4^2$ $[5] \to k_4^2 + M^2$ $[6] \to k_3^2 + M^2$	$gm2, N5b,$ $N5c$
Region 6 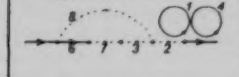	$\lvert k_1\rvert \sim m$ $\lvert k_2\rvert \gg m$ $\lvert k_3\rvert \gg m$ $\lvert k_4\rvert \sim m$	$[2] \to k_2^2$ $[3] \to k_3^2$ $[5] \to M^2$ $[6] \to k_3^2 + M^2$ $[7] \to k_3^2 = [3]$	$gm2, One$

Table 1: Expansion of topology T01 (diagrams D01,D02,D03,D04,D05,D06,D07,D08)

Topology T02 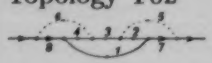	$[1] = k_1^2 + m^2$ $[2] = k_2^2 + m^2$ $[3] = k_3^2 + m^2$ $[4] = k_4^2 + m^2 [5] = (k_3 - k_2)^2$ $[6] = (k_4 - k_2)^2$ $[7] = (k_3 - k_1)^2 + M^2 [8] = (k_4 - k_1)^2 + M^2$		
Region 1 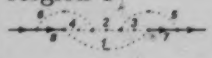	$\|k_1\| \gg m$ $\|k_2\| \gg m$ $\|k_3\| \gg m$ $\|k_4\| \gg m$	$[1] \to k_1^2$ $[2] \to k_2^2$ $[3] \to k_3^2$ $[4] \to k_4^2$	$T3k$
Region 2 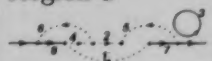	$\|k_1\| \gg m$ $\|k_2\| \gg m$ $\|k_3\| \sim m$ $\|k_4\| \gg m$	$[1] \to k_1^2$ $[2] \to k_2^2$ $[4] \to k_4^2$ $[5] \to k_2^2 = [2]$ $[7] \to k_1^2 + M^2$	$N5b, gm2$
Region 3 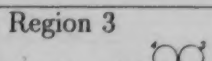	$\|k_1\| \gg m$ $\|k_2\| \gg m$ $\|k_3\| \sim m$ $\|k_4\| \sim m$	$[1] \to k_1^2$ $[2] \to k_2^2$ $[5] \to k_2^2 = [2]$ $[6] \to k_2^2 = [2]$ $[7] \to k_1^2 + M^2$ $[8] \to k_1^2 + M^2 = [7]$	$M3, gm2$
Region 4 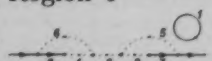	$\|k_1\| \sim m$ $\|k_2\| \gg m$ $\|k_3\| \gg m$ $\|k_4\| \gg m$	$[2] \to k_2^2$ $[3] \to k_3^2$ $[4] \to k_4^2$ $[7] \to k_3^2 + M^2$ $[8] \to k_4^2 + M^2$	$One,$ $Onshell,$ $gm2$
Region 5 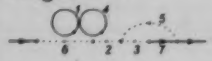	$\|k_1\| \sim m$ $\|k_2\| \gg m$ $\|k_3\| \gg m$ $\|k_4\| \sim m$	$[2] \to k_2^2$ $[3] \to k_3^2$ $[5] \to k_2^2 = [2]$ $[7] \to k_3^2 + M^2$ $[8] \to M^2$	$One, gm2$
Region 6 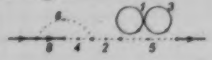	$\|k_1\| \sim m$ $\|k_2\| \gg m$ $\|k_3\| \sim m$ $\|k_4\| \gg m$	$[2] \to k_2^2$ $[4] \to k_4^2$ $[5] \to k_2^2 = [2]$ $[7] \to M^2$ $[8] \to k_4^2 + M^2$	$One, gm2$

Table 2: Expansion of topology T02 (diagrams D09,D10,D11)

Topology T03 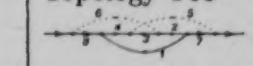	$[1] = k_1^2 + m^2$ $[2] = k_2^2 + m^2$ $[3] = k_3^2 + m^2$ $[4] = k_4^2 + m^2$ $[5] = (k_2 - k_4)^2$ $[6] = (k_2 - k_3)^2$ $[7] = (k_3 - k_1)^2 + M^2$ $[8] = (k_4 - k_1)^2 + M^2$		
Region 1 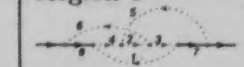	$\|k_1\| \gg m$ $\|k_2\| \gg m$ $\|k_3\| \gg m$ $\|k_4\| \gg m$	$[1] \to k_1^2$ $[2] \to k_2^2$ $[3] \to k_3^2$ $[4] \to k_4^2$	$T3i$
Region 2 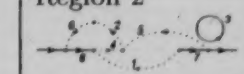	$\|k_1\| \gg m$ $\|k_2\| \gg m$ $\|k_3\| \sim m$ $\|k_4\| \gg m$	$[1] \to k_1^2$ $[2] \to k_2^2$ $[4] \to k_4^2$ $[6] \to k_2^2 = [2]$ $[7] \to k_1^2 + M^2$	$N5b, gm2$
Region 3 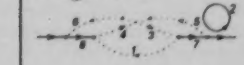	$\|k_1\| \gg m$ $\|k_2\| \sim m$ $\|k_3\| \gg m$ $\|k_4\| \gg m$	$[1] \to k_1^2$ $[3] \to k_3^2$ $[4] \to k_4^2$ $[5] \to k_4^2 = [4]$ $[6] \to k_3^2 = [3]$	$N5d, gm2$
Region 4 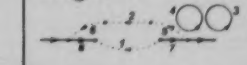	$\|k_1\| \gg m$ $\|k_2\| \gg m$ $\|k_3\| \sim m$ $\|k_4\| \sim m$	$[1] \to k_1^2$ $[2] \to k_2^2$ $[5] \to k_2^2 = [2]$ $[6] \to k_2^2 = [2]$ $[7] \to k_1^2 + M^2$ $[8] \to k_1^2 + M^2 = [7]$	$M3, gm2$
Region 5 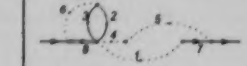	$\|k_1\| \gg m$ $\|k_2\| \sim m$ $\|k_3\| \sim m$ $\|k_4\| \gg m$	$[1] \to k_1^2$ $[4] \to k_4^2$ $[5] \to k_4^2 = [4]$ $[7] \to k_1^2 + M^2$ $[8] \to 2p(k_2 - k_3)$	$E2, M3$
Region 6 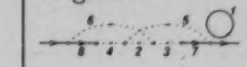	$\|k_1\| \sim m$ $\|k_2\| \gg m$ $\|k_3\| \gg m$ $\|k_4\| \gg m$	$[2] \to k_2^2$ $[3] \to k_3^2$ $[4] \to k_4^2$ $[7] \to k_3^2 + M^2$ $[8] \to k_4^2 + M^2$	$N5b, N5c,$ $N5d, gm2$
Region 7 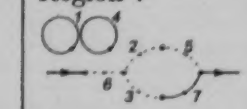	$\|k_1\| \sim m$ $\|k_2\| \gg m$ $\|k_3\| \gg m$ $\|k_4\| \sim m$	$[2] \to k_2^2$ $[3] \to k_3^2$ $[5] \to k_2^2 = [2]$ $[6] \to M^2$ $[7] \to k_3^2 + M^2$ $[8] \to M^2$	$One, gm2$

(continued on next page)

Region 8 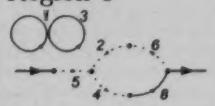	$\lvert k_1\rvert \sim m$ $\lvert k_2\rvert \gg m$ $\lvert k_3\rvert \sim m$ $\lvert k_4\rvert \gg m$	$[2] \to k_2^2$ $[4] \to k_4^2$ $[5] \to M^2$ $[6] \to k_2^2 = [2]$ $[7] \to M^2$ $[8] \to k_4^2 + M^2$	$One, gm2$
Region 9 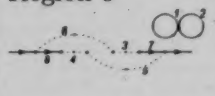	$\lvert k_1\rvert \sim m$ $\lvert k_2\rvert \sim m$ $\lvert k_3\rvert \gg m$ $\lvert k_4\rvert \gg m$	$[3] \to k_3^2$ $[4] \to k_4^2$ $[5] \to k_4^2 = [4]$ $[6] \to k_3^2 = [3]$ $[7] \to k_3^2 + M^2$ $[8] \to k_4^2 + M^2$	$One, gm2$

Table 3: Expansion of topology T03 (diagrams D15)

Topology T04 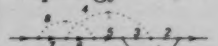	$[1] = k_1^2 + m^2$ $[2] = k_2^2 + m^2$ $[3] = k_3^2 + m^2$ $[4] = (k_3 - k_2)^2$ $[5] = (k_3 - k_1)^2 + M^2$ $[6] = (k_4 + k_3 - k_1)^2 + M^2$ $[7] = (p + k_4)^2 + M^2$ $[8] = k_4^2$		
Region 1 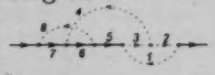	$\lvert k_1\rvert \gg m$ $\lvert k_2\rvert \gg m$ $\lvert k_3\rvert \gg m$	$[1] \to k_1^2$ $[2] \to k_2^2$ $[3] \to k_3^2$	$T3a$
Region 2	$\lvert k_1\rvert \gg m$ $\lvert k_2\rvert \gg m$ $\lvert k_3\rvert \sim m$	$[1] \to k_1^2$ $[2] \to k_2^2$ $[4] \to k_2^2 = [2]$ $[5] \to k_1^2 + M^2$ $[6] \to (k_4 - k_1)^2 + M^2$	$N5a, gm2$
Region 3	$\lvert k_1\rvert \sim m$ $\lvert k_2\rvert \gg m$ $\lvert k_3\rvert \gg m$	$[2] \to k_2^2$ $[3] \to k_3^2$ $[5] \to k_3^2 + M^2$ $[6] \to (k_3 + k_4)^2 + M^2$	$N5a, gm2$

Table 4: Expansion of topology T04 (diagrams D13,D18,D31,D32,D33)

Topology T05 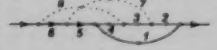	$[1] = k_1^2 + m^2$ $[2] = k_2^2 + m^2$ $[3] = k_3^2 + m^2$ $[4] = k_4^2 + m^2$ $[5] = (k_4 - k_1)^2 + M^2$ $[6] = (k_4 - k_3 + p)^2 + M^2$ $[7] = (k_3 - k_2)^2$ $[8] = (k_4 - k_3)^2$		
Region 1 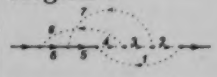	$\|k_1\| \gg m$ $\|k_2\| \gg m$ $\|k_3\| \gg m$ $\|k_4\| \gg m$	$[1] \to k_1^2$ $[2] \to k_2^2$ $[3] \to k_3^2$ $[4] \to k_4^2$	$T3b$
Region 2	$\|k_1\| \gg m$ $\|k_2\| \gg m$ $\|k_3\| \sim m$ $\|k_4\| \gg m$	$[1] \to k_1^2$ $[2] \to k_2^2$ $[4] \to k_4^2$ $[6] \to (p + k_4)^2 + M^2$ $[7] \to k_2^2 = [2]$ $[8] \to k_4^2 = [4]$	$N5a, gm2$
Region 3	$\|k_1\| \gg m$ $\|k_2\| \gg m$ $\|k_3\| \gg m$ $\|k_4\| \sim m$	$[1] \to k_1^2$ $[2] \to k_2^2$ $[3] \to k_3^2$ $[5] \to k_1^2 + M^2$ $[6] \to (p - k_3)^2 + M^2$ $[8] \to k_3^2 = [3]$	$T1, gm2$
Region 4 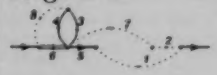	$\|k_1\| \gg m$ $\|k_2\| \gg m$ $\|k_3\| \sim m$ $\|k_4\| \sim m$	$[1] \to k_1^2$ $[2] \to k_2^2$ $[5] \to k_1^2 + M^2$ $[6] \to 2p(k_4 - k_3)$ $[7] \to k_2^2$	$One, E2$
Region 5 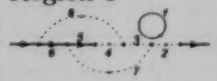	$\|k_1\| \sim m$ $\|k_2\| \gg m$ $\|k_3\| \gg m$ $\|k_4\| \gg m$	$[2] \to k_2^2$ $[3] \to k_3^2$ $[4] \to k_4^2$ $[5] \to k_4^2 + M^2$	$N5a, N5b,$ $gm2$
Region 6 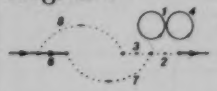	$\|k_1\| \sim m$ $\|k_2\| \gg m$ $\|k_3\| \gg m$ $\|k_4\| \sim m$	$[2] \to k_2^2$ $[3] \to k_3^2$ $[5] \to M^2$ $[6] \to (p - k_3)^2 + M^2$ $[8] \to k_4^2$	$One, gm2$

Table 5: Expansion of topology T05 (diagram D16)

Topology T06	$[1] = k_1^2 + m^2$ $[2] = k_2^2 + m^2$ $[3] = k_3^2 + m^2$ $[4] = k_4^2 + m^2$ $[5] = k_5^2 + m^2$ $[6] = (k_3 - k_2)^2$ $[7] = (k_4 - k_3)^2$ $[8] = (k_5 - k_1)^2 + M^2$ $k_5 = k_2 - k_3 + k_4$		
Region 1 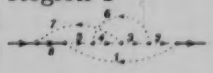	$\|k_1\| \gg m$ $\|k_2\| \gg m$ $\|k_3\| \gg m$ $\|k_4\| \gg m$ $\|k_5\| \gg m$	$[1] \to k_1^2$ $[2] \to k_2^2$ $[3] \to k_3^2$ $[4] \to k_4^2$ $[5] \to k_5^2$	$T3h(T3ng)$
Region 2 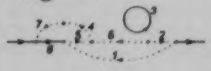	$\|k_1\| \gg m$ $\|k_2\| \gg m$ $\|k_3\| \sim m$ $\|k_4\| \gg m$ $\|k_5\| \gg m$	$[1] \to k_1^2$ $[2] \to k_2^2$ $[4] \to k_4^2$ $[5] \to k_5^2$ $[7] \to k_4^2 = [4]$ $[8] \to k_5^2 + M^2$	$N5b, gm2$
Region 3 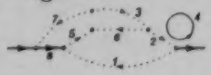	$\|k_1\| \gg m$ $\|k_2\| \gg m$ $\|k_3\| \gg m$ $\|k_4\| \sim m$ $\|k_5\| \gg m$	$[1] \to k_1^2$ $[2] \to k_2^2$ $[3] \to k_3^2$ $[5] \to k_5^2$ $[6] \to k_5^2 = [5]$ $[7] \to k_3^2 = [3]$	$T1, gm2$
Region 4 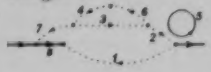	$\|k_1\| \gg m$ $\|k_2\| \gg m$ $\|k_3\| \gg m$ $\|k_4\| \gg m$ $\|k_5\| \sim m$	$[1] \to k_1^2$ $[2] \to k_2^2$ $[3] \to k_3^2$ $[4] \to k_4^2$ $[6] \to k_4^2 = [4]$ $[7] \to k_2^2 = [2]$ $[8] \to k_1^2 + M^2$	$One, gm2$
Region 5 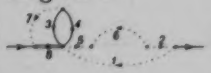	$\|k_1\| \gg m$ $\|k_2\| \gg m$ $\|k_3\| \gg m$ $\|k_4\| \gg m$ $\|k_5\| \sim m$	$[1] \to k_1^2$ $[2] \to k_2^2$ $[3] \to k_3^2$ $[4] \to k_4^2$ $[6] \to k_4^2 = [4]$ $[7] \to k_2^2 + M^2$ $[8] \to k_1^2 + M^2$	$E2, One$
Region 6 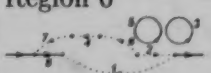	$\|k_1\| \gg m$ $\|k_2\| \gg m$ $\|k_3\| \sim m$ $\|k_4\| \gg m$ $\|k_5\| \sim m$	$[1] \to k_1^2$ $[2] \to k_4^2 = [4]$ $[4] \to k_4^2$ $[6] \to k_4^2 = [4]$ $[7] \to k_4^2 + M^2$ $[8] \to k_1^2 + M^2$	$M3, gm2$

(continued on next page)

Region 7 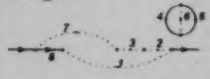	$\|k_1\| \gg m$ $\|k_2\| \gg m$ $\|k_3\| \gg m$ $\|k_4\| \sim m$ $\|k_5\| \sim m$	$[1] \to k_1^2$ $[2] \to k_2^2$ $[3] \to k_2^2 = [2]$ $[7] \to k_2^2 + M^2$ $[8] \to k_1^2 + M^2$	$M3, gm3$
Region 8 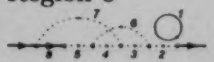	$\|k_1\| \sim m$ $\|k_2\| \gg m$ $\|k_3\| \gg m$ $\|k_4\| \gg m$ $\|k_5\| \gg m$	$[2] \to k_2^2$ $[3] \to k_3^2$ $[4] \to k_4^2$ $[5] \to k_5^2$ $[8] \to k_5^2 + M^2$	$N5b, N5c,$ $gm2$
Region 9	$\|k_1\| \sim m$ $\|k_2\| \gg m$ $\|k_3\| \gg m$ $\|k_4\| \gg m$ $\|k_5\| \sim m$	$[2] \to k_2^2$ $[3] \to k_3^2$ $[4] \to k_4^2$ $[6] \to k_4^2 = [4]$ $[7] \to k_2^2 = [2]$ $[8] \to M^2$	$One, gm2$
Region 10 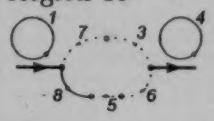	$\|k_1\| \sim m$ $\|k_2\| \gg m$ $\|k_3\| \gg m$ $\|k_4\| \sim m$ $\|k_5\| \gg m$	$[2] \to k_2^2$ $[3] \to k_3^2$ $[5] \to k_5^2$ $[6] \to k_5^2 = [5]$ $[7] \to k_3^2 = [3]$ $[8] \to k_5^2 + M^2$	$One, gm2$
Region 11 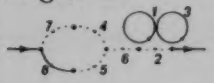	$\|k_1\| \sim m$ $\|k_2\| \gg m$ $\|k_3\| \sim m$ $\|k_4\| \gg m$ $\|k_5\| \gg m$	$[2] \to k_2^2$ $[4] \to k_4^2$ $[5] \to k_5^2$ $[6] \to k_2^2 = [2]$ $[7] \to k_4^2 = [4]$ $[8] \to k_5^2 + M^2$	$One, gm2$

Table 6: Expansion of topology T06 (diagrams D17,D19,D37,D38,D39)

Topology T07 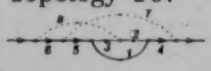	$[1] = k_1^2 + m^2$ $[2] = k_2^2 + m^2$ $[3] = k_3^2 + m^2$ $[4] = (k_2 - k_1)^2 + M^2$ $[5] = (k_3 - k_1)^2 + M^2$ $[6] = (k_3 - k_2 + p)^2 + M^2$ $[7] = (k_2 - k_1 - p)^2$ $[8] = (k_3 - k_2)^2$		
Region 1 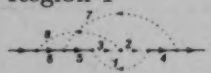	$\|k_1\| \gg m$ $\|k_2\| \gg m$ $\|k_3\| \gg m$	$[1] \to k_1^2$ $[2] \to k_2^2$ $[3] \to k_3^2$	$T3c$
Region 2 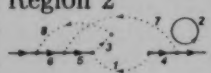	$\|k_1\| \gg m$ $\|k_2\| \sim m$ $\|k_3\| \gg m$	$[1] \to k_1^2$ $[3] \to k_3^2$ $[4] \to k_1^2 + M^2$ $[6] \to (p + k_3)^2 + M^2$ $[7] \to (p + k_1)^2$ $[8] \to k_3^2 = [3]$	$N5a, gm2$
Region 3 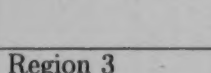	$\|k_1\| \gg m$ $\|k_2\| \gg m$ $\|k_3\| \sim m$	$[1] \to k_1^2$ $[2] \to k_2^2$ $[5] \to k_1^2 + M^2$ $[6] \to (p - k_2)^2 + M^2$ $[8] \to k_2^2 = [2]$	$N5d, gm2$
Region 4	$\|k_1\| \gg m$ $\|k_2\| \sim m$ $\|k_3\| \sim m$	$[1] \to k_1^2$ $[4] \to k_1^2 + M^2$ $[5] \to k_1^2 + M^2 = [4]$ $[6] \to 2p(k_3 - k_2)$	$E2, M3$
Region 5	$\|k_1\| \sim m$ $\|k_2\| \gg m$ $\|k_3\| \gg m$	$[2] \to k_2^2$ $[3] \to k_3^2$ $[4] \to k_2^2 + M^2$ $[5] \to k_3^2 + M^2$ $[7] \to (k_2 - p)^2$	$N5a, N5b,$ $N5d, gm2$
Region 6 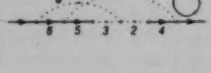	$\|k_1\| \sim m$ $\|k_2\| \gg m$ $\|k_3\| \sim m$	$[2] \to k_2^2$ $[4] \to k_2^2 + M^2$ $[5] \to M^2$ $[6] \to (p - k_2)^2 + M^2$ $[7] \to (p - k_2)^2$	$One, gm2$

Table 7: Expansion of topology T07 (diagrams D12,D14)

Topology T08 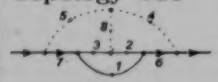	$[1] = k_1^2 + m^2$ $[2] = k_2^2 + m^2$ $[3] = k_3^2 + m^2$ $[4] = (k_2 - k_1 - p)^2$ $[5] = (k_3 - k_1 - p)^2$ $[6] = (k_2 - k_1)^2 + M^2$ $[7] = (k_3 - k_1)^2 + M^2$ $[8] = (k_2 - k_3)^2$		
Region 1 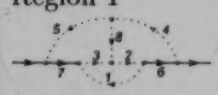	$\|k_1\| \gg m$ $\|k_2\| \gg m$ $\|k_3\| \gg m$	$[1] \to k_1^2$ $[2] \to k_2^2$ $[3] \to k_3^2$	$T3nd$
Region 2 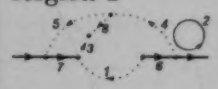	$\|k_1\| \gg m$ $\|k_2\| \gg m$ $\|k_3\| \sim m$ $+k_1 \to k_2$	$[1] \to k_1^2$ $[2] \to k_2^2$ $[5] \to (k_3 - p)^2$ $[7] \to k_3^2 + M^2$ $[8] \to k_1^2 + M^2$	$T1, gm2$
Region 3	$\|k_1\| \gg m$ $\|k_2\| \sim m$ $\|k_3\| \sim m$	$[1] \to k_1^2$ $[4] \to (p + k_1)^2$ $[5] \to (p + k_1)^2 = [4]$ $[6] \to k_1^2 + M^2$ $[7] \to k_1^2 + M^2 = [6]$	$M3, gm3$
Region 4 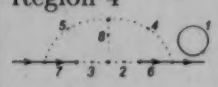	$\|k_1\| \sim m$ $\|k_2\| \gg m$ $\|k_3\| \gg m$	$[2] \to k_2^2$ $[3] \to k_3^2$ $[4] \to (k_2 - p)^2$ $[5] \to (k_3 - p)^2$ $[6] \to k_2^2 + M^2$ $[7] \to k_3^2 + M^2$	$N5b, N5c,$ $gm2$
Region 5	$\|k_1\| \sim m$ $\|k_2\| \gg m$ $\|k_3\| \sim m$	$[2] \to k_2^2$ $[4] \to (k_2 - p)^2$ $[5] \to p^2$ $[6] \to k_2^2 + M^2$ $[7] \to M^2$ $[8] \to k_2^2 = [2]$	$One, gm2$
Region 6	$\|k_1\| \sim m$ $\|k_2\| \sim m$ $\|k_3\| \gg m$	$[3] \to k_3^2$ $[4] \to p^2$ $[5] \to (k_3 - p)^2$ $[6] \to M^2$ $[7] \to k_3^2 + M^2$ $[8] \to k_3^2 = [3]$	$One, gm2$

Table 8: Expansion of topology T08 (diagram D20)

Topology T09 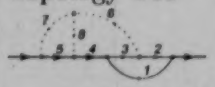	$[1] = k_1^2 + m^2$ $[2] = k_2^2 + m^2$ $[3] = k_3^2 + m^2$ $[4] = (k_3 - k_1)^2 + M^2$ $[5] = k_4^2 + M^2$ $[6] = (k_3 - k_2)^2$ $[7] = (k_4 - p)^2$ $[8] = (p + k_3 - k_2 - k_4)^2$		
Region 1 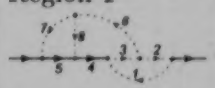	$\|k_1\| \gg m$ $\|k_2\| \gg m$ $\|k_3\| \gg m$	$[1] \to k_1^2$ $[2] \to k_2^2$ $[3] \to k_3^2$	$T3ne$
Region 2	$\|k_1\| \gg m$ $\|k_2\| \gg m$ $\|k_3\| \sim m$	$[1] \to k_1^2$ $[2] \to k_2^2$ $[4] \to k_1^2 + M^2$ $[6] \to k_2^2 = [2]$ $[8] \to (p - k_2 - k_4)^2$	$T1, gm2$
Region 3 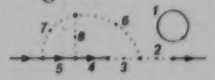	$\|k_1\| \sim m$ $\|k_2\| \gg m$ $\|k_3\| \gg m$	$[2] \to k_2^2$ $[3] \to k_3^2$ $[4] \to k_3^2 + M^2$	$N5d, gm2$
Region 4 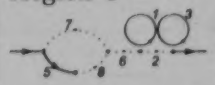	$\|k_1\| \sim m$ $\|k_2\| \gg m$ $\|k_3\| \sim m$	$[2] \to k_2^2$ $[4] \to M^2$ $[6] \to k_2^2$ $[8] \to k_4^2$	$One, gm2$

Table 9: Expansion of topology T09 (diagram D22,D23)

Topology T10 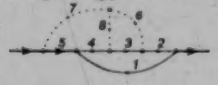	$[1] = k_1^2 + m^2$ $[2] = k_2^2 + m^2$ $[3] = k_3^2 + m^2$ $[4] = k_4^2 + m^2$ $[5] = (k_4 - k_1)^2 + M^2$ $[6] = (k_3 - k_2)^2$ $[7] = (k_4 - k_1 - p)^2$ $[8] = (k_3 - k_4)^2$		
Region 1 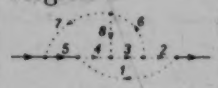	$\|k_1\| \gg m$ $\|k_2\| \gg m$ $\|k_3\| \gg m$ $\|k_4\| \gg m$	$[1] \to k_1^2$ $[2] \to k_2^2$ $[3] \to k_3^2$ $[4] \to k_4^2$	$T3ng(T3h)$
Region 2 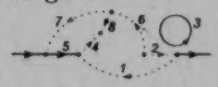	$\|k_1\| \gg m$ $\|k_2\| \gg m$ $\|k_3\| \sim m$ $\|k_4\| \gg m$	$[1] \to k_1^2$ $[2] \to k_2^2$ $[4] \to k_4^2$ $[6] \to k_2^2 = [2]$ $[8] \to k_4^2 = [4]$	$N5b, gm2$
Region 3 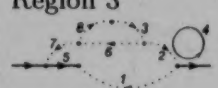	$\|k_1\| \gg m$ $\|k_2\| \gg m$ $\|k_3\| \gg m$ $\|k_4\| \sim m$	$[1] \to k_1^2$ $[2] \to k_2^2$ $[3] \to k_3^2$ $[5] \to k_1^2 + M^2$ $[7] \to k_2^2 = [2]$ $[8] \to k_3^2 = [3]$	$N5c, gm2$
Region 4 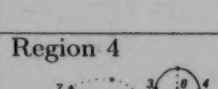	$\|k_1\| \gg m$ $\|k_2\| \gg m$ $\|k_3\| \sim m$ $\|k_4\| \sim m$	$[1] \to k_1^2$ $[2] \to k_2^2$ $[5] \to k_1^2 + M^2$ $[6] \to k_2^2 = [2]$ $[7] \to k_2^2 = [2]$	$M3, gm3$
Region 5 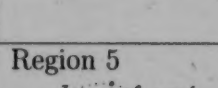	$\|k_1\| \sim m$ $\|k_2\| \gg m$ $\|k_3\| \gg m$ $\|k_4\| \gg m$	$[2] \to k_2^2$ $[3] \to k_3^2$ $[4] \to k_4^2$ $[5] \to k_4^2 + M^2$ $[6] \to (k_3 - p)^2$ $[7] \to (k_4 - p)^2$	$N5b, N5c,$ $gm2$
Region 6	$\|k_1\| \sim m$ $\|k_2\| \gg m$ $\|k_3\| \gg m$ $\|k_4\| \sim m$	$[2] \to k_2^2$ $[3] \to k_3^2$ $[5] \to M^2$ $[6] \to (k_3 - p)^2$ $[7] \to p^2$ $[8] \to k_3^2 = [3]$	$One, gm2$
Region 7	$\|k_1\| \sim m$ $\|k_2\| \gg m$ $\|k_3\| \sim m$ $\|k_4\| \gg m$	$[2] \to k_2^2$ $[4] \to k_4^2$ $[5] \to k_4^2 + M^2$ $[6] \to p^2$ $[7] \to (k_4 - p)^2$ $[8] \to k_4^2 = [4]$	$One, gm2$

Table 10: Expansion of topology T10 (diagrams D21,D24-D30,D34,D35,D36)

Appendix C

Full NNLO Expansions

For completeness, in this appendix we present the full NNLO results for both the expansion from zero recoil and the expansion from zero mass. The same colour factor separation and definitions as presented in Chapter 4 are used here and both expansions are presented in the S_2 scheme.

C.1 Expansion From Zero Recoil

$$
\begin{aligned}
X_H \;= \sqrt{\beta}\;\Bigg[&\frac{509}{48}+\frac{999}{32}R_2+\frac{87}{16}\ln 2+\frac{337}{64}\ln^2 2+\frac{75\pi^2}{128}\\
&+\beta\left(\frac{7937}{864}+\frac{1449}{32}R_2+\frac{275}{144}\ln 2+\frac{767}{64}\ln^2 2+\frac{655\pi^2}{384}\right)\\
&+\beta^2\left(\frac{610309}{51840}+\frac{204969}{2560}R_2+\frac{59519}{17280}\ln 2+\frac{973327}{46080}\ln^2 2+\frac{317957\pi^2}{92160}\right)\\
&+\beta^3\left(\frac{559481}{43200}+\frac{489121}{4480}R_2+\frac{17743}{10080}\ln 2+\frac{832541}{26880}\ln^2 2+\frac{275551\pi^2}{53760}\right)\\
&+\beta^4\left(\frac{65321021}{4838400}+\frac{11797175}{86016}R_2-\frac{305099}{322560}\ln 2+\frac{7077193}{172032}\ln^2 2\right.\\
&\left.+\frac{7052617\pi^2}{1032192}\right)\\
&+\beta^5\left(\frac{45630434489}{3353011200}+\frac{22241075}{135168}R_2-\frac{133936361}{31933440}\ln 2\right.\\
&\left.+\frac{125347637}{2433024}\ln^2 2+\frac{41697895\pi^2}{4866048}\right)\\
&+\beta^6\left(\frac{138502225529}{10332241920}+\frac{3590593927}{18743296}R_2-\frac{11536715287}{1476034560}\ln 2\right.\\
&\left.+\frac{6978512747}{112459776}\ln^2 2+\frac{2323112569\pi^2}{224919552}\right)
\end{aligned}
$$

$$+\beta^7 \left(\frac{45203268520457}{3487131648000}+\frac{214621597}{983040}R_2-\frac{302266607}{25804800}\ln 2 + \frac{142942819}{1966080}\ln^2 2+\frac{142811747\pi^2}{11796480}\right)$$

$$+\beta^8 \left(\frac{245387073590867}{19898597376000}+\frac{196431898241}{802160640}R_2-\frac{8997835501817}{568531353600}\ln 2 + \frac{44625976789}{534773760}\ln^2 2+\frac{133787752831\pi^2}{9625927680}\right)\Bigg]$$

$$X_L = \sqrt{\beta}\ \Bigg[\frac{11}{12}+\frac{1}{16}\ln 2-\frac{9}{8}\ln^2 2$$

$$+\beta \left(\frac{3131}{864}-\frac{13}{9}\ln\beta+\frac{1}{6}\ln^2\beta-\frac{503}{144}\ln 2+\frac{2}{3}\ln 2\ln\beta-\frac{1}{24}\ln^2 2-\frac{\pi^2}{9}\right)$$

$$+\beta^2 \left(\frac{1505969}{648000}-\frac{1667}{1350}\ln\beta+\frac{7}{45}\ln^2\beta-\frac{13613}{10800}\ln 2+\frac{28}{45}\ln 2\ln\beta + \frac{14}{45}\ln^2 2-\frac{14\pi^2}{135}\right)$$

$$+\beta^3 \left(\frac{152217113}{74088000}-\frac{11056}{11025}\ln\beta+\frac{11}{105}\ln^2\beta-\frac{228593}{176400}\ln 2 + \frac{44}{105}\ln 2\ln\beta+\frac{22}{105}\ln^2 2-\frac{22\pi^2}{315}\right)$$

$$+\beta^4 \left(\frac{42184943}{33339600}-\frac{1937}{2646}\ln\beta+\frac{5}{63}\ln^2\beta-\frac{515617}{635040}\ln 2+\frac{20}{63}\ln 2\ln\beta + \frac{10}{63}\ln^2 2-\frac{10\pi^2}{189}\right)$$

$$+\beta^5 \left(\frac{68030086321}{76071441600}-\frac{162025}{274428}\ln\beta+\frac{19}{297}\ln^2\beta-\frac{3569219}{6586272}\ln 2 + \frac{76}{297}\ln 2\ln\beta+\frac{38}{297}\ln^2 2-\frac{38\pi^2}{891}\right)$$

$$+\beta^6 \left(\frac{24534728569669}{37139768265600}-\frac{1923512}{3864861}\ln\beta+\frac{23}{429}\ln^2\beta-\frac{352795}{981552}\ln 2 + \frac{92}{429}\ln 2\ln\beta+\frac{46}{429}\ln^2 2-\frac{46\pi^2}{1287}\right)$$

$$+\beta^7 \left(\frac{25223352346307}{50645138544000}-\frac{7580887}{17567550}\ln\beta+\frac{3}{65}\ln^2\beta-\frac{4555351}{20077200}\ln 2 + \frac{12}{65}\ln 2\ln\beta+\frac{6}{65}\ln^2 2-\frac{2\pi^2}{65}\right)$$

$$+\beta^8 \left(\frac{86798855874227773}{229679599076928000}-\frac{74533181}{195270075}\ln\beta+\frac{31}{765}\ln^2\beta\right.$$

$$-\frac{4722926209}{37491854400}\ln 2+\frac{124}{765}\ln 2\ln\beta+\frac{62}{765}\ln^2 2-\frac{62\pi^2}{2295}\Big)\Big]$$

$$\begin{aligned}
X_S \;=\sqrt{\beta}\;&\Big[\frac{361}{96}-\frac{621}{256}R_2-\frac{25}{64}\ln 2-\frac{531}{512}\ln^2 2-\frac{1445\pi^2}{3072}\\
&-\beta\;\Big(\frac{757}{864}+\frac{207}{256}R_2+\frac{91}{576}\ln 2+\frac{1}{3}\ln 2\ln\beta+\frac{2579}{1536}\ln^2 2-\frac{433\pi^2}{3072}\Big)\\
&+\beta^2\;\Big(\frac{287639}{414720}-\frac{1}{6}\ln\beta-\frac{3243}{20480}R_2+\frac{1120967}{691200}\ln 2-\frac{14}{45}\ln 2\ln\beta\\
&\quad-\frac{85913}{73728}\ln^2 2-\frac{51907\pi^2}{442368}\Big)\\
&+\beta^3\;\Big(\frac{237277}{967680}-\frac{43}{180}\ln\beta-\frac{66027}{143360}R_2+\frac{10336187}{11289600}\ln 2-\frac{22}{105}\ln 2\ln\beta\\
&\quad-\frac{104563}{172032}\ln^2 2-\frac{62849\pi^2}{1032192}\Big)\\
&+\beta^4\;\Big(\frac{29369849}{270950400}-\frac{5}{21}\ln\beta-\frac{767311}{3440640}R_2+\frac{105336121}{162570240}\ln 2\\
&\quad-\frac{10}{63}\ln 2\ln\beta-\frac{10805267}{20643840}\ln^2 2-\frac{177487\pi^2}{8257536}\Big)\\
&+\beta^5\;\Big(\frac{2346322057}{26824089600}-\frac{1703}{7560}\ln\beta-\frac{6493703}{37847040}R_2+\frac{4231170007}{8430428160}\ln 2\\
&\quad-\frac{38}{297}\ln 2\ln\beta-\frac{26382563}{61931520}\ln^2 2-\frac{13682239\pi^2}{817496064}\Big)\\
&+\beta^6\;\Big(\frac{5710531034333}{122747034009600}-\frac{1753}{8316}\ln\beta-\frac{450064037}{3148873728}R_2\\
&\quad+\frac{6784395955399}{15197251829760}\ln 2-\frac{46}{429}\ln 2\ln\beta-\frac{750355913}{2099249152}\ln^2 2\\
&\quad-\frac{180380435\pi^2}{12595494912}\Big)\\
&+\beta^7\;\Big(\frac{56144856613663}{7978557210624000}-\frac{88799}{450450}\ln\beta-\frac{7113891}{57671680}R_2\\
&\quad+\frac{2920127357507}{6907841740800}\ln 2-\frac{6}{65}\ln 2\ln\beta-\frac{92233509}{299892736}\ln^2 2\\
&\quad-\frac{15790523\pi^2}{1245708288}\Big)\\
&-\beta^8\;\Big(\frac{92242933789654507}{3255251341934592000}+\frac{1498489}{8108100}\ln\beta+\frac{99837139559}{917671772160}R_2\\
&\quad-\frac{4576565816272799}{11056797764812800}\ln 2+\frac{62}{765}\ln 2\ln\beta+\frac{99030009733}{367068708864}\ln^2 2\\
&\quad+\frac{931916709\pi^2}{81570824192}\Big)\Big]
\end{aligned}$$

$$
\begin{aligned}
X_A \;=\sqrt{\beta}\;\Bigg[&\frac{3}{32}\zeta_3-\frac{151}{48}+\frac{291}{64}R_2+\frac{3}{16}f_3+\frac{5}{128}f_4+\frac{7}{64}\ln 2+\frac{345}{128}\ln^2 2\\
&+\frac{415\pi^2}{768}-\frac{71\pi^2}{96}\ln 2+\frac{19}{256}f_1\\
+\beta\;&\Bigg(\zeta_3-\frac{13453}{864}+\frac{325}{72}\ln\beta-\frac{11}{24}\ln^2\beta-\frac{465}{512}R_2+\frac{1}{32}f_3-\frac{7}{192}f_4\\
&+\frac{1913}{128}\ln 2-\frac{11}{6}\ln 2\ln\beta-\frac{25301}{27648}\ln^2(2)+\frac{30839\pi^2}{55296}-\frac{\pi^2}{12}\ln\beta\\
&-\frac{\pi^2}{4}\ln 2+\frac{37}{384}f_1\Bigg)\\
-\beta^2\;&\Bigg(\frac{24620749}{2592000}+\frac{11}{40}\zeta_3-\frac{21937}{5400}\ln\beta+\frac{77}{180}\ln^2\beta-\frac{9779}{3840}R_2+\frac{1}{20}f_3\\
&+\frac{47}{640}f_4-\frac{1213}{200}\ln 2+\frac{77}{45}\ln 2\ln\beta+\frac{332033}{207360}\ln^2 2-\frac{1788217\pi^2}{2073600}\\
&+\frac{7\pi^2}{90}\ln\beta+\frac{71\pi^2}{480}\ln 2+\frac{19}{3840}f_1\Bigg)\\
+\beta^3\;&\Bigg(\frac{143}{280}\zeta_3-\frac{306021494399}{42674688000}+\frac{199637}{66150}\ln\beta-\frac{121}{420}\ln^2\beta+\frac{761419}{1720320}R_2\\
&+\frac{2}{105}f_3-\frac{1}{60}f_4+\frac{17586639079}{3657830400}\ln 2-\frac{121}{105}\ln 2\ln\beta\\
&-\frac{135914773}{358318080}\ln^2 2+\frac{55337441843\pi^2}{175575859200}-\frac{11\pi^2}{210}\ln\beta-\frac{163\pi^2}{1260}\ln 2\\
&-\frac{1}{280}f_1\Bigg)\\
+\beta^4\;&\Bigg(\frac{253}{840}\zeta_3-\frac{31554158310737}{5761082880000}+\frac{9158899}{3969000}\ln\beta+\frac{28131181}{25804800}R_2\\
&-\frac{55}{252}\ln^2\beta+\frac{1}{420}f_3-\frac{11}{1260}f_4+\frac{1838523203161}{493807104000}\ln 2-\frac{55}{63}\ln 2\ln\beta\\
&-\frac{33304290763}{48372940800}\ln^2 2+\frac{1759880112133\pi^2}{4740548198400}-\frac{5\pi^2}{126}\ln\beta-\frac{127\pi^2}{1260}\ln 2\\
&-\frac{1}{630}f_1\Bigg)\\
+\beta^5\;&\Bigg(\frac{439}{1848}\zeta_3-\frac{4144742338781819}{1195013191680000}+\frac{22898593}{12474000}\ln\beta+\frac{216371011}{378470400}R_2\\
&-\frac{19}{108}\ln^2\beta+\frac{1}{2310}f_3-\frac{5}{924}f_4+\frac{20544855025817}{9311791104000}\ln 2-\frac{19}{27}\ln 2\ln\beta\\
&-\frac{18438671811899}{44696597299200}\ln^2 2+\frac{35053470717493\pi^2}{140475020083200}-\frac{19\pi^2}{594}\ln\beta\\
&-\frac{1181\pi^2}{13860}\ln 2-\frac{5}{5544}f_1\Bigg)
\end{aligned}
$$

$$
\begin{aligned}
&+\beta^6 \quad \left(\frac{4787}{24024}\zeta_3 - \frac{263591499991597941509}{90971633980491264000} + \frac{5305903765}{3408807402}\ln\beta\right.\\
&\quad -\frac{23}{156}\ln^2\beta + \frac{3376621229}{5166120960}R_2 + \frac{671133099613976429}{381699163554508800}\ln 2\\
&\quad -\frac{23}{39}\ln 2\ln\beta - \frac{1}{36036}f_3 - \frac{19}{5148}f_4 - \frac{807494967124639}{1830325659402240}\ln^2 2\\
&\quad \left.-\frac{1141\pi^2}{15444}\ln 2 + \frac{12509819248109819\pi^2}{52347313858904064} - \frac{23\pi^2}{858}\ln\beta - \frac{1}{1716}f_1\right)\\
&+\beta^7 \quad \left(\frac{2957}{17160}\zeta_3 - \frac{4378705818571605642806317}{20959864469105187225600000} + \frac{19599846143}{14567553000}\ln\beta\right.\\
&\quad -\frac{33}{260}\ln^2\beta - \frac{1}{6435}f_3 - \frac{23}{8580}f_4 + \frac{1966537403323028633561}{1758869745659176550400}\ln 2\\
&\quad +\frac{17304456498367}{39675808972800}R_2 - \frac{33}{65}\ln 2\ln\beta - \frac{13615427593349080271}{42170703192627609600}\ln^2 2\\
&\quad \left.+\frac{405991007361016947 97\pi^2}{219287656601663569920} - \frac{3\pi^2}{130}\ln\beta - \frac{5033\pi^2}{77220}\ln 2 - \frac{7}{17160}f_1\right)\\
&+\beta^8 \quad \left(\frac{14783}{97240}\zeta_3 - \frac{50050009410668813377666683931}{28084312946376486774374400000} + \frac{7770892507}{6527599650}\ln\beta\right.\\
&\quad +\frac{44883901561063}{96355536076800}R_2 + \frac{17079399912473708158441}{19804416486837741158400}\ln 2\\
&\quad -\frac{20272170727481170913}{61448738937828802560}\ln^2 2 + \frac{1420067336922129323 99\pi^2}{803560432263915110400}\\
&\quad -\frac{341}{3060}\ln^2\beta - \frac{9}{48620}f_3 - \frac{9}{4420}f_4 - \frac{341}{765}\ln 2\ln\beta - \frac{31\pi^2}{1530}\ln\beta\\
&\quad \left.\left.-\frac{8501\pi^2}{145860}\ln 2 - \frac{1}{3315}f_1\right)\right]
\end{aligned}
$$

$$
\begin{aligned}
X_F \;&= \sqrt{\beta}\;\left[\frac{117}{16} - \frac{57}{32}\zeta_3 - \frac{291}{32}R_2 - \frac{3}{8}f_3 - \frac{5}{64}f_4 - \frac{957}{64}\ln 2 + \frac{409}{64}\ln^2 2\right.\\
&\quad \left.-\frac{173\pi^2}{384} + \frac{13\pi^2}{12}\ln 2 - \frac{19}{128}f_1\right.\\
&+\beta \quad \left(\frac{313}{128} + \frac{25}{32}\zeta_3 - 2\ln\beta + \frac{465}{256}R_2 - \frac{1}{16}f_3 + \frac{7}{96}f_4 - \frac{1825}{144}\ln 2\right.\\
&\quad \left.+\frac{9}{4}\ln 2\ln\beta + \frac{179813}{13824}\ln^2 2 - \frac{6071\pi^2}{27648} + \frac{55\pi^2}{144}\ln 2 - \frac{37}{192}f_1\right)\\
&+\beta^2 \quad \left(\frac{1961473}{172800} - \frac{1}{5}\zeta_3 - \frac{907}{360}\ln\beta + \frac{1}{6}\ln^2\beta - \frac{9779}{1920}R_2 + \frac{1}{10}f_3 + \frac{47}{320}f_4\right.\\
&\quad -\frac{951211}{43200}\ln 2 + \frac{103}{30}\ln 2\ln\beta + \frac{1274369}{103680}\ln^2 2 - \frac{49733\pi^2}{207360}\\
&\quad \left.-\frac{193\pi^2}{240}\ln 2 + \frac{19}{1920}f_1\right)
\end{aligned}
$$

$$
\begin{aligned}
&+\beta^3 \quad \left(\frac{5937450497}{3048192000}+\frac{27}{70}\zeta_3-\frac{230359}{75600}\ln\beta+\frac{23}{90}\ln^2\beta-\frac{761419}{860160}R_2\right.\\
&\quad -\frac{4}{105}f_3+\frac{1}{30}f_4+\frac{11493917587}{1254113280}\ln^2 2+\frac{311118671\pi^2}{2508226560}\\
&\quad \left.-\frac{20159773639}{1828915200}\ln 2+\frac{2179}{630}\ln 2\ln\beta-\frac{2\pi^2}{21}\ln 2+\frac{1}{140}f_1\right)\\
&+\beta^4 \quad \left(\frac{522094668017}{115221657600}+\frac{5}{21}\zeta_3-\frac{1904759}{661500}\ln\beta-\frac{28131181}{12902400}R_2-\frac{1}{210}f_3\right.\\
&\quad -\frac{2749179423913}{246903552000}\ln 2+\frac{3389}{1050}\ln 2\ln\beta+\frac{1507989932173}{169305292800}\ln^2 2\\
&\quad \left.+\frac{283}{1050}\ln^2\beta+\frac{11}{630}f_4-\frac{55213660051\pi^2}{338610585600}-\frac{139\pi^2}{945}\ln 2+\frac{1}{315}f_1\right)\\
&+\beta^5 \quad \left(\frac{126350435017}{44341862400}+\frac{443}{2310}\zeta_3+\frac{119}{450}\ln^2\beta-\frac{216371011}{189235200}R_2\right.\\
&\quad -\frac{22744297}{8316000}\ln\beta-\frac{1}{1155}f_3+\frac{5}{462}f_4-\frac{450130690189651}{51214851072000}\ln 2\\
&\quad +\frac{14747}{4950}\ln 2\ln\beta+\frac{170186952000827}{22348298649600}\ln^2 2-\frac{1730791200569\pi^2}{44696597299200}\\
&\quad \left.-\frac{446\pi^2}{3465}\ln 2+\frac{5}{2772}f_1\right)\\
&+\beta^6 \quad \left(\frac{57998933463276174371}{24492362994747648000}-\frac{933522061}{388468080}\ln\beta+\frac{7387}{29106}\ln^2\beta\right.\\
&\quad -\frac{3376621229}{2583060480}R_2+\frac{1}{18018}f_3+\frac{19}{2574}f_4-\frac{126728876077850311}{17349961979750400}\ln 2\\
&\quad +\frac{163}{1001}\zeta_3+\frac{6472416203154079}{915162829701120}\ln^2 2-\frac{178706339563 09\pi^2}{183032565940224}\\
&\quad \left.+\frac{1042109}{378378}\ln 2\ln\beta-\frac{1003\pi^2}{9009}\ln 2+\frac{1}{858}f_1\right)\\
&+\beta^7 \quad \left(\frac{11052212985169752020129083}{7335952564186815528960000}+\frac{203}{1430}\zeta_3-\frac{429093000827}{189378189000}\ln\beta\right.\\
&\quad +\frac{152497}{630630}\ln^2\beta-\frac{17304456498367}{19837904486400}R_2+\frac{2}{6435}f_3+\frac{23}{4290}f_4\\
&\quad +\frac{133792959866261710031}{21085351596313804800}\ln^2 2-\frac{19862438969692106 93\pi^2}{42170703192627609600}\\
&\quad -\frac{1882\pi^2}{19305}\ln 2+\frac{7}{8580}f_1-\frac{260182796917434762586 21}{4397174364147941376000}\ln 2\\
&\quad \left.+\frac{1612907}{630630}\ln 2\ln\beta\right)\\
&+\beta^8 \quad \left(\frac{954114049822352647477003 31}{82600920430519078748160000}+\frac{1531}{12155}\zeta_3-\frac{1553400235001}{752593842000}\ln\beta\right.\\
&\quad \left.-\frac{44883901561063}{48177768038400}R_2+\frac{9}{2210}f_4-\frac{35201911157547612242123}{7073005888156336128000}\ln 2\right.
\end{aligned}
$$

$$+\frac{10048418532335365951}{1688152168621670400}\ln^2 2 - \frac{3204468415729060213\pi^2}{43891956384163430400}$$
$$-\frac{631\pi^2}{7293}\ln 2 + \frac{2}{3315}f_1 + \frac{5651}{24570}\ln^2\beta + \frac{9}{24310}f_3$$
$$+\frac{997037}{417690}\ln 2\ln\beta\Big)\Big]$$

The values of f_1, f_3, f_4, and R_2 from [11] are

$$f_1 = 3.2244598, \quad f_3 = 12.3200632, \quad f_4 = 7.8319492, \quad R_2 = -0.7294612.$$

C.2 Expansion From Zero Mass

$$\begin{aligned}
X_H &= \frac{12991}{1296} - \frac{1}{3}\zeta_3 - \frac{53\pi^2}{54} \\
&+\rho^2 \left(\frac{89\pi^2}{54} + \frac{13}{3}\zeta_3 - \frac{137567}{6480}\right) \\
&+\rho^4 \left(\frac{4\pi^2}{3} - \frac{10081601}{705600} - \frac{23}{840}\ln\rho\right) \\
&+\rho^6 \left(\frac{79\pi^2}{27} + \frac{311162923}{11430720} - \frac{20107}{22680}\ln\rho\right) \\
&+\rho^8 \left(\frac{239\pi^2}{27} - \frac{53677950653}{628689600} - \frac{12703}{45360}\ln\rho\right) \\
&+\rho^{10} \left(\frac{289\pi^2}{9} - \frac{608580026081197}{1947889944000} + \frac{6391951}{10810800}\ln\rho\right)
\end{aligned}$$

$$\begin{aligned}
X_S &= \frac{23\pi^2}{108} - \frac{4}{9} + \zeta_3 \\
&-\rho \left(\frac{3\pi^2}{4}\right) \\
&+\rho^2 \left(\frac{4}{9} + \frac{13}{2}\ln\rho - 3\ln^2\rho - \zeta_3 + \frac{157\pi^2}{108}\right) \\
&-\rho^3 \left(\frac{25\pi^2}{18}\right) \\
&+\rho^4 \left(\frac{1193}{36} - \frac{61}{3}\ln\rho + 9\ln^2\rho - \frac{16\pi^2}{3}\right) \\
&+\rho^5 \left(\frac{113\pi^2}{36}\right) \\
&-\rho^6 \left(\frac{1513}{36} - \frac{2273}{54}\ln\rho + 12\ln^2\rho + 12\zeta_3 - \frac{235\pi^2}{54} + \frac{8\pi^2}{3}\log\rho\right)
\end{aligned}$$

$$+\rho^7 \quad \left(\frac{13\pi^2}{2}\right)$$

$$+\rho^8 \quad \left(\frac{164233}{43200} + \frac{6043}{135}\ln\rho + 8\ln^2\rho - \frac{205\pi^2}{54}\right)$$

$$+\rho^9 \quad \left(\frac{104\pi^2}{9}\right)$$

$$+\rho^{10} \quad \left(\frac{88799687}{1512000} + \frac{27319}{180}\ln\rho + 34\ln^2\rho - \frac{541\pi^2}{90}\right)$$

$$X_L = \frac{23\pi^2}{108} - \frac{4}{9} + \zeta_3$$

$$-\rho^2 \quad \left(\frac{77\pi^2}{108} + \frac{1}{18} - \frac{13}{2}\ln\rho + 3\ln^2\rho + \zeta_3\right)$$

$$+\rho^4 \quad \left(\frac{865}{72} - \frac{34}{3}\ln\rho + 6\ln^2\rho\right)$$

$$+\rho^6 \quad \left(\frac{235}{108} + \frac{521}{27}\ln\rho - 6\ln^2\rho - \frac{40\pi^2}{27}\right)$$

$$+\rho^8 \quad \left(\frac{63853}{1440} + \frac{961}{27}\ln\rho - 18\ln^2\rho - \frac{71\pi^2}{27}\right)$$

$$+\rho^{10} \quad \left(\frac{17785273}{108000} + \frac{22733}{225}\ln\rho - 76\ln^2\rho - \frac{383\pi^2}{45}\right)$$

$$X_A = \frac{521}{576} + \frac{9}{16}\zeta_3 + \frac{505\pi^2}{864} - \frac{19\pi^2}{8}\ln 2 + \frac{11\pi^4}{1440}$$

$$-\rho^2 \quad \left(\frac{1223}{576} + \frac{185}{8}\ln\rho - \frac{33}{4}\ln^2\rho + \frac{107}{16}\zeta_3 + \frac{145\pi^2}{864} - \frac{57\pi^2}{8}\ln 2 + \frac{161\pi^4}{720}\right)$$

$$+\rho^3 \quad \left(\frac{2\pi^2}{3}\right)$$

$$+\rho^4 \quad \left(\frac{27\pi^2}{8} - \frac{13391}{288} + \frac{2027}{48}\ln\rho - \frac{33}{2}\ln^2\rho - \frac{403}{64}\zeta_3 - \frac{23\pi^2}{8}\ln\rho - \frac{201\pi^2}{32}\ln 2 - \frac{31\pi^4}{720}\right)$$

$$+\rho^5 \quad \left(\frac{118\pi^2}{15}\right)$$

$$+\rho^6 \quad \left(\frac{3843029}{129600} - \frac{9997}{135}\ln\rho + \frac{85}{6}\ln^2\rho - \frac{4519}{192}\zeta_3 - \frac{2677\pi^2}{432} - \frac{323\pi^2}{144}\ln\rho + \frac{113\pi^2}{32}\ln 2 - \frac{1309\pi^4}{1440}\right)$$

$$
\begin{aligned}
&+\rho^7 \quad \left(\frac{1234\pi^2}{45}\right) \\
&-\rho^8 \quad \left(\frac{7938960101}{50803200} + \frac{14713471}{120960}\ln\rho - \frac{2881}{72}\ln^2\rho + \frac{182}{3}\zeta_3 + \frac{119861\pi^2}{4608}\right. \\
&\qquad \left. + \frac{277\pi^2}{24}\ln\rho - 2\pi^2\ln 2 + \frac{575\pi^4}{288}\right) \\
&+\rho^9 \quad \left(\frac{155266\pi^2}{1575}\right) \\
&-\rho^{10} \quad \left(\frac{410660471567}{846720000} + \frac{1085474549}{3024000}\ln\rho - \frac{2939}{60}\ln^2\rho + \frac{191113}{960}\zeta_3\right. \\
&\qquad \left. + \frac{1265407\pi^2}{13824} + \frac{50591\pi^2}{1440}\ln\rho - \frac{39\pi^2}{32}\ln 2 + \frac{2093\pi^4}{288}\right)
\end{aligned}
$$

$$
\begin{aligned}
X_F \quad = \quad & 5 - \frac{53}{8}\zeta_3 - \frac{119\pi^2}{48} + \frac{19\pi^2}{4}\ln 2 - \frac{11\pi^4}{720} \\
&+\rho^2 \quad \left(\frac{743\pi^2}{48} - \frac{97}{2} - \frac{75}{8}\ln\rho - \frac{27}{2}\ln^2\rho + \frac{151}{8}\zeta_3 + \pi^2\ln\rho - \frac{57\pi^2}{4}\ln 2\right. \\
&\qquad \left. - \frac{127\pi^4}{360}\right) \\
&-\rho^3 \quad \left(\frac{4\pi^2}{3}\right) \\
&+\rho^4 \quad \left(\frac{7145}{288} - \frac{329}{24}\ln\rho + 18\ln^2\rho + \frac{547}{32}\zeta_3 - \frac{83\pi^2}{12} + \frac{25\pi^2}{12}\ln\rho\right. \\
&\qquad \left. + \frac{201\pi^2}{16}\ln 2 + \frac{19\pi^4}{72}\right) \\
&-\rho^5 \quad \left(\frac{236\pi^2}{15}\right) \\
&+\rho^6 \quad \left(\frac{745007}{21600} - \frac{7381}{360}\ln\rho - \frac{602}{9}\ln^2\rho + \frac{3895}{96}\zeta_3 + \frac{274\pi^2}{27} + \frac{427\pi^2}{72}\ln\rho\right. \\
&\qquad \left. - \frac{113\pi^2}{16}\ln 2 + \frac{941\pi^4}{720}\right) \\
&-\rho^7 \quad \left(\frac{2468\pi^2}{45}\right) \\
&+\rho^8 \quad \left(\frac{391125283}{8467200} - \frac{15587891}{60480}\ln\rho - \frac{5893}{24}\ln^2\rho + \frac{1435}{12}\zeta_3 + \frac{251863\pi^2}{6912}\right. \\
&\qquad \left. + \frac{787\pi^2}{36}\ln\rho - 4\pi^2\ln 2 + \frac{895\pi^4}{144}\right) \\
&-\rho^9 \quad \left(\frac{310532\pi^2}{1575}\right)
\end{aligned}
$$

$$+\rho^{10}\left(\frac{20467679\pi^2}{172800}-\frac{72627657751}{1270080000}-\frac{1796140691}{1512000}\ln\rho-\frac{439783}{600}\ln^2\rho\right.$$
$$\left.+\frac{188881}{480}\zeta_3+\frac{49007\pi^2}{720}\ln\rho-\frac{39\pi^2}{16}\ln 2+\frac{16289\pi^4}{720}\right)$$